Structural and functional characterisation of tRNA modifying enzymes

Dissertation

for the award of the degree

Doctor rerum naturalium

of the Georg-August-Universität Göttingen

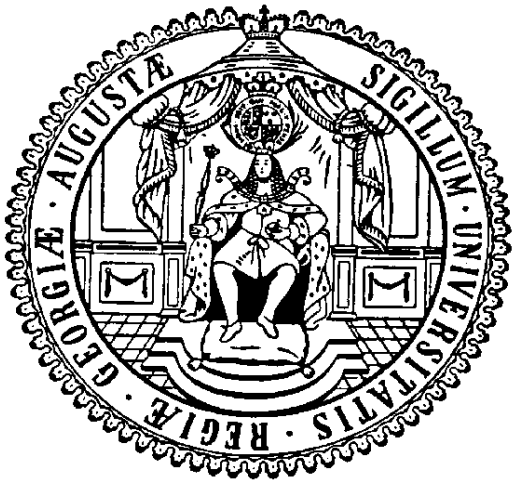

Within the doctoral program

Biomolecules: Structure – Function – Dynamics

of the Georg-August-University School of Science (GAUSS)

submitted by

Katharina Franziska Blersch

From Albstadt-Ebingen, Germany

Göttingen, 2021

Members of the Thesis Committee:

Prof. Dr. Ralf Ficner (Reviewer 1)
Department of Molecular Structural Biology
Institute for Microbiology and Genetics
Georg-August-University Göttingen

Prof. Dr. Jörg Stülke (Reviewer 2)
Department of General Microbiology
Institute for Microbiology and Genetics
Georg-August-University Göttingen

Prof. Dr. Markus Bohnsack
Department of Molecular Biology
University Medical Centre Göttingen
Georg-August-University Göttingen

Members of the Extended Examination Board:

Dr. Sarah Adio
Department of Molecular Structural Biology
Institute for Microbiology and Genetics
Georg-August-University Göttingen

Prof. Dr. Kai Tittmann
Department of Molecular Enzymology
Schwann-Schleiden Research Centre
Georg-August-University Göttingen

Prof. Dr. Henning Urlaub
Max Planck Institute for Biophysical Chemistry
Bioanalytical Mass Spectrometry Group

Date of oral examination: May 19, 2021

I hereby declare that the PhD thesis "Structural and functional characterisation of tRNA modifying enzymes" is my own work that was prepared with no other sources and aids than quoted. This thesis, or parts thereof, have not been submitted elsewhere.

31th March 2021, Göttingen

Table of content

Abstract

Posttranscriptional and posttranslational modifications are key regulatory mechanisms to expand biological properties of proteins and nucleic acids in living cells. A tremendous number of chemical modifications is found on all RNA species, with the highest diversity in composition and density found in transfer RNA (tRNA). Occurring all over the tRNA body, modifications increase tRNA stability, induce proper folding, and modulate translational fidelity. Non-canonical nucleobases include simple modifications as methylations and alkylations to highly complex extensions as seen in wybutosine and queuosine (Q), of which the latter requires a complete base exchange. Because mammalian tRNA molecules can harbour on average 13 modification at the same time, studying single modifications can be challenging. Especially since modifications exhibit a certain degree of "cross-talk" by influencing each other as seen for Q. Recent studies revealed a link between the hypermodified 7-deaza guanine derivative Q occurring at the wobble base position 34 (Q34) of $tRNA^{Asp}$ and the methylation of cytosine at position 38 (m^5C38) introduced by Dnmt2. Here, deposition of m^5C38 is stimulated upon prior Q34 modification with an enigmatic underlying biochemical mechanism. Thus, the aim of this study was to gain structural and biochemical insights into RNA modifying enzymes introducing (i) a methyl group to guanine at position 7 (m^7G) by TrmB, (ii) methylation of cytosine at position 4 (m^5C) by Dnmt2, and (iii) ribosyl transfer and isomerisation to $preQ_1$ by QueA.

m^7G is found not only as the mRNA-cap structure to protect mRNA from degradation, but also in tRNAs at position 46 in the variable loop introduced by the TrmB/Trm8 enzyme family. Prior to this thesis, several crystal structures of TrmB/Trm8 enzymes have been determined, revealing differences in their biological assembly. In this thesis, the first crystal structure of the homodimeric *B. subtilis* TrmB in complex with the methyl group donor S-Adenosylmethionine (SAM) and post catalytic product SAH is reported. Analysis of the SAM/SAH crystal structures revealed conserved ligand binding across TrmB/Trm8 enzymes. Structural, biochemical, and computational approaches revealed a 2:2 binding stoichiometry of tRNA to protein, and resulted in the TrmB-$tRNA^{Phe}$ complex model in which two tRNA molecules bind to the homodimeric TrmB. Interestingly, biochemical analysis of TrmB activity at physiological SAM conditions showed a half-of-the sites reactivity, even though each monomer of TrmB is capable of tRNA and ligand binding. Subsequently, the presented biochemical and structural data give valuable insights into TrmB activity and substrate binding.

The second part of the thesis focusses on the m^5C writer enzyme Dnmt2. Dnmt2 substrate specificity was long enigmatic, as Dnmt2 was first identified as DNA methyltransferase (MTase), however, exhibiting weak methyltransferase activity on DNA. Since the discovery of highly specific MTase activity of Dnmt2 on $tRNA^{Asp}$, a few more substrates have been identified, including

$tRNA^{Gly}$ and $tRNA^{Val}$. However, only $tRNA^{Asp}$ harbours Q at position 34 which was identified to increase Dnmt2 methylation activity. Of the four Q34 tRNAs $tRNA^{Asp}$, $tRNA^{Asn}$, $tRNA^{Tyr}$, and $tRNA^{His}$ only the latter harbours a cytosine at position 38, rendering $tRNA^{His}$ a putative Dnmt2 substrate. Even though m^5C38 in $tRNA^{His}$ could not be observed so far, human Dnmt2 was identified to modify human $tRNA^{His}$ during the course of this thesis. In contrast to prior work on *S. pombe* Dnmt2, stimulating effects upon Q modification could not be observed in the human context, implying different functions of Q34 in *S. pombe* and humans. Furthermore, Dnmt2 activity on $tRNA^{His}$ was found to be highly pH-dependent rendering $tRNA^{His}$ from cognate to non-cognate tRNA by shifting the pH from 8.0 to 7.4. The identification of $tRNA^{His}$ as Dnmt2 substrate gives more insight into Dnmt2 substrate specificity.

The S-adenosylmethionine:tRNA ribosyltransferase isomerase (QueA) was the study focus of the last part of this thesis. QueA is of special interest as (i) QueA catalyses the ribosyl-transfer in the penultimate step of Q-biosynthesis, (ii) Q is a major driving force in the virulence of *Shigella* bacteria, and (iii) QueA inhibition represents and interesting starting point in treating *Shigella* infection. Prior to this thesis incomplete QueA crystal structures have been determined. During this work, a full length QueA structure model on basis of a QueA crystal structure determined in this thesis was proposed. Investigation of this model enabled the identification of a putative SAM-binding pocket and amino acids possibly involved during catalysis. Furthermore, molecular docking experiments gave rise to a putative QueA-tRNA complex model. The proposed complex model gives valuable insight into QueA activity and provides a model for initial computer-based fragment screening in order to perform structure-based drug design to inhibit *Shigella* bacterial infection and treat shigellosis.

Overall, this thesis provides insights into protein-RNA complexation and substrate specificity by studying complex formation by means of biochemical, structural, and computational methods. Even though, both subunits of the homodimeric TrmB are capable of binding SAM and tRNA, TrmB exhibits at physiological SAM concentration a half-of-the sites reactivity. Furthermore, a connection of enzyme activity to stress response was identified, as human Dnmt2 shows altered enzyme activity on $tRNA^{His}$ depending on the used pH value. Lastly, the identification of the putative SAM-binding pocket and proposition of a QueA-tRNA complex model represents a valuable starting model for computational and experimental methods in structure-based drug design.

Chapter 1 Introduction

The identification of deoxyribonucleic acid (DNA) and its composition forming the genetic code was one of the most ground-breaking discoveries in recent history. First, the unravelling of the DNA structure by Watson and Crick in 1953 significantly changed the understanding of DNA (Watson and Crick, 1953a, 1953b). But not until the mid 1960s with the elucidation of the genetic code, the era of molecular genetics began. For a long period of time, DNA was thought to be too simple to store the genetic information, as it consists of only four nucleoside building blocks. Namely, these are the canonical nucleosides deoxyadenosine (dA) and deoxyguanosine (dG) classified as heterocyclic purines and the monocyclic pyrimidines deoxycytosine (dC) and deoxythimidine (dT)(Dahm, 2008). Corresponding to these deoxynucleosides are the ribonucleosides A, G, C, and uracil (U) in the DNA transcript ribonucleic acid (RNA). With these four nucleosides, DNA and RNA are able to carry the genetic information and are the building blocks of life.

In general, DNA forms a three-dimensional double wounded helix, which requires prior formation of a polynucleotide chain. To form this chain, the canonical nucleosides consisting of a nitrogenous base and the 2-deoxyribose, are connected to an additional phosphate group, then called nucleotide. These nucleotides are then covalently linked to each other to form polynucleotide sequences (Watson and Crick, 1953a, 1953b). In this polynucleotide strand, 2-deoxyribose (sugar) and phosphate groups are composed in an alternating manner connected via phosphodiester bonds to form the sugar phosphate backbone. In detail, the phosphate group links two adjacent sugar rings via the 5´carbon of one nucleotide sugar and the free hydroxyl-group on the 3´ carbon belonging to the neighbouring nucleotide. With this 5´ to 3´ extension, DNA can form large polymers which are able to store the genetic information via a unique arrangement of these four bases. As described by Watson and Crick, DNA is built up by two wounded strands complementary to each other, leading to a stable 3D structure (Watson and Crick, 1953a, 1953b). In this double-stranded helix, hydrogen bonds are formed between purine bases with opposing pyrimidine bases, allowing the interaction of A/T and C/G nucleotide pairs. On the way from DNA to protein, the information stored in DNA is read and transcribed to RNA molecules, maintaining the “storage only” attribute of DNA. In RNA, the above mentioned base pairing rules apply, with the difference of using U instead of T which results in the pairings A/U and G/C. In contrast to the uniform structure and function of DNA, RNA comes in many different flavours depending on their purpose. Beside the coding messenger RNA (mRNA) which contains the genetic information of a specific gene that is to be translated to a protein, there are several non-coding RNAs. Part of these

non-coding RNAs are micro RNA (miRNA), small nuclear (snRNA), small nucleolar RNA (snoRNA) and long non-coding RNA (lncRNA) which are involved in gene expression by regulating mRNA degradation and translational repression, modification of ribosomal RNA (rRNA), and splicing of mRNA, respectively (Cao et al., 2018; Catalanotto et al., 2016). However, the most abundant RNA molecule in living cells is transfer RNA (tRNA) involved in protein synthesis and therefore common to the bacterial, archaeal, and eukaryotic kingdoms of life.

1.0 Transfer RNA

Transfer RNA (tRNA) is a key component in the life of a cell and was discovered with a fully sequenced tRNA molecule in 1965 (Schimmel, 2017; Shepherd and Ibba, 2015). tRNAs are linker molecules, bridging the informational level of DNA and the functional level of proteins. These are rather small non-coding RNAs of 76 to 90 nucleotides, carrying amino acids to the ribosome to decode the mRNA sequence for protein synthesis. The human genome encodes more than 500 tRNA genes to decode 61 codons (Chan and Lowe, 2016). Given this high amount of tRNA genes, it is not surprising that tRNAs show a large sequence diversity. However, tRNAs exhibit a conserved secondary structure, also referred to as "cloverleaf" named after their similar appearance (Figure 1.1). The main features of this cloverleaf are formed by the acceptor stem, the dihydrouidine (D)- arm, the anticodon arm, the variable loop, and the TψC (T)- arm. The acceptor stem contains the 5´- and 3´-end of the tRNA and serves as recognition motif for the aminoacyl-tRNA-synthetases (Cavarelli and Moras, 1993; McClain, 1993), the anticodon arm harbours the name giving anticodon which serves as recognition motif to decipher mRNA during translation, and the TψC (T)- arm contains the highly conserved pseudouridine (ψ, Figure 1.1).

Before tRNA molecules can participate in protein synthesis, they undergo specific maturation processes to ensure structural integrity and proper function of the tRNA. These maturation processes include trimming of the 5´- and 3´- ends, excision of introns, specific base modifications, and the addition of the conserved CCA-end (Betat et al., 2014). These modifications enable the tRNA molecule to fold into the functional three-dimensional L-shaped form. Before the tRNA fulfils its role in protein translation, aminoacyl-tRNA-synthetases activate and charge the tRNA molecule with its cognate amino acid. This reaction is highly dependent on the proper structure of the 3´-end as well as the anticodon, resulting in a proof-reading mechanism for tRNA integrity and thereby ensuring correct translational activity (Hou, 1997; Ibba and Söll, 2000; Shepherd and Ibba, 2015).

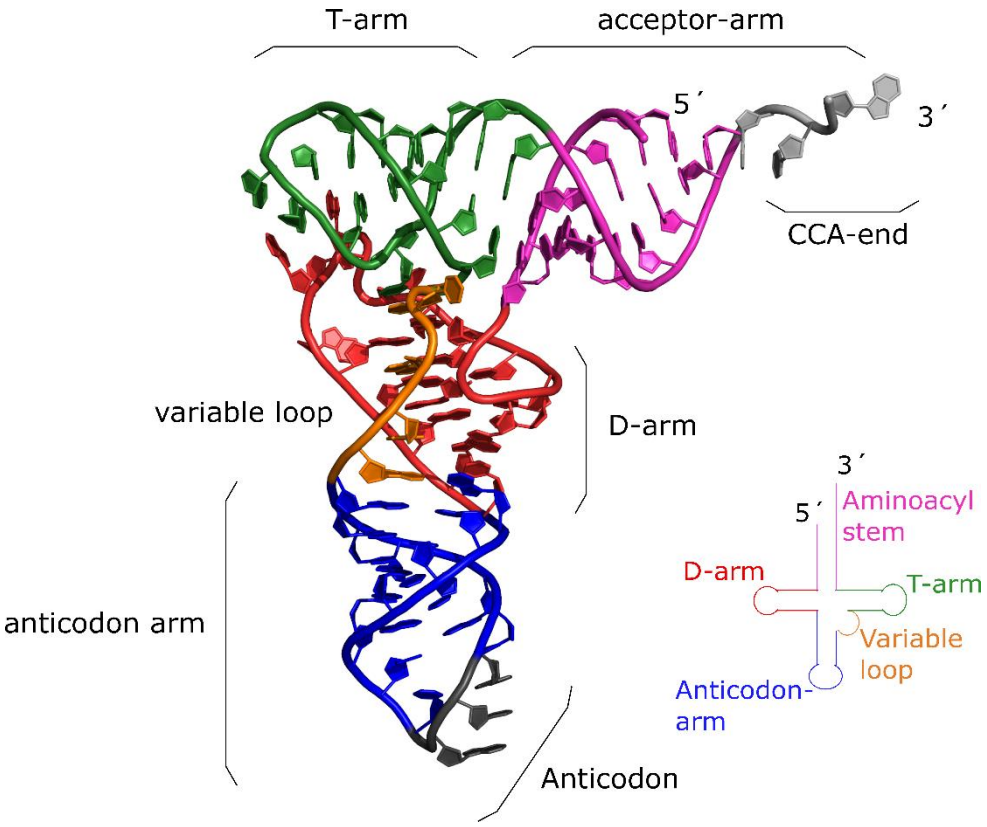

Figure 1.1: Tertiary structure of transfer RNA (tRNA). The canonical L-shaped tertiary structure is shown as cartoon with acceptor stem (magenta), D-arm (red), anticodon arm (blue), variable loop (orange), and TψC-arm (green). The anticodon is shown in grey (PDB ID: 1ehz). The classic cloverleaf structure is depicted on the right bottom corner, showing the typical tRNA features, coloured according to the L-shaped tRNA.

1.1 Extending the genetic code: non canonical bases

DNA consists of four canonical bases, namely dA, dG, dC, and dT, with the corresponding canonical RNA bases A, G, C, and U. This rather limited set of building blocks is expanded by the introduction of special chemical modifications, altering canonical to non-canonical bases. The extent to which RNA and DNA bases are modified is highly different. While in DNA only a hand full base modifications are detected to date, the non-canonical nucleobase pool of which RNA can choose from is tremendous. DNA base modification occurs in three of the four canonical nucleotides dC, dA, and dG (listed according to their abundance) (Carell et al., 2018). The first non-canonical DNA base identified was 5-methyl-deoxycytidine (5-mC). Introduction of 5-mC can have strong effects on the cellular metabolism, such as silencing of gene expression upon 5-mC insertion in promoter regions and thereby preventing binding of transcription factors to their designated target site (Murín et al., 2018; Razin and Cedar, 1991).

In contrast to the rather small set of DNA modifications, there are more than 170 unique modifications known to broaden the RNA information content (Boccaletto et al., 2018). RNA

modifications are found on all four canonical nucleotides at a variety of positions within the corresponding bases, and span from simple modifications like methylations and alkylations to highly complex alterations, even introducing a nucleobase exchange as seen in queuine (q) , which is called hyper-modification (Carell et al., 2012). Of all modified RNA species, tRNAs are most extensively and diversely modified with a total of 93 modifications found to date (Cantara et al., 2011). These modifications vary in their composition, as well as in their density, generally increasing from bacteria (on average ~ 6.5 % of total residues are modified) to eukaryotic tRNAs with up to 16.5 % of all bases modified in tRNA (Machnicka et al., 2014). The abundance of these modifications changes dramatically when taking a closer look on single tRNA sequences. For example, the mitochondrial $tRNA^{Ser}$ of *Mesocricetus auratus*, contains only one modification, whereas the cytoplasmic $tRNA^{Trp}$ of *Triticum aestivum* harbours 18 modified residues. Despite the high fluctuation of tRNA modifications, there are modifications common to nearly all tRNA molecules. Examples include pseudouridine (ψ) which is a highly conserved modification occurring at position 55 in the TψC-arm, and more elaborate modifications that are present in only one or a few tRNA species like wybutosine (yW), and queuosine (Q)(Machnicka et al., 2014). Queuosine modification and its biological role will be discussed in detail in chapter 1.7.

The diversity seen in tRNA modification, composition, and density is also mirrored in their chemical properties, and cellular effects as for instance (i) induction of proper folding, (ii) stabilization of the three-dimensional structure or (iii) fine tuning of the translational machinery (Helm et al., 1998; Konevega, 2004). However, from the complexity of the introduced modification it is not possible to deduce their function, as seen for the methylation of human mitochondrial $tRNA^{Lys}$ (Helm et al., 1999, 1998). The absence of methylation of A9 at position 1 (m^1A9) would permit Watson-Crick pairing of A9-U64 and consequently enable the formation of an extended hairpin. In the presence of m^1A9, this base pairing would be prevented, which allows the formation of the T- and D-stems and results in the folding of the canonical cloverleaf structure (Helm et al., 1999, 1998).

Further, Chen and colleagues described the modification level dependent binding of Mg^{2+} ions (Chen et al., 1993) in yeast $tRNA^{Phe}$. Here, methylation of carbon 5 at position 40 (m^5C40) leads to a m^5C40-dependent conformational change within the tRNA molecule and results in the formation of the canonical anticodon stem-loop. However, this process is induced by Mg^{2+} and results in a m^5C40-dependent Mg^{2+} induced conformational change of yeast $tRNA^{Phe}$, not possible for unmodified $tRNA^{Phe}$ (Chen et al., 1993).

One of the more frequently modified positions in tRNA is located adjacent to the anticodon at position 37, with 13 known different modifications. One of these modifications represents the methylation of guanine at position 1, resulting in m^1G37, and ensures reading frame maintenance

(Urbonavicius et al., 2001). Elimination of m^1G37 in bacteria leads to accumulation of ribosomal +1 frameshifts, which results in a prematurely terminated aberrant peptide. Therefore, m^1G37 plays a vital role in maintaining the reading frame and preventing energetically costly translational errors (Urbonavicius et al., 2001). Albeit tRNA modifications are immensely complex in their composition and chemistry, two thirds of the known modifications consist of simple methylations. Two of these methylations will be discussed in chapters 1.4 and 1.6, as they play a vital role in this thesis.

The previously mentioned examples give first insights into the dependency between a modifications position and the resulting cellular effect. Indeed, in recent years it could be shown that modifications within the tRNA core correlate mostly with tRNA folding and stability, whereas modifications in the anticodon, and nucleotides surrounding this region, are associated with translational fine tuning during decoding (Gu et al., 2014; Helm, 2006; Väre et al., 2017). As discussed before, the lack of modifications within the anticodon region can have severe effects within the cell. However, in most cases, the loss of a single modification often has little to no effect during growth and cell homeostasis, suggesting that there is a level of redundancy and loss of a modification can be compensated, as seen in yeast (Alexandrov et al., 2006). This indicates the presence of a modification network, where several modifications act together to ensure and maintain biologically functional tRNAs within the cell.

Recent findings further broaden the complexity of the tRNA modification field. The view of tRNA modifications as a steady "once introduced never erased" static posttranscriptional feature has changed toward a more dynamic regulation of the modification status of RNAs (Gu et al., 2014). Specifically, the degree of tRNA modification were shown to respond dynamically to extrinsic stimuli, such as nutritional stress, suggesting a participation of tRNA in the regulation of molecular responses that can cause tRNA reprogramming (Endres et al., 2015). Furthermore, tRNA fragments (tRFs), which have been long considered degradation intermediates or tRNA preparation artefacts, were revealed to be the product of specific enzymes and harbour biological activity. tRFs are the result of nucleolytic cleavage, such as the stress induced activity of angiogenin (Schaefer et al., 2010). Angiogenin cleaves tRNAs in the anticodon, resulting in 5´- and 3´- halves. tRF activity has been identified in various processes like translation interference and cancer progression (Fish et al., 2018; Guzzi, 2020; Magee and Rigoutsos, 2020). With the existence of nearly 60 million tRNA molecules in a single mammalian cell (Lodish, 2002), tRNA modification, and fragmentation add another layer to the complex tRNA world.

1.2 Common Methyltransferases

Over half of the modifications specific to RNA involve the addition of a single or sometimes two methyl groups (Boccaletto et al., 2018; Cantara et al., 2011). The dynamic deposition and removal of these modifications is ensured by the so called "writer" and "eraser" proteins. These proteins effect the dynamic modification of RNAs to modulate RNA metabolism, such as stability and effective protein synthesis, as demonstrated for methylation of adenosine at position 6 (m^6A) (Cao et al., 2016; Yang et al., 2018). m^6A plays a crucial role during splicing and in epigenetic gene regulation. The realization of the dynamic deposition and removal of m^6A renewed the interested of scientists to study RNA modification in a dynamic context.

1.3 m^7G Methyltransferase

One of the most important modifications in eukaryotes is added to the 5´ end of each mRNA, snoRNA, and snRNA transcript and known as the 5´-cap structure. The 5´-cap is built up by a N7 methylated guanosine base (m^7G) connected via a 5´-5´- triphosphate linker with the first nucleotide in a multistep reaction mechanism (Fabrega et al., 2004; Shatkin, 1976; Trotman and Schoenberg, 2019). The m^7G-cap together with further accessory modifications function in the cell to mark nucleotides as "self" and to differentiate from foreign viral RNA, e.g. to (i) prevent self RNA from degradation or RIG-I mediated immune response (Schuberth-Wagner et al., 2015), and (ii) to enhance translation efficiency (Kuge, 1998). Apart from the role of the m^7G modification in guarding eukaryotic self RNA, m^7G is further common to eubacterial and archaeal tRNAs (Edmonds et al., 1991; Juhling et al., 2009). In eubacterial tRNAs, m^7G is found exclusively at position 46 in the variable loop (Okamoto et al., 2004; Purta et al., 2005; Tomikawa et al., 2018; Zegers, 2006; Zhou et al., 2009), with additional regions at positions 49 in archaeal $tRNA^{Leu}$ (Edmonds et al., 1991; Tomikawa et al., 2013), and position 34 in mitochondrial $tRNA^{Ser}$ of some eukaryotes (Matsuyama et al., 1998; Tomita et al., 1998). Methylation of G46 induces base pairing of m^7G46 with G22 and C13, resulting in the stabilization of the tRNA tertiary structure, further enhanced by the m^7G46 introduced positive charge (Agris et al., 1986). The enzyme depositing m^7G is the S-Adenosyl-L-methionine- (SAM)-dependent tRNA (guanine-7-)-methyltransferase, in eubacteria called TrmB. Interestingly, while the *E. coli* enzyme consist of a single functional subunit (Zhou et al., 2009), the *B. subtilis* TrmB is a homodimer (Zegers, 2006), and the eukaryotic yeast TrmB consists of two unrelated subunits Trm8/Trm82, with known homologues in human (METTL1/WDR4) (Alexandrov, 2005, p. 8; Alexandrov et al., 2002).

1.4 TrmB

M^{7}G46 belongs to one of the most common modifications and is spread through all kingdoms of life. The m^{7}G46 writer enzyme TrmB has been studied from several organisms, belonging to different kingdoms of life. TrmB belongs to the classic class I methyltransferase (MTase) superfamily harbouring a Rossmann-like fold (Leulliot et al., 2008; Martin and McMillan, 2002; Schubert et al., 2003; Zegers, 2006; Zhou et al., 2009). The canonical Rossmann-fold consists of a six-stranded central β-sheet flanked by α-helices (Hanukoglu, 2015), resulting in a double wound αβα sandwich (Figure 1.2). Interestingly, the central β-sheet of the class I methyltransferases contains a topological switch-point, resulting in a deep cleft within the MTase. A part of this cleft is formed by the first β- strand ending in a GxGxGx motif. This motif is a hallmark for nucleotide binding sites and is part of the SAM binding pocket in TrmB. However, the TrmB/Trm8 family differs from the canonical Rossmann-fold by the insertion of an additional β-strand between β-strands 5 and 6 (Figure 1.2) (Bujnicki, 1991; Zegers et al., 2005). Despite the overall conserved fold of the TrmB/Trm8 enzyme family, the domain architecture varies from mesophilic organisms containing an extended N-terminus to thermophilic organisms harbouring an elongated C-terminus. The thermophile organism *Aquifex aeolicus* contains an extended C-terminal domain important for protein stability at high temperatures (Tomikawa et al., 2007). Deletion of this extension resulted in unspecific N^7-methylation of tRNA transcripts and the reduction in methyl transfer activity.

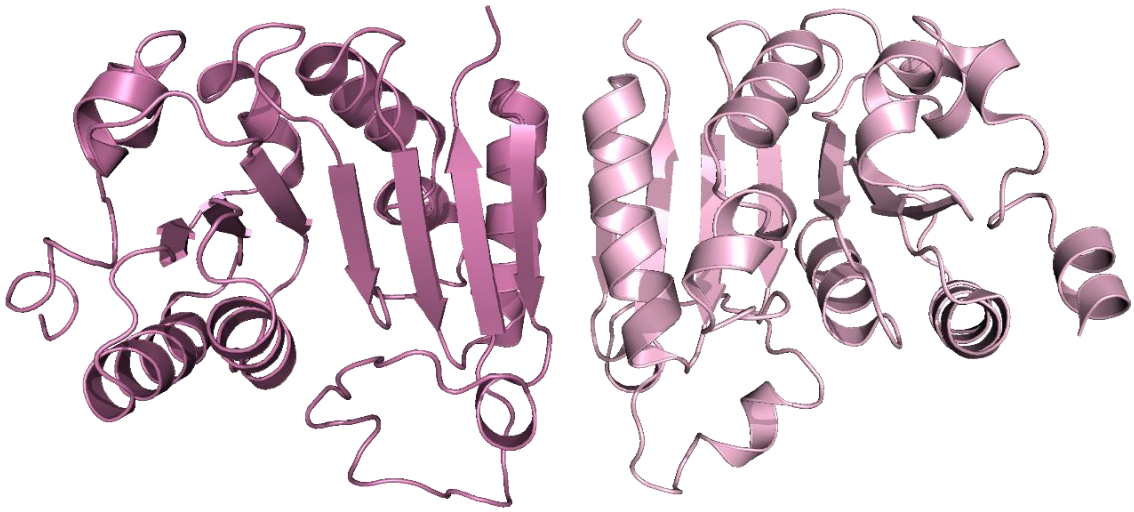

Figure 1.2: Structure of *Bacillus subtilis* TrmB. Crystal structure of the homodimeric TrmB presented in cartoon mode. Single subunits are indicated by colour in light and dark pink, respectively (PDB ID: 2FCA).

Since its discovery, the only known cognate tRNA annotated for TrmB encoded tRNA^{Phe}. A recent study on *Pseudomonas aeruginosa* TrmB revealed 23 different tRNAs substrates, including

$tRNA^{Ala}_{(GGC)}$, $tRNA^{Asp}_{(GUC)}$, and $tRNA^{Ile}_{(GAU)}$ (Thongdee et al., 2019). However, $tRNA^{Phe}$ emerged as a common substrate for TrmB.

1.4.1 tRNA recognition

Crystallization of protein-RNA complexes is a challenging task, which is reflected in only 4% of the total deposited structural entries in the Protein Databank (Berman et al., 2000), with even fewer structures (about 0.1%) involving tRNAs. Hence, extensive biochemical analyses have been conducted to map important amino acids on the TrmB enzyme to determine protein-RNA interaction sites and recognition motifs. Apparently, the mechanisms by which eukaryotic and eubacterial TrmB enzymes bind their cognate tRNA seem to follow different rules, as the enzymes already differ in their architectural composition. The yeast TrmB homolog Trm8/Trm82 distinguishes its substrate via the D-stem and T-stem structure on the tRNA molecule, as upon disruption of these structures, methyltransferase activity is shown to be severely decreased (Matsumoto et al., 2007a). Further mutations addressing the disruption of base pairing within the T-stem loop and D-stem loop structures revealed that Trm8/Trm82 recognizes the G46 base from the T-stem side. Interactions of the D- and T-stem were disrupted by mutagenesis of the D-loop, which perturbed the distance and angle of the G46 base relative to the T-stem (Matsumoto et al., 2007a). Indeed, Leulliot *et al.* (2008) present a Trm8/Trm82-tRNA complex model, based on molecular docking and cross validated by small-angle X-ray scattering (SAXS), where most of the protein-RNA contacts were made via the D- and T-arm, even though the anticodon was detected in close proximity to the protein (Leulliot et al., 2008). In contrast, the *A. aeolicus* TrmB accesses its tRNA target only via the T-stem side, with the tertiary base pair in the tRNA core being not essential for methylation (Okamoto et al., 2004). In summary, the tRNA recognition mechanism of the various TrmB proteins commonly address the substrate tRNA from the D-stem and T-stem facing site, albeit differing in their strictness of structural features to be recognized.

1.4.2 Reaction mechanism

Despite the variety of reported crystal structures of TrmB, the catalytic mechanism of the methyltransfer is still not fully elucidated. Even though TrmB belongs to the SAM-dependent MTases and harbours sequence motifs conserved in this class of enzymes, comparison of TrmB to the mRNA cap m^7G methyltransferase (Abd1), showed no striking structural similarities (De Bie et al., 2003; Fabrega et al., 2004). Hence, it is impossible to infer the TrmB catalytic mechanism from related enzymes such as Abd1. Therefore, elaborate mutation studies of TrmB proteins from different organisms have been conducted and identified Asp133 (nomenclature according to *A. aeolicus* TrmB) as possible catalytic centre. Asp133 is thought to be important for capturing the G46 base of the tRNA molecule, as alanine substitution of Asp133 reduced activity severely or

abolished activity completely (Purta et al., 2005; Tomikawa et al., 2018). This finding led to a hypothetic reaction mechanism, where the carboxyl group of Asp133 captures the N1 proton of the guanine base with a subsequent attack of the guanine-N7 atom against the activated methyl group of SAM. This reaction further requires the disruption of the G46-C13-G22 base pairing and leads to flipping of G46 into the binding pocket. However, this hypothetical reaction mechanism needs to be confirmed by biochemical and structural analyses.

1.4.3 Functional importance

m^7G46 gains more importance, as its physiological role is slowly uncovered. Since m^7G46 is located in the core region of tRNAs, it can be assumed that this particular modification acts in the stabilization of the tertiary tRNA fold, as the effect of a modification in cellular processes depends on the position of the modification. Concordantly, deletion of the TrmB gene in *E. coli* resulted in unnoticeable defects (De Bie et al., 2003). Intriguingly, deletion of the yeast homolog Trm8 and Trm82 is associated with a growth phenotype in a temperature sensitive manner (Alexandrov, 2005). This was an important discovery, as it was the first report on a conditional temperature sensitivity connected to m^7G modification in tRNA. Even more so, due to the finding of the existence of a complex modification network in *Thermus thermophilus* TrmB. The authors described a positive effect of m^7G46 on other modifications enhancing MTase activity for m^1G37 by TrmD, m^1A58 by TrmI, and Gm18 by TrmH (Tomikawa et al., 2010). Furthermore, recent studies have linked the human Trm8/Trm82 homolog METTL1/WDR4 to genetic diseases. In patients suffering from microcephalic primordial dwarfism, missense mutations in the gene coding for the non-catalytic subunit WDR4 were found, that caused defects in m^7G46 modification level (Shaheen et al., 2015). The catalytic subunit METTL1 (human homolog of Trm8) was further found to be regulated via phosphorylation and growth factors, proposing the involvement in a vast variety of cellular processes (Cartlidge et al., 2005). These studies clearly show the importance of m^7G46 modification of tRNAs and the necessity of studying tRNA modifications, since increasing numbers of human diseases are linked to atypical tRNA modifications.

1.5 m^5C Methyltransferase

Methylation of carbon 5 of cytosine (m^5C) is a widespread modification in both, DNA and RNA (Boccaletto et al., 2018; Cantara et al., 2011). In eukaryotic tRNAs, m^5C modification occurs most frequently at the junction between the variable loop and the T-stem at positions 48 and 49 (Boccaletto et al., 2018). Further modifications can be found at position C38 in animal tRNAs, where it results in a stimulated $tRNA^{Asp}$ charging activity and a subsequent enrichment of $tRNA^{Asp}$ containing proteins, upon other functions (Shanmugam et al., 2015). Confirmed m^5C writer

enzymes belong to the NSUN and Dnmt2 (a Dnmt homologue) enzyme family (Bohnsack et al., 2019; Motorin et al., 2009). Dnmt2 utilizes SAM as methyl donor to transfer the methyl moiety to the C5 atom of cysteine, to form m^5C38.

DNA Methyltransferases (Dnmts) are broadly distributed in vertebrates. In eukaryotes, Dnmts are divided in three major groups based on their substrate specificity: Dnmt1, Dnmt2, and Dnmt3 of which the latter is further divided into Dnmt3A, 3B, and 3L subfamilies (Goll and Bestor, 2005). Dnmt1, Dnmt3A, and Dnmt3B represent canonical cytosine-5 Dnmts that catalyse the modification of genomic DNA, whereas Dnmt3L and Dntm2 are non-canonical Dnmts lacking classic Dnmt activity. In most cases, the presence of Dnmt1 enzymes coincides with the presence of members of the Dnmt3 family (Goll and Bestor, 2005). Furthermore, organisms expressing members of the Dnmt1 and Dnmt3 families also encode for Dnmt2. Dnmt2 on the other hand was found to be the only Dnmt protein common in organisms such as *Saccharomyces pombe*, *Drosophila melanogaster*, and *Enantiomobea histolytica*. Thus, these Dnmt2-only organisms are interesting model organisms to study Dnmt2 function.

1.6 Dnmt2

Dnmt2 is the most conserved and widely distributed Dnmt member with a size of about 40 kDa. Dnmts consist of an N-terminal regulatory domain and a C-terminal catalytic domain, of which Dnmt2 only contains the C-terminal catalytic domain. Even though the eukaryotic Dnmt1, Dnmt2, and Dnmt3 families are conserved, it is thought that most likely, they evolved from independent origins in the prokaryotic DNA methyltransferase field and were derived from the methyltransferase and restriction modification systems (Jurkowski and Jeltsch, 2011). Dnmt2 was at first classified as a DNA-methyltransferase as it contains all of the 10 described motifs conserved in DNA cytosine-5 methyltransferases (Dong, 2001; Jeltsch et al., 2006; Johannsson et al., 2018; Schulz et al., 2012). Additional high structural conservation across species, such as the prokaryotic m^5C DNA MTase M.HhaI, strengthened the classification for Dnmt2 as DNA methyltransferase (Dong, 2001). Despite different methods employed to study Dnmt2 including bisulfate sequencing, thin-layer chromatography, and high-performance liquid chromatography, no or only very weak DNA methyltransferase activity could be detected (Dong, 2001; Hermann et al., 2003; Phalke et al., 2009). However, although an organism contains a Dnmt2 homologue, this does not mean that methylation of DNA has to occur. The genome of nematodes is in general considered to be unmethylated and *Caenorhabditis elegans* belongs to a group of organisms that lack any Dnmt2-like gene. Although this group lacking Dnmt2 is rather small (Gutierrez, 2004). In 2006, an important article reported knockout studies, conducted in different organisms (*A.*

thaliana, *D. melanogaster* and mice), where a highly specific Dnmt2-dependent RNA methyltransferase activity was discovered. This specific activity could be verified on $tRNA^{Asp}$ at position C38 positioned in the anticodon loop only (Goll et al., 2006). This high specificity of Dnmt2 towards its cognate tRNA was softened during the course of the last few years, as new tRNA substrates were confirmed. Additional to the common substrate $tRNA^{Asp}$, studies conducted in *D. melanogaster* and mouse revealed further substrates to be $tRNA^{Gly}$ and $tRNA^{Val}$ (Goll et al., 2006; Schaefer et al., 2010). Currently, these three tRNAs are the known cognate Dnmt2 substrates in mammals and further confirmed in *S. pombe*. However, this does not hold true for every organism, as seen in *Geobacter sulfurreducens*. *Geobacter* Dnmt2 specifically methylates $tRNA^{Glu}$ *in vitro* and *in vivo*, whereas no methyl transfer activity can be detected for $tRNA^{Asp}$ (Shanmugam et al., 2014). Apart from this altered substrate specificity, $tRNA^{Asp}$, $tRNA^{Gly}$, and $tRNA^{Val}$ manifested as common Dnmt2 targets (Jeltsch et al., 2017).

1.6.1 Catalytic mechanism

Dnmt2 displays dual specificity in catalysing m^5C modification on both, DNA and RNA in form of $tRNA^{Asp}$ (Goll et al., 2006). C5 methylation is not a trivial mechanism, since cytosine is an electron-poor heterocyclic aromatic ring and cytosine C5 is not able to perform a nucleophilic attack on the methyl group of SAM without prior activation. This is why RNA- and DNA (cytosine-5) methyltransferases perform the methyl transfer via Michael addition. In brief, DNA methylation is initiated by a first nucleophilic attack of the catalytic cysteine, located in the conserved motif IV, on the target cytosine (Liu and Santi, 2000; Santi et al., 1984) (Figure 1.3). This first attack leads to the formation of a covalent protein-DNA adduct, leading to the activation of the C5 position of the target cytosine. The activated C5 in turn performs the second and last nucleophilic attack on the SAM methyl group and the covalent protein-DNA adduct is resolved by the deprotonation at C5 and re-establishment of the aromatic ring. Subsequently, the methylated base and the co-factor product S-adenosyl-L-homocystein (SAH) are released. In contrast, RNA-methyltransferases use a cysteine residue located in motif VI and replace a catalytic glutamate residue from motif VI used in DNA-methyltransferases with an aspartate residue from motif IV (Motorin et al., 2009).

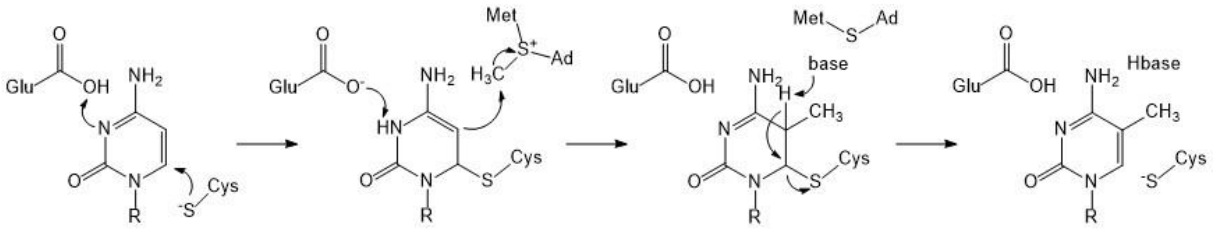

Figure 1.3: Dnmt2 catalytic mechanism. Catalysis is started with the nucleophilic attack of the catalytic cysteine on the target cytosine, resulting in a covalent enzyme-substrate adduct. The activated C5 of cytosine in turn performs nucleophilic attack on the SAM methyl group, leading to the reestablishment of the aromatic ring and breakage of the intermediate complex and the release of the reaction products SAH and m^5C38-tRNA.

1.6.2 tRNA recognition

Key prerequisite for Dnmt2 catalysis is the existence of a cytosine at position 38 of tRNAs. Consequently, a common feature of Dnmt2 substrates is the C38, however, not every C38 containing tRNA is a Dnmt2 substrate. This raises the question how Dnmt2 discriminates between cognate and non-cognate tRNAs. Mutation studies tried to tackle this question by mutagenesis of conserved amino acids followed by studying tRNA binding and methylation activity. Several conserved basic amino acids form a cleft on Dnmt2. This cleft is large enough to accommodate the anticodon loop, suggesting that the main interaction points are within the anticodon loop and stem of the tRNA molecule, while the acceptor stem points away from the protein (Jurkowski et al., 2012). However, the anticodon stem-loop alone does not seem to be the sole determinant, since Dnmt2 interacts with the anticodon stem-loop very weakly (Schulz et al., 2012). An additional determinant could be the variable loop which is located close to the anticodon stem in the L-shaped tRNA structure. The exchange of the variable loop of murine $tRNA^{Asp}$ with that of murine $tRNA^{Glu}$ (differing in sequence from AGAC to CGCG) led to a strong decrease in methyltransferase activity in *Geobacter* and human Dnmt2 (Shanmugam et al., 2014). Contradicting, replacement of the murine $tRNA^{Glu}$ with $tRNA^{Asp}$ did not lead to an increase in MTase activity of human Dnmt2. These results show the influence of the variable loop as further substrate recognition determinant in Dnmt2 enzymes. To further complicate substrate recognition, tRNA/DNA chimeras were prepared and tested for MTase activity. In these chimeras, small DNA stretches were inserted close to the tRNA target site, still maintaining the tRNA tertiary structure. The generated tRNA/DNA chimeras improved methylation over the canonical $tRNA^{Asp}$ (Kaiser, 2017). It is important to note, that in this context, MTase activity gradually fades with increasing DNA content, as the chimera loses its tRNA resemblance. Even though this Dnmt2 feature has only been recorded *in vitro*, this report shows the importance of the tRNA tertiary structure for proper Dnmt2 activity.

1.6.3 Dnmt2 structure

So far, crystal structures of Dnmt2 enzymes were reported from human, *S. pombe*, *D. frugiperda*, and *E. histolytica* (Dong, 2001; Johannsson et al., 2018; Li et al., 2013; Schulz et al., 2012). All of them were obtained in complex with SAH, the reaction product (Figure 1.4). However, neither of these four structures was co-crystallized with tRNA. The overall Dnmt2 fold comprises a large and a small domain. The large domain consists of a highly conserved central seven stranded β-sheet, flanked by α-helices, harbouring the SAM-binding pocket. In contrast, the small domain is built by a short antiparallel β-propeller surrounded by α-helices. The main differences in the reported structures can be observed in flexible loop regions, of which several are not resolved in the electron density. In the human Dnmt2, one of these un-resolved loops contains the catalytic

residue Cys79 (Dong, 2001). In *S. frugiperda*, *E. histolytica*, and *S. pombe* this active site loop is resolved and adopts either (i) a two antiparallel β-stranded structure (Li et al., 2013), (ii) a α-helical conformation (Schulz et al., 2012), or (iii) does not contain any secondary structure elements (Johannsson et al., 2018). It should be noted that these active site loops are all stabilized by crystal packing and may not resolve the true conformation, as seen for instance in the structurally related M.HhaI, where the corresponding active site loop interacts with the DNA substrate (Klimasauskas et al., 1994), resembling a putative feature of the Dnmt2 active site loop.

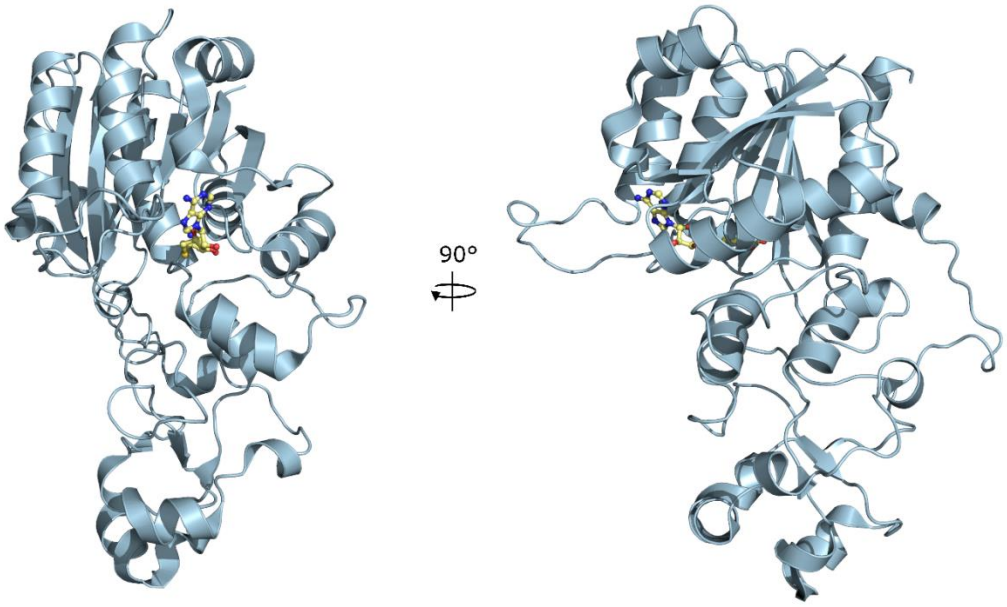

Figure 1.4: Dnmt2 crystal strucutre. The crystal structure of *S. pombe* Dnmt2 is presented in cartoon mode with the bound methyl dondor SAM as ball and stick in light yellow (PDB ID: 6FDF). The domain architecture is displayed in two orientations with 90° rotation.

1.6.4 Physiological importance

In the previous chapters, the importance of the modification location within the tRNA body for determining its function was discussed. The target position 38 methylated by Dnmt2 is next to the anticodon, and its involvement in protein translation is easily assumed. Indeed, Dnmt2-mediated m^5C38 modification in $tRNA^{Asp}$ promotes the association of aspartyl-tRNA synthetase to $tRNA^{Asp}$, resulting in a more efficient aminoacylation, and a final enhancement of poly-Asp-containing proteins (Shanmugam et al., 2015). Furthermore, Dnmt2 deposited m^5C38 enables discrimination between cognate and near-cognate codons (Tuorto et al., 2015), adding an additional layer in the impact on translation. The lack of m^5C38 in $tRNA^{Asp}$ during the translation of Asp(GAC/GAU) codons reduces the ability of $tRNA^{Asp}$ to compete with near-cognate tRNAs at the ribosome. This in turn allows the misincorporation of amino acids in the peptide chain and shows the effect of Dnmt2-mediated m^5C modification in translational accuracy. Further stimulating conditions for Dnmt2 activity were found in *S. pombe* and *D. discoideum*. The authors could show significant

changes in Dnmt2 activity depending on the modification state of $tRNA^{Asp}$ at position 34. $tRNA^{Asp}$ is one of four tRNAs to be modified with queuine, and will be discussed in detail in the following chapter. Cultivation of *S. pombe* cells in medium containing queuine resulted in a substantial induction of Dnmt2 activity. This also holds true for *D. discoideum* showing the conservation level of queuine induced fidelity of Dnmt2 (Müller et al., 2015; Tuorto et al., 2018). A physiological link to the cellular stress response was made, when Dnmt2 re-localization to stress granules was observed. Upon heat-shock, Dnmt2 localizes to stress granules, leading to the lack of m^5C38 modification, and to the production of tRNA fragments, indicating a Dnmt2-mediated stress response via tRNA modification (Schaefer et al., 2010).

1.7 Hypermodification Queuosine

In the late 1960s, an unidentified nucleoside at the first position of the anticodon of $tRNA^{Tyr}$ in *E. coli*, designated as Q, was discovered (Goodman et al., 1968). In the following five years, additional tRNAs containing this nucleoside were identified, namely $tRNA^{Asp}$, $tRNA^{His}$, and $tRNA^{Asn}$. They all have the hypermodification Q at the wobble position 34 in common, and harbour the anticodon sequence $G_{34}U_{35}N_{36}$ (Harada and Nishimura, 1972). Later on, the structure of Q was determined based on UV absorption, NMR spectra, and its chemical properties (Kasai et al., 1975; Ohgi et al., 1979). Queuosine is a guanosine derivative with the exchange of nitrogen at position 7 by a carbon atom (Figure 1.5). Appended to the C7 atom is a cyclopentanediol ring via an aminomethyl linker.

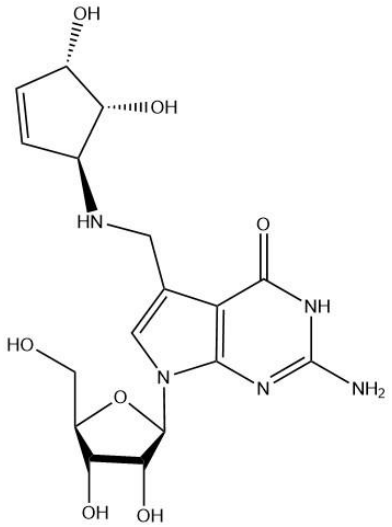

Figure 1.5: Chemical structure of the hypermodification queuosine (Q).

1.7.1 Q biosynthesis

Queuosine is the product of an elaborate biosynthesis pathway starting from guanosine-5´-triphosphate (GTP) and ending in a deazaguanosine base decorated with additional functional groups. As a modification of the wobble base, Q is shared by eukaryotes and prokaryotes. In archaea, a structurally similar modification of the 7-deazaguanosine, archaeosine (G^+), is found. G^+ is introduced at position 15 in the D-loop and acts in the stabilization of the tRNA structure (Gregson et al., 1993). Albeit prokaryotic and eukaryotic tRNAs carry Q, the modification pathways are quite different. While eukaryotes need to rescue queuine as dietary nutrient or salvage it from the gut microbiome (Katze et al., 1984), bacteria are able to synthesize queuine *de novo*. Hence, Q biosynthesis is unique to the prokaryotic kingdom.

The synthesis of Q is a multistep reaction mechanism involving seven enzymes. In general, Q biosynthesis can be divided into two major phases, first, the synthesis of the queuine precursor $preQ_1$ and second, incorporation into tRNA accompanied with the final maturation steps to form Q (Figure 1.6).

The queuine precursor 7-ammoniomethyl-7-deazaguanine ($preQ_1$) is synthesized in a multi-step process within the bacterial cytoplasm involving five different enzymes. Starting from guanosine-5´-triphosphate (GTP), GTP cyclohydrolase I catalyses the protonation of the N7 atom resulting in cleavage of the imidazole ring at position C8, with additional opening of the furanose ring. Subsequent re-cyclization leads to a 7,8-dihydroneopterin triphosphate (H_2NTP) (Nar et al., 1995; Phillips et al., 2008). Next, QueD binds the pterin moiety to form 6-carboxy-5,6,7,8-tetrahydropterin (CPH_4) (McCarty et al., 2009a), followed by QueE which catalyses the formation of 7-carboxy-7-deazaguanine (CDG) via a radical-mediated ring contraction in which N7 is replaced by a carbon atom and a covalently linked carboxy group (Bandarian and Drennan, 2015; McCarty et al., 2009b). QueC is next in line to form $preQ_0$, where the cyano nitrogen is derived from ammonia to form a nitrile, in two ATP-dependent reactions (McCarty et al., 2009b; Nelp and Bandarian, 2015). And lastly, QueF performs the conversion from $preQ_0$ to $preQ_1$ in a $NADPH/H^+$ dependant manner. The nitrile group of $preQ_0$ is reduced to a primary amine under the consumption of 4 electrons (Lee et al., 2007). Finally, the queuine precursor $preQ_1$ is incorporated into the tRNA substrate by the bacterial tRNA-guanine transglycosylase (TGT) at position 34, involving transglycosylation (Boland et al., 2009; Garcia and Kittendorf, 2005). TGT brakes the glycosydic bond between the sugar and the base and exchanges the guanine base with queuine (Iwata-Reuyl, 2003).

During the last step, which involves the action of two enzmyes, $preQ_1$-34tRNA is fully modified to Q34tRNA. The first step is performed by QueA, adding a cyclopentane-diol ring to the base and isomerization to epoxy-queuosine-tRNA (oQ-34tRNA), which is described in detail in section

1.8.1. (Van Lanen and Iwata-Reuyl, 2003). In a last, until recently not completely understood reaction, oQ-34tRNA is converted to the final Q34tRNA by QueG and its co-factor cobalamin. This reaction involves a two-electron reduction of the epoxide, leading to the formation of the distinct cyclopentane-diol moiety and the formation of queuosine (Miles et al., 2015, 2011).

1.7.2 Physiological consequences of Queuine modification

The hypermodified base queuine is involved in a variety of cellular processes spanning from efficient translation on a biochemical level, differentiation and development on a cellular level, to human diseases like cancer. Over decades, tRNA abundance and composition in mice and rats were measured and compared between developmental stages of both organisms. Analyses, including the level of Q-modified tRNAs, showed that Q-modified tRNAs in pre-natal mice and young rats increase with age (Frazer and Yang, 1972; Singhal, 1981). Furthermore, the extent of Q hypermodified tRNAs in murine erythro-leukemic cells differs between undifferentiated and differentiated cells, corroborating the impact of Q on development (Shindo-Okada et al., 1981). In undifferentiated cells, more than 90% of the $tRNA^{Asp}$ population was hypomodified, harbouring G34 instead of Q34. In contrast, in differentiated cells (120 h after induction of differentiation), most of the $tRNA^{Asp}$ molecules contained a queuine derivative at position 34 (mannose-Q). These studies suggest the influence of queuine in cell differentiation and development with a relation of queuine-incorporation and modification depending on the metabolic state of the cell.

The involvement of queuine-hypomodification in cancer tissue is poorly understood and currently under debate, due to conflicting reports. However, a recent study proposed that queuine-hypomodification in cancer is an intentional, rather than a passive mechanism (Hayes et al., 2020). The authors describe that the promotion of a Warburg-type metabolism is due to queuine depletion in human cervical HeLa cells. This altered metabolism typically is accompanied with increased ammonia and lactate production and increased aerobic glycolysis, and results in the hyperpolarization of the inner mitochondrial membrane (Hayes et al., 2020). As a result, queuine-hypomodification is expected to improve cell survival and immune resistance through the altered metabolism towards the Warburg metabolism, with additional resistance to apoptotic cell death. However, even though for many cancer tissues and cancer cell lines a decrease in queuine-modification could be observed, this does not mean that this phenomenon is universal for cancer, as some studies could provide data of fully queuine-modified tRNAs in neoplastic tissues from patients (Emmerich et al., 1985).

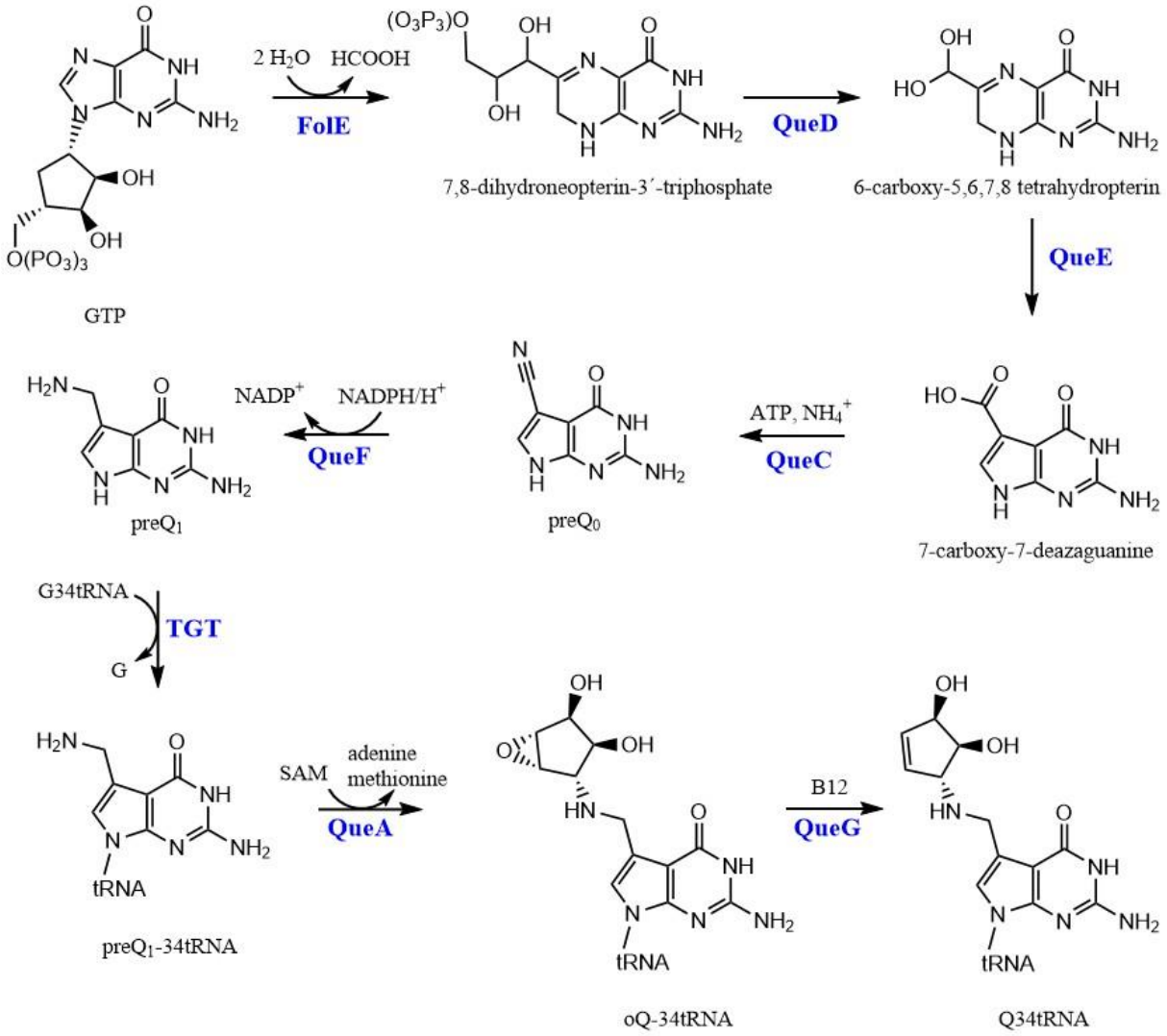

Figure 1.6: *De novo* biosynthesis of queuosine in bacteria. Q biosynthesis is exclusive to the eubacterial kingdom and incorporated at the wobble position 34 in tRNAs. Biosynthesis starts with guanosine 5´-triphosphate (GTP) and its hydrolysis followed by five sequential reactions of the enzymes FolE, QueD, QueE, QueC, and QueF. After the incorporation of $preQ_1$ into the tRNA by TGT, final modifications by QueA and QueG are established to form the mature Q34tRNA.

A more direct and also well-established impact of queuine lies within translation of proteins. In recent years, it became more evident that tRNA modifications act within a modification network. In these networks, modifications can contribute to tasks of other modifications, rather than act as stand-alone modification. As described previously, Dnmt2 mediated C38 methylation is driven by the presence of the neighbouring modification Q at position 34. Müller and colleagues showed that *S. pombe* cultures grown in standard, full medium conditions (lacking queuine) resulted in a low modification level of $tRNA^{Asp}$ (Müller et al., 2015). However, this changes upon addition of queuine which leads to the full methylation of $tRNA^{Asp}$ at position 38. Thus, Dnmt2-dependent methylation of C38 $tRNA^{Asp}$ strongly depends on the presence of Q at position 34. A few years later, this relationship between Q and m^5C38 methylation was also observed in mammalian cells, where Dnmt2-mediated $tRNA^{Asp}$ methylation drops upon queuine starvation, while the modification

level of other Dnmt2 targets remained unaffected ($tRNA^{Gly}$ and $tRNA^{Val}$) (Tuorto et al., 2018). Additionally, both modifications influence translational speed and accuracy, since the lack of m^5C38 and Q34 in $tRNA^{Asp}$ affects discrimination of cognate from near-cognate codons. This in turn results in the accumulation of Asp codons within the ribosome, the misincorporation of amino acids, and the subsequent accumulation of misfolded proteins and aggregates (Tuorto et al., 2018, 2015). These wrongly translated peptides in turn can lead to ER stress and the subsequent activation of the unfolded protein response.

1.8 QueA

The enzyme catalysing the penultimate step in Q-biosynthesis is the S-adenosylmethionine:tRNA ribosyltransferase-isomerase (QueA). QueA adds in an unprecedented reaction an epoxycyclopentandiol ring to $preQ_1$, forming epoxyQ (oQ). The epoxycyclopentandiol ring originates from the ribosyl moiety of SAM, representing the first reported example of the use of SAM as ribosyl-donor. The reaction catalysed by QueA includes the elimination of both adenine and methionine from SAM, the transfer of the ribosyl moiety to the $preQ_1$-tRNA, and the rearrangement of the transferred ribosyl group to form an epoxy carbocycle (Slany et al., 1994; Van Lanen and Iwata-Reuyl, 2003).

1.8.1 QueA structure

QueA is a rather small protein of about 38 kDa in size consisting of a small and a large subunit. The small subunit folds into a 6-stranded β-barrel, analogous to trypsin-like serine proteases (Figure 1.7). The large subunit comprises a central β-sheet built by seven β-strands that is flanked by five α-helices, resembling an αβα sandwich topology, (Grimm et al., 2006; Mathews et al., 2005). β-strands 5, 6, and 8, together with α-helix 3 form the interface between both domains, with the small domain being inserted into the large domain between strand β3 and α-helix 2. Both domains are connected via two extended loop regions of which one loop forms a straight connection between both domains and the other loop is not resolved in the electron density and is assumed to be disordered. Interestingly, this disordered loop harbours several conserved amino acids considered to be important during catalysis and QueA-tRNA complex stabilization. Comparison of *B. subtilis* and *T. maritima* QueA suggests a high domain flexibility, as the small domain is rotated around an imaginary axis (Grimm et al., 2006; Mathews et al., 2005). This

suggests a conformational rearrangement of the small domain upon substrate binding, in order to fully accommodate its cognate tRNA.

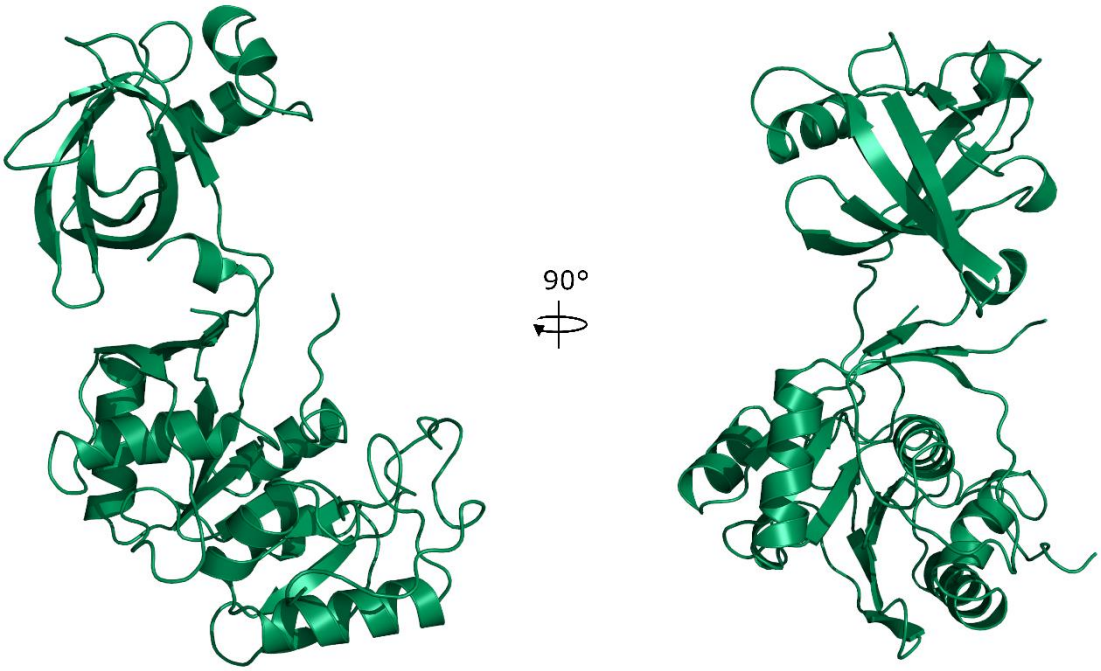

Figure 1.7: QueA crystal structure. The crystal structure of *B. subtilis* QueA is shown in cartoon mode. The domain architecture of the large and small domain is shown in two orientations (PDB ID: 1YY3).

1.8.2 Catalytic mechanism of QueA

The catalytic mechanism of QueA is still poorly understood. In general, unlike other RNA-modifying enzymes such as Dnmt2, there is no evidence of a covalent association between QueA and its tRNA substrate (Mueller and Slany, 1995; Van Lanen and Iwata-Reuyl, 2003). This is supported by sequential binding and dissociating of the ternary complex. The ordered mechanism allows the binding of preQ$_1$-tRNA first, followed by SAM, forming the ternary complex. Once catalysis is completed, ordered product release is conducted, where first adenine, then methionine, and lastly oQ-tRNA are released (Van Lanen and Iwata-Reuyl, 2003). Based on competition assays and steady-state kinetics, a hypothetical catalytic reaction mechanism was proposed for the ribosyl transfer (Figure 1.8). The reaction mechanism starts with deprotonation of SAM at the C5 atom, resulting in a sulfonium ylide, collapsing to a vinyl sulfonium. This results in ring opening of the ribose and elimination of adenine. Subsequently, the preQ$_1$ amine performs a nucleophilic attack at C4 which in turn generates a new sulfonium ylide. This newly formed sulfonium ylide in turn attacks the C1 atom of the aldehyde to generate an alkoxy carbocycle. A subsequent S_N2 attack of the alkoxy oxygen on the adjacent carbon 2 results in the formation of the epoxide and elimination of methionine, leading to the final product oQ. Substrate recognition

of QueA was shown to not require the full tRNA molecule, since interactions could be established between QueA and the anticodon stem-loop of the cognate tRNA (Slany et al., 1994).

Aside the so far gathered information about QueA catalysis, structural information about QueA in complex with SAM and its cognate tRNA would be desirable to understand this unique reaction mechanism.

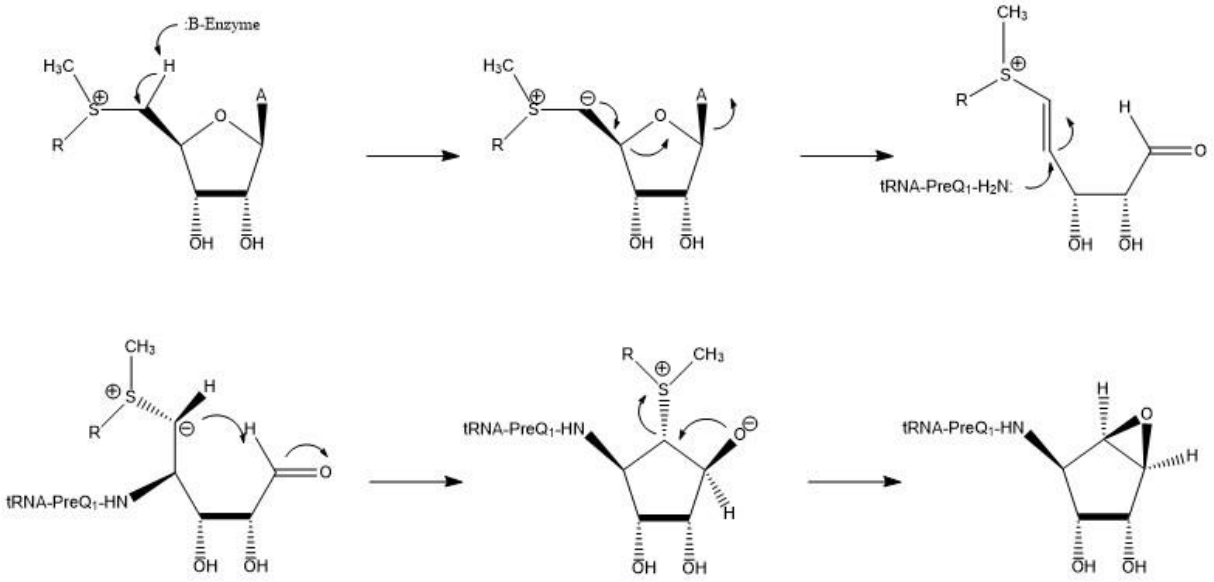

Figure 1.8: Hypothetical catalytic mechanism of QueA. The reaction mechanism starts off with the enzyme catalysed deprotonation of C5' of SAM. Followed by the ring opening and elimination of adenine. Nucleophilic attack of preQ1-tRNA at C4' of SAM results in two steps in the formation of the alkoxy carbocycle. Intramolecular S_N2 attack of the oxygen leads to the elimination of the methionine moiety and gives rise to the mature epoxy-queuosine-tRNA (adapted from Van Lanen and Iwata-Reuyl, 2003).

1.8.3 Physiological role of QueA

Even though our knowledge about queuine modification in the physiological context is increasing, little studies have been conducted on QueA. Shortly after the identification of the QueA crystal structure, Liu *et al.* (2008) reported a connection of QueA with the arginine deiminase system (ADS) in *Streptococus gordonii* (Y. Liu et al., 2008). The ADS contributes to pH homeostasis, providing ATP for growth and protects cells from lethal acidification. In this system, QueA modulates translational efficiency of ADS genes, such as ArcR (an activator of the arc operon induced by arginine). However, QueA-deficient *S. gordonii* cells showed no growth phenotype in different media. Only upon serial passage of mutant cells, a decline of mutant cells could be observed, indicating, that the lack of queuine may reduce fitness of the organism. In a broad study focussing on cell survival under UV- and X-radiation in *Escherichia coli*, QueA was one of the genes found to reduce fitness upon deletion. The authors proposed effects of the identified genes upon DNA repair (Sargentini et al., 2016).

So far, the most important impact of QueA has been reported for the Q biosynthesis of *Shigella flexneri*. Q induces the translation of the vacC gene which in turn results in reduced synthesis of VirF. VirF is a key regulator for the full development of virulence of *Shigella* (Durand et al., 1994). *Shigella* bacteria are the cause of bacillary dysentery and result in the deaths of some 600.000 infants per year, predominantly in developing countries as cause of sub-standard water supplies and hygiene (cdc.gov; Louise K. Francois Watkins and Grace D. Appiah, 2019). The upstream enzyme of QueA in Q-biosynthesis is TGT and was subject to structure-based drug design. Impairing TGT activity using designed inhibitors resulted in the termination of the Q-biosynthesis at the TGT stage, which resulted in the lack of *Shigella* virulence (Grädler, 2001). In contrast to TGT, which is part of the human queuine-cycle, QueA has no homologue in humans. This renders QueA a promising drug target to treat shigellosis.

1.9 Aim of this Thesis

During the last years, it became increasingly clear that tRNA modifications are dynamically regulated. With this high modularity, tRNA modifications act in response to environmental cues. Cross talk between modifications and their pathways contribute to the complexity of tRNA modifications. Due to the interconnectivity of tRNA modifications, studying the role and impact of single modifications is challenging. Analysis of enzymes introducing the respective modifications can help to infer their role within these modification networks. Structural analysis of protein-tRNA complexes help to elucidate the underlying mechanism of tRNA substrate recognition and enzyme catalysis. However, only few complex crystal structures are available in the literature. The aim of this thesis is to gain insight in RNA modifying enzyme substrate recognition and catalysis.

The first chapter of this thesis aims to get insights into protein:RNA interactions of the methyltransferase TrmB. So far, TrmB-SAM/SAH crystal structures are only available for *E. coli*, yeast, and humans (Leulliot et al., 2008; Q. Liu et al., 2008; Zegers et al., 2005). Therefore, *Bacillus subtilis* TrmB is co-crystallized with SAM and SAH to gain insights into *B. subtilis* TrmB enzyme activity. Furthermore, structural data obtained from small-angle x-ray scattering, mass-spectrometry of cross-linked complexes, and molecular docking approaches led to the determination of a TrmB-tRNA^{Phe} complex structure. Lastly, TrmB enzyme activity is studied to gain insights into the impact of homodimerization of TrmB.

The second chapter focuses on the m^{5}C methyltransferase Dnmt2. Since the discovery of the dual specificity of Dnmt2 on DNA and tRNA in 2006, several new tRNA substrates were identified (Goll et al., 2006; Schaefer et al., 2010). The knowledge, that queuine-modified tRNAs enhances Dnmt2-mediated C38 methylation, raised the question, whether other queuine-modified tRNAs are also

subject to Dnmt2 modification. Of the four queuine-modified tRNAs, only two contain at position 38 a cytosine, of which $tRNA^{Asp}$ is the commonly known Dnmt2 target. The remaining tRNA codes for $tRNA^{His}$. Therefore, the capability of human Dnmt2 to bind and modify human $tRNA^{His}$ is analysed, in both queuine-modified and unmodified states. These experiments will help to gain more insights into Dnmt2 substrate specificity.

Lastly, the third chapter focusses on QueA which is one of the least understood enzymes within the Q-biosynthesis pathway. It is identified as the enzyme catalysing the penultimate step of the Q-biosynthesis (Slany et al., 1994; Van Lanen and Iwata-Reuyl, 2003). QueA uses SAM as ribosyl donor to attach the ribosyl moiety to the $preQ_1$ base and rearranges it to an epoxycyclopentane ring. This is the first mechanism reported so far, for the use of the ribose moiety of SAM. However, little is known about the catalytic mechanism and structural recognition of QueA and its tRNA substrate. Therefore, QueA has been crystallized to gain more insights into enzyme activity and substrate binding. To infer the location of the putative active site pocket, a full length QueA model is generated, by modelling unresolved loop regions not refined in the electron. With the resulting model, molecular docking was performed to gain insight into QueA-tRNA binding.

This manuscript was submitted to the Journal for RNA Biology

Chapter 2 tRNA complex structure of the M7G46 Methyltransferase TrmB

Blersch Katharina F.[1], Burchert Jan-Philipp[2], August Sophie C.[2], Welp Luisa[3], Neumann Piotr[1], Köster Sarah[2], Urlaub Henning[3,4], Ficner Ralf[1*]

[1] Department of Molecular Structural Biology, Institute of Microbiology and Genetics, GZMB, Georg August University Göttingen, Justus-von-Liebig Weg 11, 37077 Göttingen, Germany

[2] Institute for X-Ray Physics, Georg August University Göttingen, Friedrich-Hund-Platz 1, 37077, Göttingen, Germany

[3] Bioanalytical Mass Spectrometry Research Group, Max Planck Institute for Biophysical Chemistry, Am Faßberg 11, 37077, Göttingen, Germany

[4] Bioanalytics Group, Institute for Clinical Chemistry, University Medical Center Göttingen, 37075 Göttingen, Germany

* To whom correspondence should be addressed: Ralf Ficner, Department of Molecular Structural Biology, Institute for Microbiology and Genetics, Georg-August-University Göttingen, 37077 Göttingen, Germany; rficner@uni-goettingen.de

Abstract

TrmB belongs to the class I S-adenosylmethionine (SAM)-dependent methyltransferases (MTases) and introduces a methyl group to guanine at position 7 (m^7G) in tRNA. In tRNAs m^7G is most frequently found at position 46 in the variable loop and forms a tertiary base pair with C13 and U22, introducing a positive charge at G46. The TrmB/Trm8 enzyme family is structurally diverse, as TrmB proteins exist in a monomeric, homodimeric, and heterodimeric form. So far, the exact enzymatic mechanism, as well as the tRNA-TrmB crystal structure is not known. Here we present the first crystal structures of *B. subtilis* TrmB in complex with SAM and SAH. The crystal structures of TrmB apo and in complex with SAM and SAH have been determined by X-ray crystallography to 1.9 Å (apo), 2.5 Å (SAM), and 3.1 Å (SAH). The obtained crystal structures revealed Tyr193 to be important during SAM binding and MTase activity. Applying fluorescence polarization, the dissociation constant K_d of TrmB and $tRNA^{Phe}$ was determined to be 0.12 µM ± 0.002 µM. Luminescence based methyltransferase activity assays revealed cooperative effects during TrmB catalysis with a half-of-the sites reactivity at physiological SAM concentrations. Structural data retrieved from small-angle x-ray scattering (SAXS), mass-spectrometry of cross-linked complexes, and molecular docking experiments led to the determination of the TrmB-$tRNA^{Phe}$ complex structure.

Keywords: tRNA modification, 7-methylguanosine, m7G, TrmB, Trm8

2.1 Introduction

Ribonucleic acids (RNA) are subject to a vast number of post-transcriptional modifications. Currently, about 172 post-transcriptional RNA modifications are known, introducing an enormous diversity to the basic four RNA nucleotides adenine (A), thymine (T), cytosine (C), and guanine (G) (Boccaletto et al., 2018). Over 90 of these modifications are found in transfer RNAs (tRNA) across all three kingdoms of life, rendering them highly versatile molecules (see http://mods.rna.albany). Of all modifications, methylation is the most abundant one. Methylation of the guanine base at position 7 (m^7G) is a highly conserved modification and common to eubacteria, eukaryotes, and a few archaea (Juhling et al., 2009). m^7G occurs not only in tRNA (Boccaletto et al., 2018; Machnicka et al., 2012), but also in other RNA species such as messenger RNA (mRNAs) as the 5´-cap, ribosomal RNA (rRNA), small nuclear RNA (snRNA), and small nucleolar RNA (snoRNA) (Okamoto et al., 2007; Wang et al., 2012). In tRNAs, m^7G is frequently found at position 46 in the variable loop and forms a tertiary base pair with C13 and G22 leading to the stabilization of the tRNA core. The formation of the tertiary base pair in turn introduces a positive charge at the N7 of the guanine base (Agris et al., 1986; Hoburg et al., 1979; Quigley and

Rich, 1976). The enzyme introducing the m^7G modification in tRNA is the tRNA(guanine-N7-)-Methyltransferase (MTase), also denoted as TrmB or Trm8 (TRMT8, EC 2.1.1.33) (Boccaletto et al., 2018; Machnicka et al., 2012). The TrmB/Trm8 protein family belongs to the SAM-dependent MTases and is structurally diverse, ranging from monomeric or homodimeric to heterodimeric functional assemblies, e.g. the heterodimeric yeast Trm8-Trm82 (Leulliot et al., 2008; Liu et al., 2008; Zegers et al., 2005).

Crystallographic studies of eubacterial and eukaryotic tRNA(guanine-N7-)-MTases revealed a class I MTase fold (Dong et al., 2008; Leulliot et al., 2008; Martin and McMillan, 2002; Schubert et al., 2003; Zegers et al., 2005; Zhou et al., 2009), hence these enzymes belong to the Rossmann-like fold (RFM) MTase superfamily (Ahn, 2003; Zegers et al., 2005). The Rossmann-fold consists of six β-strands forming the central β-sheet flanked by α-helices, giving rise to a doubly wound αβα sandwich. The central β-sheet harbours a switch-point introduced by an antiparallel β-strand, forming the S-Adenosylmethionine (SAM) binding pocket. However, the tRNA(guanine-N7-) MTases, also called TrmB/Trm8, differ from the canonical Rossmann-fold by an additional β-strand inserted between β-strands 5 and 6 (Bujnicki, 1991; Zegers et al., 2005).

The lack of TrmB/Trm8 - tRNA complex crystal structures renders biochemical characterization of this enzyme family extremely valuable, in particular concerning the protein-RNA interaction. Mutagenesis studies on the *Aquifex aeolicus* TrmB (*Aa*TrmB) showed that replacing the highly conserved Asp133 by alanine or asparagine abolishes MTase activity completely (Tomikawa et al., 2018). Furthermore, *Aa*TrmB recognizes its cognate tRNA via the T-stem with the tertiary base pair in the tRNA core being not essential for methylation (Okamoto et al., 2004). In agreement with biochemical characterisation of *Aa*TrmB, mutation of the *Escherichia coli* TrmB (*Ec*TrmB) Arg180 to alanine (in *Aa*TrmB Asp133) reduced MTase activity by 90% (Purta et al., 2005). Additionally, single mutations of Arg26, Asp144, His151, Arg154, Arg155, Thr217, and Glu220 to alanine either caused at least 10-fold reduction of MTase activity, or in case of Asp144, Arg154, and Arg155, abolished it completely. In the yeast homolog Trm8, Asp220, which corresponds to the *A. aeolicus* and *E. coli* Asp133 and Arg180, respectively, adopts the same side chain orientation and position within the TrmB structure. This led to the conclusion that *Aa*TrmB Asp133 forms the catalytic centre of the TrmB/Trm8 enzyme family (Tomikawa et al., 2018). The proposed reaction mechanism includes the capture of the N-H of the guanine base by the carboxyl group of Asp133 (nomenclature according to *Aa*TrmB), and the subsequent nucleophilic attack of the methyl group of SAM by the N7 atom of the guanine base.

The physiological role of m^7G46 has been subject to recent studies. The m^7G46 modification is located in the tRNA core. The influence of the modification on other cellular processes depends on the position of the modification. In general, modifications in the tRNA body mostly enhance

RNA processing and stability, whereas modifications within the anticodon can influence translational accuracy and stress response. Hence, the lack of modifications outside the anticodon rarely lead to phenotypic defects as for *TrmB* gene disruption in *E. coli* (De Bie et al., 2003). Interestingly, deletion of the yeast homolog Trm8/Trm82 either as single mutant or double mutant coupled to other genes leads to phenotypic defects (Alexandrov, 2005). Alexandrov *et al.* described a conditional temperature sensitivity on basis of a physiological function for the m^7G modification in tRNA. *Thermus thermophilus* TrmB knockout mutants showed severe growth defects in high temperatures and hypo-modification of m^1G37 leading to the specific degradation of $tRNA^{Phe}$ and $tRNA^{Ile}$. Additionally, the authors could show that m^7G46 has a positive effect on other modifications indicating the existence of a complex modification network (Tomikawa et al., 2010). Furthermore, mutations of the human TrmB homolog METTL1 are linked to genetic diseases. In humans, WDR4 gene mutation abolishes the m^7G46 modification in tRNA and causes microcephalic primordial dwarfism (Shaheen et al., 2015). These studies show the complexity and importance of m^7G46 modification of tRNAs.

In this study, we present the crystal structures of *Bacillus subtilis* TrmB (*bs*TrmB) in complex with its substrate SAM, the post-catalytic product SAH as well as an unliganded state. We show that under near physiological SAM concentrations, the TrmB homodimer methylates tRNA in a negative cooperative manner and shows a half-of-the sites reactivity. Furthermore, using protein-RNA cross-linking, we could map the RNA interaction sites on TrmB and propose a cross-link based three-dimensional model of TrmB-$tRNA^{Phe}$ complex, which has been verified by SAXS measurements.

2.2 Material and Methods

2.2.1 Cloning of *bs*TrmB

Bacillus subtilis TrmB (*bs*TrmB) was amplified from genomic *B. subtilis* DNA introducing BamHI and PstI restriction sites at the 5´ and 3´position, respectively (forward primer: BamHI- CG GGATCC atgagaatgcgccacaagcc, reverse primer: AA CTGCAG ttacgttctccattcaacctcagc- PstI). *bs*TrmB was cloned in the expression vector pQE80 introducing a N-terminal 6x His-tag. The Y193A mutant was obtained by site directed mutagenesis and both, the wild type and mutant genes verified by sequencing.

2.2.2 Protein expression and purification

Wild type and mutant His_6-*bs*TrmB fusion proteins were expressed in *Escherichia coli* BL21(DE3) cells and cultivated in 2YT medium containing 100 µg/ml Ampicillin. The expression cultures

were grown at 37°C until the optical density (OD_{600}) reached 0.5 and protein expression was induced by the addition of 1 mM Isopropy β-$_D$-1-thiogalactopyranoside (IPTG). After 4h at 37°C cells were harvested, frozen in liquid nitrogen, and stored at -20°C until further use.

Frozen cells were thawed in Lysis buffer (50 mM Tris/HCl pH 8.5, 500 mM KCl) and disrupted by micro fluidization for 7 cycles at 90 psi (M-110S Microfluidics). The soluble protein was collected by centrifugation for 30 min at 50000 g, 4°C, and filtered through a 0.45 µm syringe filter. The lysate was applied to a His-Talon FPLC affinity column (Protino Ni-NTA MN) equilibrated against Lysis buffer. Nucleic acids were removed from the protein bound to the resin (lysis buffer + 1M $LiCl_2$) and the fusion protein was eluted with 50 mM Tris/HCl pH 8.5, 50 mM $MgCl_2$, 300 mM KCl, 500 mM imidazole. Further purification was achieved by Superdex S200 size exclusion chromatography (50 mM Tris/HCl pH 8.5, 50 mM $MgCl_2$, 300 mM KCl). Purified *bs*TrmB was concentrated to 6-9 mg/ml and stored at -80°C until further use.

2.2.3 In vitro transcription and RNA purification

Bacillus subtilis $tRNA^{Phe}$ (*bs*$tRNA^{Phe}$) was transcribed from a linearized vector in a run-off *in vitro* transcription containing T7 Polymerase, 10 mM rNTPs each, 1x HT buffer (30 mM HEPES pH 8.0, 25 mM $MgCl_2$, 10 mM DTT, 2 mM spermidine, 0.01% Triton X-100). The reaction was incubated for 3 h at 37°C, PP_i was pelleted and the reaction terminated by the addition of 50 mM EDTA. Self-cleavage of the ribozyme GlmS was induced upon glucosamine-6-phosphate (GlmN6P) addition and further incubated for 1 h at 37°C. *bs*$tRNA^{Phe}$ was purified by ion exchange chromatography (1 ml Resource-Q GE). The *in vitro* transcription reaction was applied to the resin with IEX-A buffer (20 mM HEPES pH 7.5, 20 mM KCl) and eluted with a linear gradient from 10-35% IEX-B buffer (20 mM HEPES pH 7.5, 2 M KCl). Fractions containing pure tRNA were pooled, ethanol precipitated, and subsequently dissolved in ddH_2O. tRNA was stored at -20°C until further use.

2.2.4 tRNA labelling and binding assays

tRNA was labelled with fluorescein-5-thiosemicarbazide (Sigma Aldrich) according to Johannsson *et al.* 2018 (Johannsson et al., 2018). Unreacted fluorophore was removed using Zeba Spin desalting columns (Thermofisher Scientific). *bs*TrmB was stepwise diluted in assay buffer from 0.007 to 2.1 µM (20 mM Tris/HCl pH 8.0, 200 mM KCl). Anisotropy was measured using a multimode microplate reader (PerkinElmer) and plotted with R (R Core Team, 2017).

2.2.5 Methyltransferase assay

*bs*TrmB kinetics were analysed with the MTase-Glo methyltransferase assay (Promega). The assay was performed according to the manufacturer's recommendations. 0.1 µM TrmB were mixed with 0 to 61 µM $tRNA^{Phe}$, 40 µM, 10 µM, and 1 µM SAM and incubated for 30 min at RT. The

reaction was stopped adding 0.5 % TFA. After the addition of the MTase-Glo reaction solution and MTase-Glo detection solution, luminescence was measured using a multimode microplate reader (PerkinElmer). The data was transformed to display the consumed SAM molecule using a SAH standard curve. Data were plotted with R (R Core Team, 2017) and fitted with the Hill equation $v = V_{max} * x^n / (k^n + x^n)$.

2.2.6 Crystallization

*bs*TrmB was crystallized using sitting drop vapour diffusion. 1 µL 2 mg/ml TrmB supplemented with 20-fold molar excess SAM (Sigma Aldrich) was mixed with 1 µl crystallization buffer (20% PEG 4000, 20% Glycerol, 0.06 M KAc pH 5.0, 0.08 M Ammonium sulphate, 0.01 M Trimethylamine hydrochloride). Crystals grew over night at 293 K. Soaking experiments were performed with 20-fold molar excess SAH (Sigma Aldrich). These crystals were harvested using loops and flash cooled and subsequently stored in liquid nitrogen. *bs*TrmB apo was crystallized via sitting drop vapour diffusion at 293K. 1 µl 2 mg/ml TrmB was mixed with 1 µl crystallization buffer from the commercially available MIDAS MD1-59 screen (Molecular Dimensions). Crystals grown in 0.2 M NaCl, 0.1 M MES pH 6.0, 15% *v*/*v* Pentaerythritol propoxylate (5/4PO/OH) were cryo protected by adding glycerol to a final concentration of 23%, flash frozen in liquid nitrogen, and stored at 77 K.

2.2.7 Diffraction data collection, molecular replacement and refinement

X-ray diffraction data were collected at PETRA III P13 beamline (EMBL, DESY, Hamburg, (Cianci et al., 2017)) and at MX-14.1 (BESSY, Berlin). Diffraction images were indexed, integrated and scaled using the XDS-package (Kabsch, 2010). The TrmB complex structures were solved using molecular replacement by PHASER (McCoy et al., 2007) implemented in the CCP4 suite (Winn et al., 2011) and *bs*TrmB apo structure used as model (PDB ID: 2FCA). Structure refinement was done by iterative steps using Refmac implemented in the CCP4 suite (Murshudov et al., 2011) and subsequent manual adjustments in Coot (Emsley et al., 2010). Ligand omit maps were calculated using the Phenix package (Adams et al., 2010). Figures were prepared with *PyMOL* (v.2.2, Schrödinger, LLC, 2015).

2.2.8 Protein-RNA cross-linking and LC-MS/MS analysis and data analysis

For UV cross-linking, the complex was irradiated at 254 nm for 10 min on ice using an in-house built cross-linking apparatus as described (Kramer et al., 2014). For chemical cross-linking, DEB or NM were added to a final concentration of 50 mM and 1 mM, respectively. The cross-linking reaction was performed for 30 min at 37°C. Cross-linked samples were ethanol-precipitated and further processed as described in (Kramer et al., 2014). Briefly, 10 µg RNase A (EN0531, Thermo Fisher Scientific), 1kU RNase T1 (EN0531, Thermo Fisher Scientific) and 250 U PierceTM

universal nuclease (88700, Thermo Fisher Scientific) were used for tRNA digestion followed by protein hydrolysis using trypsin (sequencing grade, Promega) at a 1:20 mass ratio. Sample clean-up was performed using C18 columns (74-4601, Harvard Apparatus) and cross-linked peptides were enriched with in-house packed TiO_2 columns (Titansphere 5 µm; GL Sciences, Japan). Peptides were dried and subjected to MS measurement.

Sample pellets from TiO_2 enrichment were dissolved in 2% *[v/v]* acetonitrile, 0.05% *[v/v]* TFA. LC-MS/MS analyses were performed on a Q Exactive HF-X (Thermo Fisher Scientific) instrument coupled to a nanoflow liquid chromatography system (1100 series, Agilent Technologies). Sample separation was performed with a flow rate of 300 nl/min using a linear gradient and a buffer system consisting of 0.1% *[v/v]* formic acid (buffer A) and 80% *[v/v]* acetonitrile, 0.08% *[v/v]* formic acid (buffer B). Peptides were separated over 58 min. Eluting heteroconjugates were analysed in positive mode using a data-dependent top 15 acquisition method. MS1 and MS2 resolution were set to 120,000 and 30,000 FWHM, respectively. AGC targets were set to 10^6 and $5x10^5$, normalized collision energy (NCE) to 28, dynamic exclusion to 21 s, and max. injection time to 104 ms (for both MS1 and MS2). MS data were analysed and manually validated using the OpenMS pipeline RNPxl and OpenMS TOPPASViewer https://www.ncbi.nlm.nih.gov/pmc/articles/PMC5995894/ - CR35 (Kramer et al., 2014).

2.2.8.1 SAXS measurements on the TrmB Complex

The scattering signal of TrmB, tRNA and the TrmB-tRNA^{Phe} complex was measured with an in-house small-angle x-ray scattering (SAXS) setup (Xeuss 2.0, Xenocs, Sassenage, France): A Cu K_α source (Genix 3D, Xenocs, Sassenage, France) generated x-rays with a wavelength of 1.54 Å, at 50 kV and 600 µA. The resulting beam was reduced to a size of approximately 0.5 x 0.5 μm^2 with multilayer optics and scatterless slits. Proteins, dissolved in buffer solutions, were measured in quartz glass capillaries with a nominal inner diameter of 1.48 mm and a wall thickness of 10 µm (Art. no. 4017515, Hilgenberg GmbH, Mansfeld, Germany). During the measurements the capillaries were sealed with wax to avoid evaporation. A Pilatus3R 1M pixel detector (Dectris Ltd., Baden, Switzerland) with 981 x 1043 px^2 and a pixel size of 172 x 172 μm^2 recorded the scattering images at a sample-to-detector distance of 575 mm. To avoid air scattering, most of the beam path was kept at low pressure (p < 0.56 mbar).

For each protein sample, the same capillary was first used for an empty measurement, filled with ultrapure water for a calibration measurement, then refilled with buffer for a background measurement and finally refilled with the protein in buffer. In each case, a transmission measurement with an exposure time of 0.1 s was performed. The scattering signal of buffers and proteins with exposure times ranging from 12 to 25 hours per capillary were recorded and

divided into 30 min intervals. During these measurements a 3 mm beam stop blocked the primary beam. The scattering signal of both TrmB and the TrmB-tRNA complex was measured at 3 protein concentrations each (3 mg/ml, 2 mg/ml, and 1 mg/ml) to ensure that no form factor influenced the measurement (Figure S2.1). The final concentration of 3 mg/ml was measured 3 times for TrmB (20 mM Tris, pH 8.5, 500 mM KCl and 10 mM MgCl), the TrmB-tRNA complex (20 mM HEPES, pH 7.4, and 50 mM KCl) and tRNA (20 mM HEPES, pH 7.4, and 50 mM KCl).

The scattering data were processed with self-written Matlab (Matlab 9.3, 2017, The MathWorks, Natick, MA, USA) scripts, based on the PSI cSAXS matlab package (www.psi.ch/en/sls/csaxs/software). Multiple scattering images were summed up, masked to exclude contributions of beam stop and detector grid, and azimuthally averaged. The resulting radial intensity profiles were functions of the absolute value of the scattering vector q:

$$q = \frac{4\,\Pi}{\lambda}\sin(\Theta),$$

where λ is the wavelength of the x-rays and Θ is half the scattering angle. The radial intensity profiles were corrected by their total exposure time and their transmission factor. Here, the transmission factor was the ratio of the summed intensities of a transmission measurement and the primary beam intensity in a 35 x 35 px^2 window around the beam centre. The scattering signal was background corrected by subtracting the radial intensity profile of the buffer from the one of the proteins in buffer. Further, it was divided by the protein concentration and the inner diameter of the capillary to be able to compare intensity profiles from capillaries with different inner diameters and with different protein concentrations. The inner diameters of the capillaries were determined with the transmission measurements of the empty and water filled capillaries as well as the density ρ = 1 g/cm^3 and the mass attenuation coefficient (μ/ρ) = 10.4 g/cm^2 of water (www.nist.gov/pml/x-ray-mass-attenuation-coefficients). Finally, an average radial intensity profile was calculated from all available profiles for every protein by using a point wise weighted average.

To further analyse the average radial intensity profiles and assuming a globular shape of the scattering proteins, Guinier analysis was performed to obtain the radius of gyration. For this purpose, the software PRIMUS (Konarev et al., 2003) (ATSAS, EMBL, Hamburg, Germany) was used and a q range of $0.21 < q < 0.41$ nm^{-1} was considered for TrmB, $0.27 < q < 0.51$ nm^{-1} for tRNA and $0.12 < q < 0.24$ nm^{-1} for the complex.

2.2.9 RNA-protein molecular docking

2.2.9.1 Preparation of protein and tRNA model

The homodimeric model of apo/holo *bs*TrmB was prepared based on the reported crystal structure by removing all non-protein atoms from the atomic model and used for *in silico* docking experiments. Atomic coordinates of the tRNA model were extracted from the crystal structure of yeast phenylalanine tRNA (PDB id: 1EHZ) and converted to a format suitable for Rosetta. All modified bases were replaced by unmodified ones, the sequence has been adjusted to match *bs*tRNA^{Phe} and the resulting model was idealized using ERRASER (Chou et al., 2013).

2.2.9.2 Protein-RNA docking combined with SAXS and cross-link based validation

Initially, the *bs*tRNA^{Phe} model was manually docked with the G46 positioned close to the active site of *bs*TrmB using spatial restrains obtained from the cross-linking experiment. However, SAXS based validation of the symmetric protein-tRNA complex, comprising two *bs*tRNA^{Phe} molecules bound in the same manner by the homodimeric *bs*TrmB, indicated not a perfect fit. This was most likely a consequence of not optimal orientation of the docked partners as well as different conformations (bending) of the tRNA molecule. Hence, two models of bend *bs*tRNA^{Phe} were prepared in Coot (Emsley et al., 2010) utilising local distance restraints (ProSMART) (Nicholls et al., 2012) in order to perform *in silico* docking, and subsequently verified by both, SAXS and cross-link experimental data.

Docking was performed with the RosettaDock application (Chaudhury et al., 2011) optimized for predicting RNA-Protein complexes (Guilhot-Gaudeffroy et al., 2014). Docking was divided into two stages: low resolution global docking and high resolution refinement of selected decoys. The former stage uses a coarse-grained representation of docking partners and facilitates quick sampling of the available search space. In order to thoroughly sample the search space, 100.000 poses have been generated for each tRNA model. Favourable low resolution (initial) docking orientations were identified as follows. First, a point in space was selected which is located in the active site of *bs*TrmB. This point corresponds to the position of the SD atom of SAM bound in the here reported *bs*TrmB structure and is located between Phe71, Trp120, and Phe197 residues which have been identified by UV cross-link experiment. Then, the distance criterion of maximum 8 Å, calculated between that point and the phosphate atom of G46, was applied to select decoys with G46 positioned in vicinity of the active site. The best 100 decoys for each of two tRNA models were selected based on the *I_sc* score (representing the energy of the interactions across the interface) and the total Rosetta score. These models have been subjected to the high resolution (second) docking step which performed rebuilding of all-atom models followed by model optimization (1000 decoys per low resolution model). The resulting decoys were first sorted by

I_sc score and the most favourable 100 models have been validated based on crosslinking data and subsequently by calculating the fit to the SAXS curve. The latter step required generation of symmetrical dimeric *bs*TrmB – *bs*tRNA^{Phe} complexes. Modelling of the flipped G46 nucleotide was performed in Coot.

2.3 Results

2.3.1 Affinity of in vitro tRNA^{Phe} to TrmB

To date, the binding affinity of TrmB enzymes to their cognate tRNAs were measured by studying methylation kinetics via the Michaelis-Menten equation and taking the K_m value as binding constant. Here, we directly measured the dissociation constant using quantitative binding analysis via fluorescently labelled, *in vitro* transcribed, unmodified tRNA^{Phe} of *Bacillus subtilis*. TrmB binds tRNA^{Phe} with a K_d of 0.12 µM ± 0.002 µM (Figure 2.1).

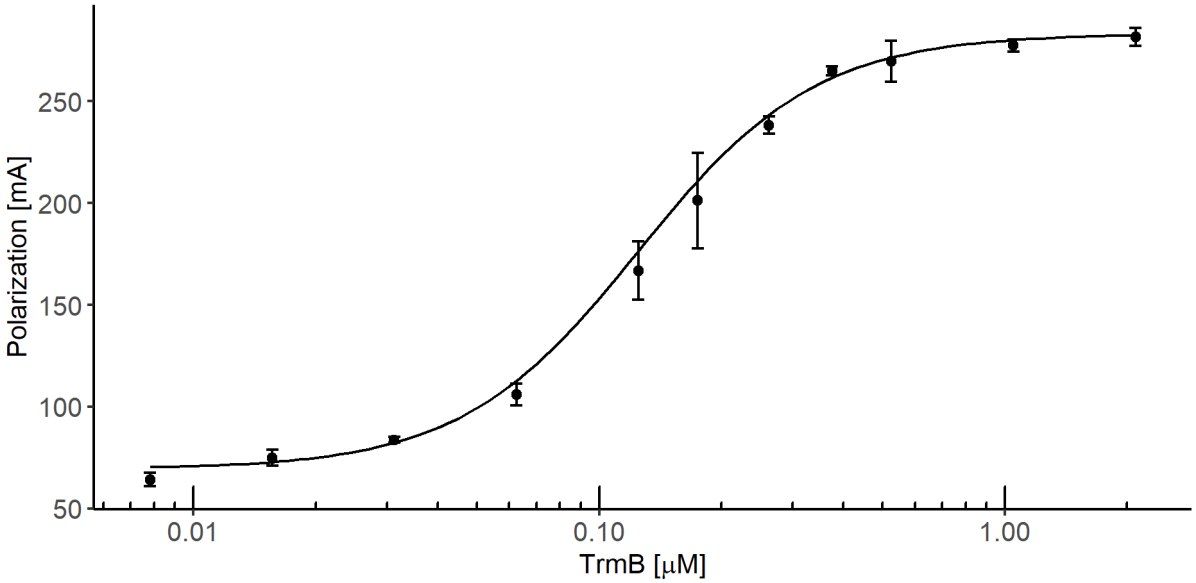

Figure 2.1: tRNA complex structure of the M7G46 Methyltransferase TrmB: Quantitative analysis of wt *bs*TrmB-tRNA^{Phe} complex formation measured by fluorescence polarization. The fluorescently labelled tRNA^{Phe} was analysed within increasing *bs*TrmB concentration, in the range of 0.007 to 2.1 µM. Complex formation was observed with fluorescence polarisation. Measurements were performed in three indepentend experimental replicates. Results are shown as Mean ± SD with error bars of SD (n=3). tRNA^{Phe} binds to TrmB in the nanomolar range of 0.12 µM ± 0.002 µM. Data were plotted with R (R Core Team, 2017).

2.3.2 TrmB half-of-the-sites reactivity under near physiological conditions

We further tested TrmB MTase activity using the MTase-Glo™ Methyltransferase Assay (Promega). The MTase assay was performed under MTase-Glo™ standard conditions using 40 µM SAM. The obtained data were described best using the Hill-equation, which provides further information about cooperativity during catalysis by the Hill coefficient *n*. In general, a Hill

coefficient of $n < 1$ describes negative cooperative effects during catalysis, $n > 1$ positive cooperative effects, and $n = 1$ independent binding (Barcroft and Hill, 1910; Weiss, 1997). TrmB methylated tRNA^{Phe} with a V_{max} of 1.7 nM/s ± 0.09 nM/s, a K_m of 4.8 µM ± 0.8 µM, and a Hill coefficient of $n = 0.8$, indicating mild negative cooperative effects during catalysis (Figure 2.2). The observed K_m value for *bs*TrmB is in the range of the previously reported K_m values of 0.7 µM for *Aa*TrmB to yeast tRNA^{Phe} and 6 µM for *Ec*TrmB to tRNA^{Phe} (Purta et al., 2005; Tomikawa et al., 2018). To further assess the degree of negative cooperativity during TrmB catalysis, additional MTase assays, using *in vitro* tRNA^{Phe} with SAM concentrations of 10 µM and 1 µM, were performed and results were summarized in Table 2.1. Comparison of the Hill coefficient of all three samples shows a shift of mild negative cooperativity at 40 µM ($n = 0.8 \pm 0.09$) to a strong negative effect of $n = 0.4 \pm 0.07$ for 10 µM and $n = 0.6 \pm 0.1$ for 1 µM SAM (Figure 2.2).

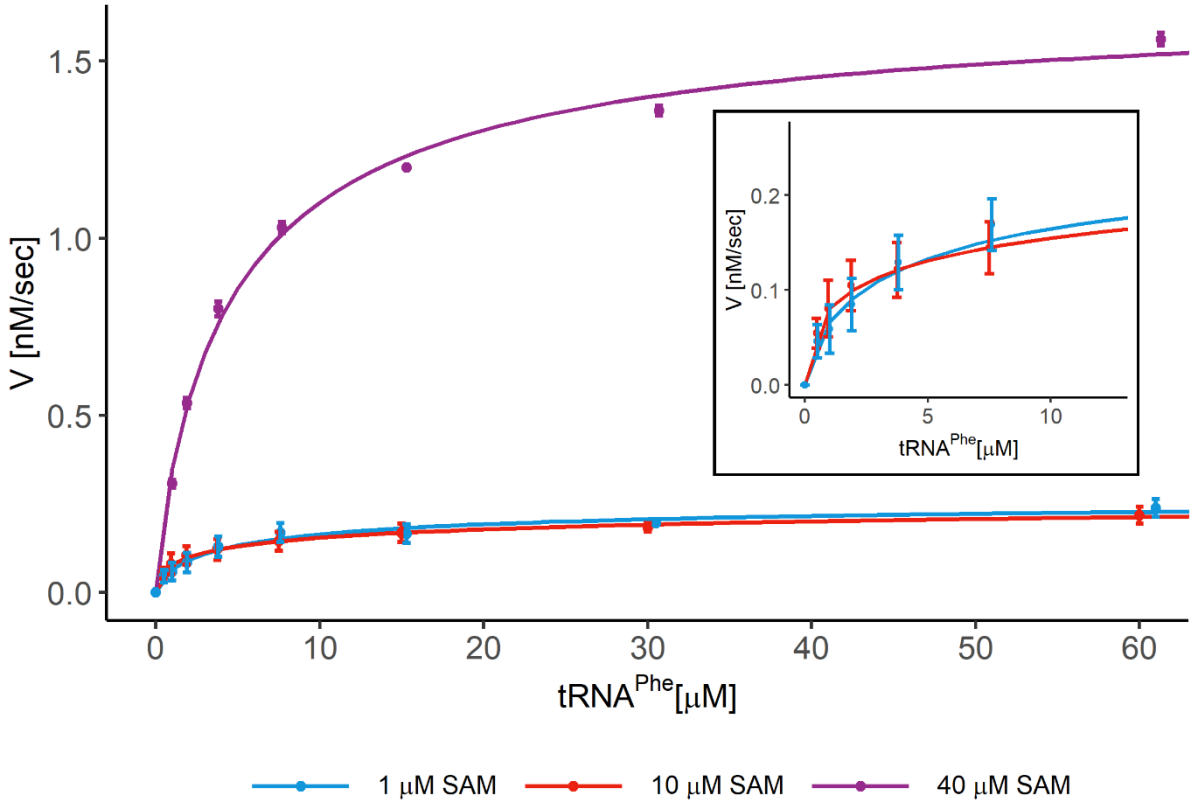

Figure 2.2: Methyltransferase assay of wt *bs*TrmB with varying SAM concentrations to analyse cooperativity. Methyltransferase assay was performed according to the Promega MTase-Glo assay and measured via luminescence. Cooperativity of the TrmB subunits was tested with increasing concentrations of SAM in the range of 1 to 40 µM (1 µM SAM in blue, 10 µM SAM in red, and 40 µM in lilac). The colour code is identical between main plot and inset. Measurements were performed as independent duplicates with increasing substrate concentrations from 0 to 60 µM tRNA^{Phe}. Data were plotted using R (R Core Team, 2017) and fitted with the Hill equation, errors are presented as standard deviation. TrmB methylated tRNA^{Phe} with a V_{max} of 1.7 nM/s ± 0.09 nM/s, a K_m of 4.8 µM ± 0.8 µM, and a Hill coefficient of n = 0.8. Lowering SAM concentrations led to a decrease in the Hill coefficient from n = 0.8 (40 µM SAM) to n = 0.4 (10 µM SAM) and n = 0.5 (1 µM SAM).

Additionally, the Hill coefficient also describes how many active sites within a macromolecule are catalytically active. A Hill coefficient of 0.5 for the homodimeric TrmB suggests that only one of two active sites is active. This leads to the hypothesis that the *bs*TrmB shows a half-of-the-sites reactivity at low SAM concentrations, with only one subunit being catalytically active at any given time.

Table 2.1: Kinetic parameters of wt *bs*TrmB using SAM concentrations from 1 to 40µM

SAM	40 µM	10 µM	1 µM
V_{max} [nM/s]	1.7 ± 0.09	0.3 ± 0.04	0.3 ± 0.04
K_m [µM]	4.8 ± 0.8	8.8 ± 6.2	5.2 ± 2.8
n	0.8 ± 0.09	0.5 ± 0.07	0.7 ± 0.2
K_{cat} x 10^3 [s^{-1}]	8.5 ± 0.45	1.5 ± 0.2	1.3 ± 0.2

2.3.3 Crystal structure of bsTrmB

To get insight into the catalytic mechanism of *B. subtilis* TrmB, we solved *bs*TrmB crystal structures of the apo state, bound with the catalytic methyl group donor SAM, and in complex with the post-catalytic ligand S-adenosyl-L-homocystein (SAH). All structures were solved by molecular replacement and determined to 1.98 Å, 2.5 Å, and 3.1 Å resolution for the apo, SAM-, and SAH complex, respectively (Figure 2.3). The details of data collection and structure refinement statistics are summarized in Table 2.2. The N-terminal regions (up to 11 residues) in all structures were not visible in the electron density and thus could not be modelled. Apparent high flexibility of this region is consistent with the prediction of the N-terminal residues 1-10 to be disordered. The determined crystal structures adopt a classic class I RFM MTase fold consisting of 7 β-strands building the central β-sheet flanked by two side layers of 6 α-helices forming an αβα sandwich (Figure 2.3A), confirming data of the apo *bs*TrmB structure (Zegers et al., 2005). Superposition of both monomers of the homodimeric apo *bs*TrmB, TrmB-SAM (Figure 2.3B), and TrmB-SAH structures revealed, that they are structurally identical (root mean square deviation between all Cα atoms of 0.119 Å (apo), 0.146 Å (SAM), and 0.181 Å (SAH)). The solvent accessible area of the dimer interface sums up 779.2 $Å^2$ indicating existence of a stable homodimer in solution. The dimer interface is formed by 22 residues constructing a hydrophobic interface with a Δ´G of -6.3 kcal/mol, as assessed by PISA (Krissinel and Henrick, 2007).

Table 2.2: Crystallographic Data Collection and Refinement Statistics

	bsTrmB-SAM	**bsTrmB-SAH**	**bsTrmB apo**
Crystallographic data			
Beamline	Petra III, P13	BESSY, 14.1	Petra III, P13
Wavelength (Å)	0.9763	0.9184	0.9763
Resolution range (Å)	44.55 - 2.5 (3.17-2.5)	44.37 - 3.1 (3.35-3.1)	44.53 - 1.98 (2.0 - 1.98)
Unique reflections	16092	9049	96395
Redundancy	10.55 (10.6)	7.8 (7.6)	3.8 (3.8)
Completeness (%)	99.9 (99.9)	99.9 (99.87)	91.5 (89.9)
Space group	H3	H3	P1
a, b, c (Å)	178.19, 178.19, 37.01	177.48, 177.48, 42.44	42.62, 103.68, 103.69
α, β, γ (deg)	90, 90, 120	90, 90, 120	118.12, 97.91, 97.84
R_{meas} (%)	11.3 (56.4)	31.8 (152.4)	8.3 (155.7)
I/σ (I)	13.31 (4.61)	7.2 (1.43)	12.47 (1.5)
$CC_{1/2}$	99.9 (96.1)	98.5 (62.2)	99.7 (54.8)
Wilson B ($Å^2$)	61.1	98.5	35.2
Refinement statistics			
R_{work}/R_{free}	0.21/0.25	0.18/0.27	0.19/0.22
Clash score	8.57	6.4	4.27
No. of atoms	3416	3422	10878
Average B-factor $(Å)^2$	70.0	65.0	44.0
Root mean square deviation			
Bonds Å	0.011	0.005	0.009
Angles (°)	1.71	1.43	1.25
Ramachandran plot			
Favoured (%)	96.55	94.13	96.79
Allowed (%)	2.96	5.38	2.72
Outlier (%)	0.49	0.49	0.49
PDB codes	7NYB	7NZI	7NZJ

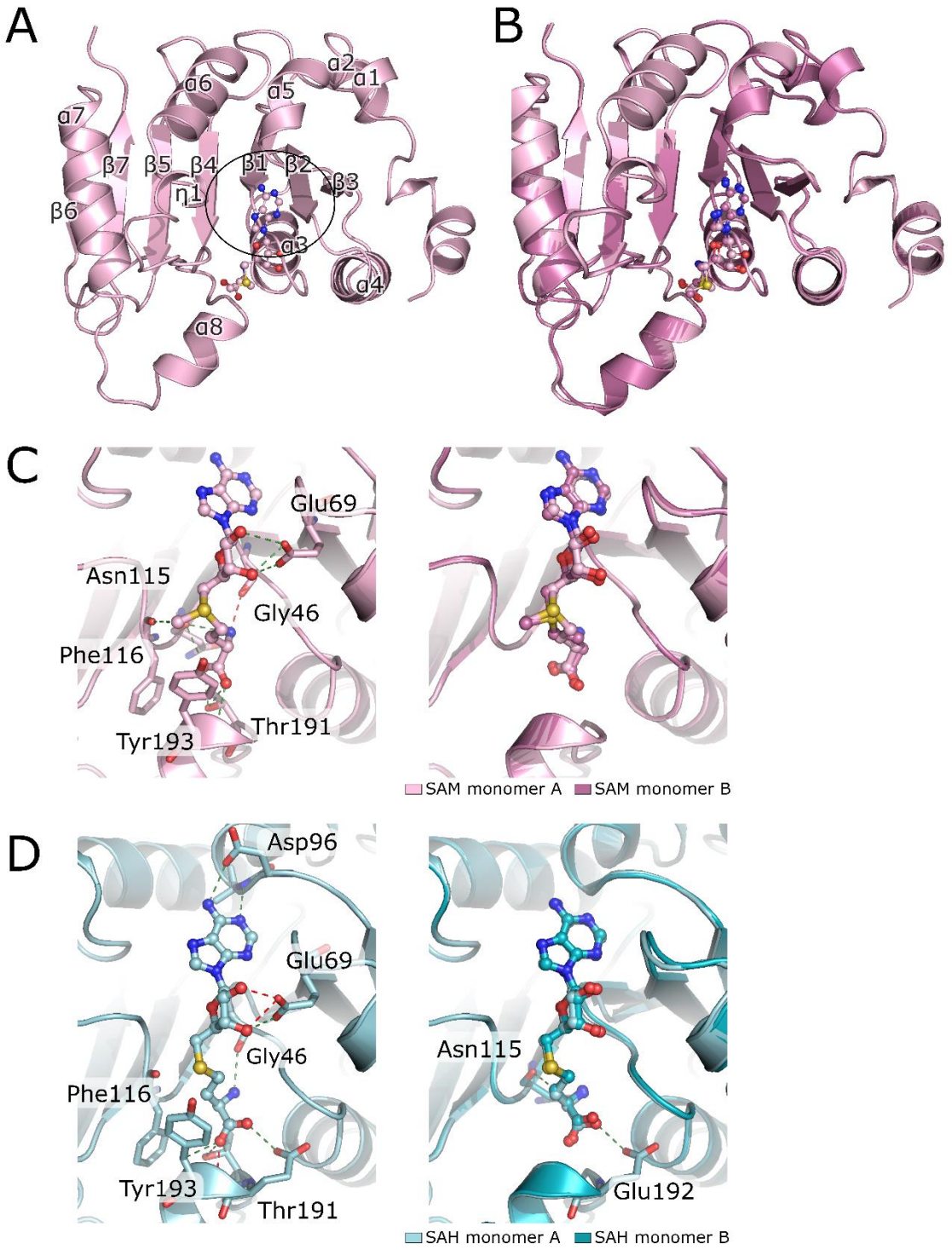

Figure 2.3: Crystal structures of SAM and SAH bound to *bs*TrmB. (A) TrmB subunit A is represented as cartoon with annotated secondary elements. SAM is shown as ball and stick model. Central switch point is highlighted by the black circle. (B) Superposition of TrmB monomer A (light pink) and monomer B (dark pink) represented in cartoon mode. SAM is shown as ball and stick. The crystal structure was determined to 2.5 Å. (C) Close-up view of the ligand binding sites of TrmB monomer A (left) and superposition of both (right) complexed with SAM. Ligand interacting residues are shown in sticks and interactions are marked as dashed lines. (D) Close up view of the SAH-TrmB complex structure. bsTrmB is depicted as cartoon (light cyan (monomer A, left) and superposition of both (right)). The soaked S-Adenosyl-L-homocysteine is depicted in ball and stick mode. SAH coordinating residues are shown as sticks and hydrogen bonds as dashed lines. The crystal structure was determined at 3.1 Å. Hydrogen bonds are colour coded for 2.2 to 2.8 Å (red) and 2.8 to 3.2 Å (green).

2.3.4 SAM binding pocket

In the SAM-TrmB crystal structure, in each monomer the electron density for SAM is clearly visible at higher sigma levels on both 2mFo-DFc as well as mFo-DFc (polder) omit maps (Figure S2.2). The SAM binding pocket is built by the C-terminal edges of β-strands β2, β3, and β5 (Figure 2.3A), forming the central topological switch-point (Figure 2.3A), common to SAM-dependent MTases. Bound SAM molecule adopts an elongated conformation (Figure 2.3C). The binding pocket of both SAM molecules consists of three motifs, motif I (Glu69 (β2), Gly46 (β1)), motif II (Asn115, Phe116, β4), and motif III (Thr191, Tyr193, α8), of which Glu69 and Thr191 are highly conserved among TrmB members (Figure 2.3C). The 2´ OH group of the ribose forms hydrogen bonds with the side chain of Glu69, the carboxyl group of the methionine moiety is hydrogen bonded to the side chain of Thr191 and the main chain of Tyr193, and the amine group to the main chain of Asn115 and Gly46.

The overall topology of the TrmB-SAH complex structure is similar to the TrmB-SAM complex. Additional hydrogen bonds are formed between the N6 amine group of the SAH adenine moiety to the side chain of Asp96 (Figure 2.3D). Interactions of Asn115 and SAH could only be seen for TrmB monomer B. Hydrogen bonds of Glu192 to the carboxyl group of SAH are established only in monomer A.

2.3.5 Conformational rearrangement of the active site

Next, we were interested in whether the binding of SAM or SAH leads to conformational changes of the active site. Therefore, we compared the TrmB-SAM/SAH complex structures with the TrmB apo structure. In both liganded structures, Tyr193 in motif VI shows a rearrangement in its side-chain orientation toward the ligand. Upon ligand binding, Tyr193 OH group is displaced by about 8 Å towards the sulphur atom of SAM/SAH. This side-chain conformational change leads to a decrease in local B-values of the loop region connecting α8-β7 (Figure 2.4). Furthermore, the observed rotation of Tyr193 pulls helix α8 on average 1.8 Å toward SAM and results in a reorientation of Phe197 (Figure 2.4C). This movement of α8 further leads to a “closing” of the catalytic pocket.

Interestingly, the Tyr193 is not conserved across the TrmB/Trm8 family. In yeast Trm8 and human METTL1, this tyrosin is replaced by glutamate at position 261 and 210, respectively. Both Glu residues adopt, like Tyr193 in *B. subtilis*, the same position relative to the sulfur group of SAM (Dong et al., 2008; Leulliot et al., 2008). However, due to lacking the active site loop harboring amino acids 260-270 in determined complex and apo Trm8 crystal structures, no structural data are available which could shed the light on similarities or dissimilarities of this region when compared to *bs*TrmB.

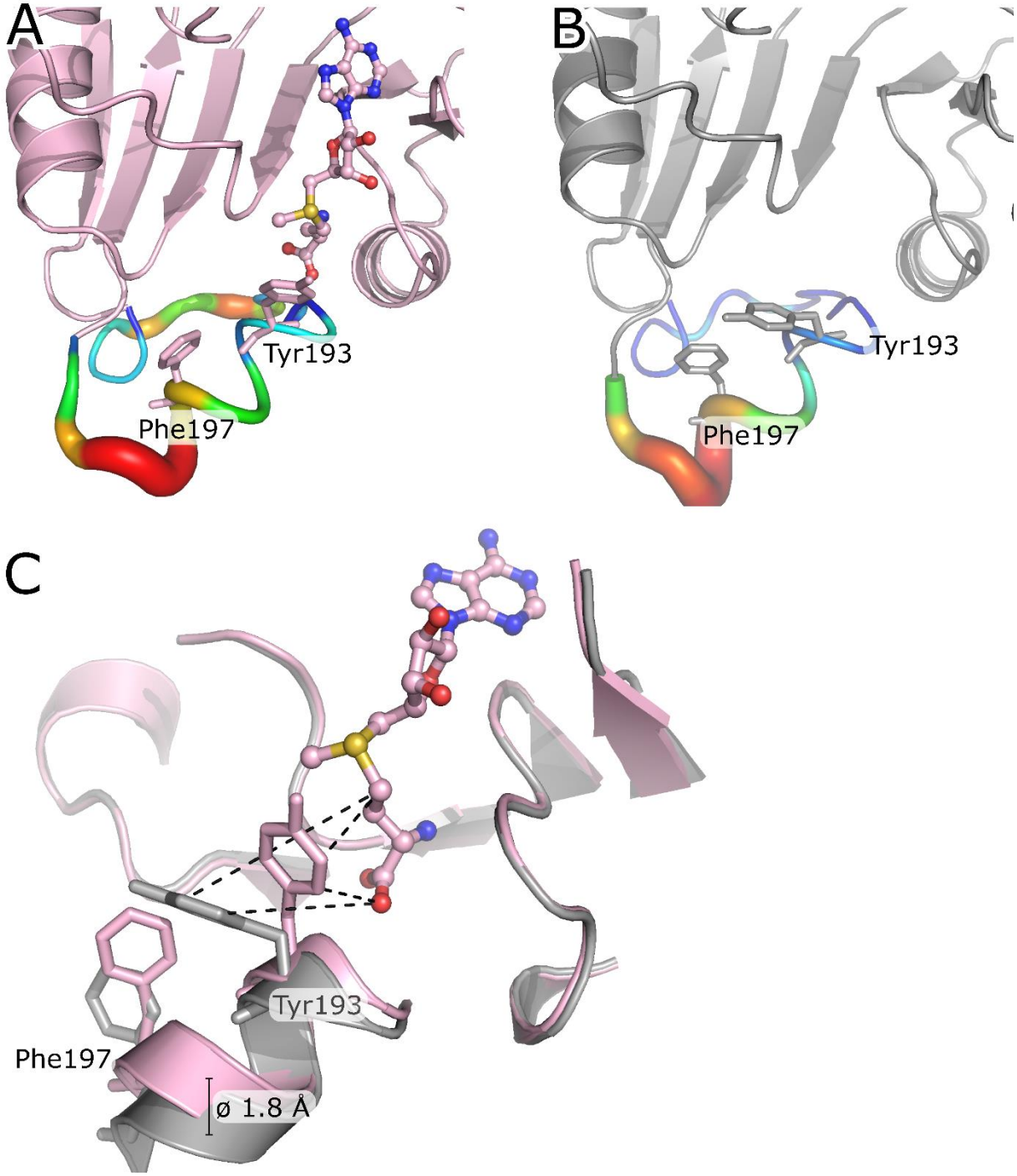

Figure 2.4: Structural rearrangement of the *bs*TrmB active site upon ligand binding. (A) TrmB (monomer A, light pink) is shown as cartoon, the bound SAM is represented as ball and stick model. Local B-factors are ramp coloured from blue to red representing regions of low and high flexibility, respectively. Tyr193 and Phe197 are shown as sticks. (B) apo TrmB (monomer A, grey) is shown as cartoon. Local B-factors are ramp coloured from blue to red representing regions of low and high flexibility, respectively. Tyr193 and Phe197 are shown as sticks. (C) Superposition of TrmB-SAM and apo TrmB. Tyr193 and Phe197 are depicted as sticks and the residue movement upon ligand binding is shown as dashed lines. Average displacement of cα of helix 8 is about 1.8 Å.

To investigate whether Tyr193 plays a crucial role in SAM binding and/or methyl group transfer, we generated a Y193A mutant of TrmB. This mutation resulted in a reduced affinity of TrmB to its cognate $tRNA^{Phe}$ from a K_d of 0.12 µM to 0.32 µM. Furthermore, MTase activity was significantly

reduced (25 fold reduction) (Figure S2.3). These results confirm the importance of Tyr193 in SAM binding and methyl group transfer.

2.3.6 Conserved water molecules in SAM binding pocket and possible reaction mechanism

Comparison of crystal structures from *bs*TrmB complexed with SAM/SAH or in the apo state with TrmB enzymes from *E. coli*, *S. cerevisiae*, and *H. sapiens* revealed the presence of a few structurally conserved water molecules surrounding the SAM binding pocket, 4 in subunit A (Figure 2.5A) and 5 in subunit B (Figure 2.5B). In both chains, one conserved water molecule (named W_2) interacts with the highly conserved residue Asp154. W_3 interacts with the side chain of the conserved Thr153 and further forms hydrogen bonds to the side chain of Ser117 and main chain of Phe116. Additionally, W_1 forms hydrogen bonds with W_2, W_3, Asp154 (monomer A), and Tyr193 (monomer B). These water molecules protrude into the putative tRNA G46 binding pocket. Prior to tRNA binding, these water molecules might just fill up the void space, but upon binding, they could play a role in aligning the guanine base for methyl group transfer or even aiding in catalysis.

The remaining two structurally conserved water molecules, W_4 and W_5 are located near the adenine binding site, possibly bridging the protein main chain with SAM. W_4 forms hydrogen bonds with the Leu130 and Asp118 main chain. W_5 in turn hydrogen bonds to Asp118 side chain and the N7 atom of the adenine SAM (Figure 2.5B).

2.3.7 $tRNA^{Phe}$-TrmB complex cross-linking

To get structural insight in how TrmB binds its tRNA substrates, we performed UV light induced cross-linking of the TrmB-$tRNA^{Phe}$ complex and analysed the cross-linked peptides by means of mass spectrometry. We found 6 residues cross-linked to RNA (Figure 2.6). Phe71, Pro121, Lys137/138, and Phe197 cross-linked to cytosine and Trp120 cross-linked to guanine. Phe71, Trp120 and, Phe197 are part of the SAM binding pocket. Residues Phe71 and Trp120 are oriented vertically upward, so they could interact with tRNA via π-stacking to fix the tRNA substrate in a proper position for catalysis. Phe197 flanks the proposed guanine base binding pocket. The electrostatic surface potential surrounding the SAM binding pocket shows positively charged areas especially in the conserved region η1 connecting β4 and α6, which could indicate possible tRNA binding sites to bind and stabilize the tRNA structure upon base flipping of G46 and catalysis (Figure 2.6). Taken together, the observed $tRNA^{Phe}$-TrmB cross-links suggest the binding of $tRNA^{Phe}$ above the SAM-binding pocket with the anticodom-stem loop aligning with the methionine moiety and the acceptor stem aligning with the adenine moiety. Additional strong interactions are established between the η1 with the tRNA molecule.

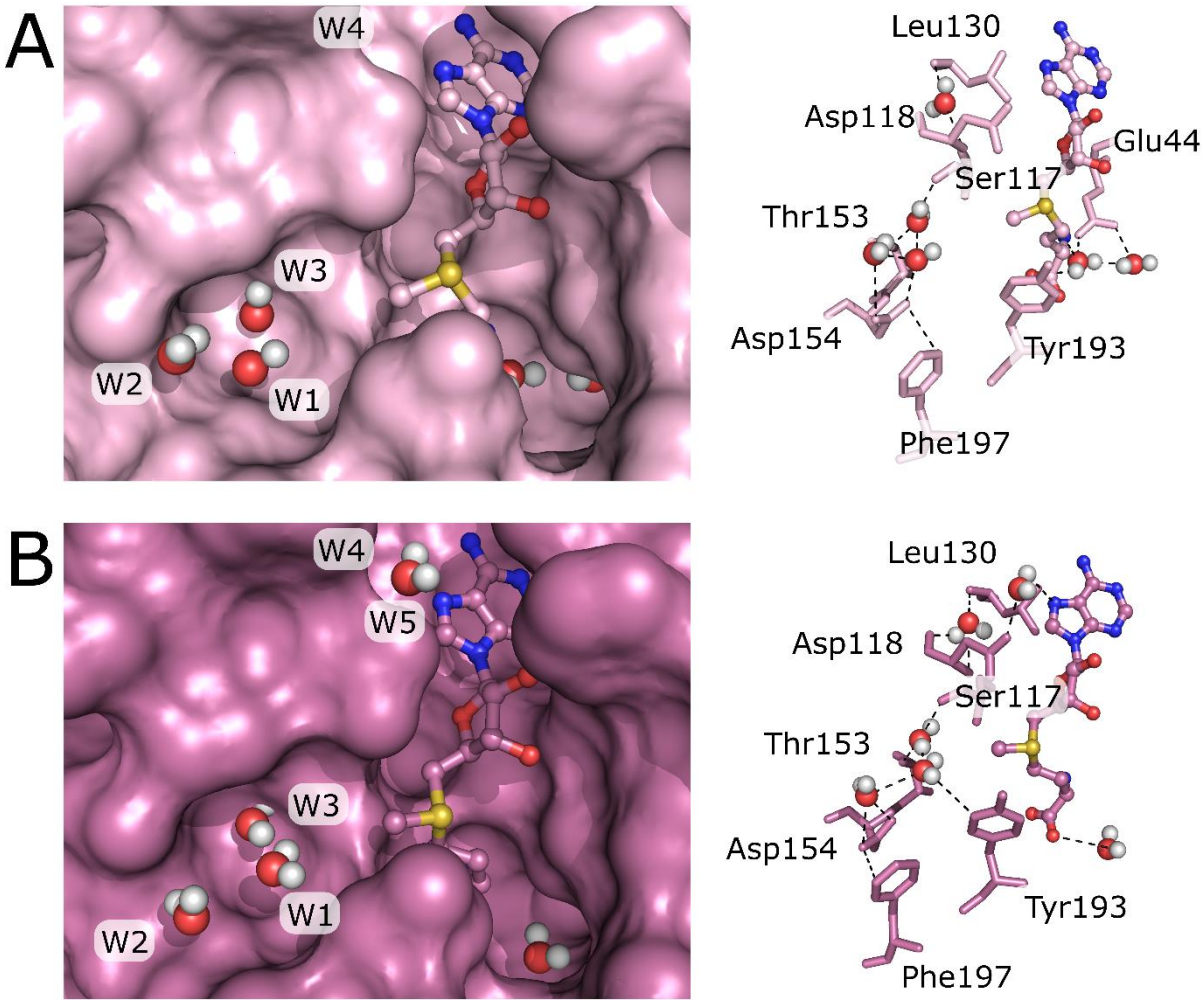

Figure 2.5: Structurally conserved water molecules in TrmB crystal structures mapped on the TrmB-SAM structure. (A) Monomer A of the TrmB-SAM complex structure is shown in surface mode (left). SAM is shown as ball and stick model and water as spheres. Water coordinating residues are represented as sticks (right), water is shown as spheres, and hydrogen bonds are shown as dashed lines. (B) Monomer B of the TrmB-SAM crystal structure shows TrmB in surface representation (left). SAM is shown as bal and stick model. Water molecules are represented as spheres. Water coordinating residues (right) are shown as sticks, water as spheres and hydrogen bonds as dashed lines.

2.3.8 Low resolution model of the TrmB-tRNA^{Phe} complex using SAXS and molecular docking

After the identification of direct TrmB-tRNA^{Phe} interaction sites, we aimed for more structural insight about the TrmB-tRNA^{Phe} complex. Therefore, we reconstituted this complex, as for the cross-linking experiments, and performed small-angle X-ray scattering (SAXS) measurements. To better evaluate the obtained SAXS data, we measured each component of the TrmB-tRNA^{Phe} complex separately. Guinier radii for the individual components were determined to be 3.29 ± 0.04 nm (TrmB), 2.67 ± 0.02 nm (tRNA), and 5.3 ± 0.05 nm (tRNA-TrmB complex). However, evaluation of the complex SAXS curves was challenging. Therefore, molecular docking experiments were performed and validated using the experimental SAXS curves. Complex models

were generated by molecular docking using Rosetta (Chaudhury et al., 2011). First, a low-resolution global docking, generating 100.000 decoys in a coarse-grained representation, was performed. These initial poses were sorted by their relative position to the sulphur atom of SAM, and the distance to the G46 of the tRNA molecule. The best 100 models were subsequently sorted by the energy of the interactions across the interface (*I_sc* score) and the total Rosetta score. Second, decoys exhibiting the best scores were used for high resolution docking, and again sorted by the *I_sc* score. Initially, the crystal structure of $tRNA^{Phe}$ (PDB ID: 1EHZ) has been used, however the validation against SAXS data indicated some structural changes of the tRNA molecule. As the G46 base needs to break hydrogen bonds in the tRNA core and flip into the active site pocket, bending of the tRNA molecule can be assumed. Indeed, much better fits of the computationally generated complex models were obtained when slightly bend tRNA molecules (Emsley et al., 2010) were used. The most favourable models were validated based on the cross-linking data and the calculated SAXS curves to fit the experimental SAXS data. Evaluation of the TrmB crystal structure against the TrmB SAXS data resulted in a good fit of the SAXS and X-ray data (Figure 2.7A). The protein-tRNA complex SAXS data could be described best with a TrmB-$tRNA^{Phe}$ complex model in a 2:2 stoichiometry (Figure 2.7B). Hence, the final TrmB-tRNA complex model comprises two slightly bend tRNA molecules bound to the homodimeric protein (Figure 2.7C). The tRNA molecules lie on top of TrmB, with the T-arm facing toward the protein (Figure 2.7E), agreeing with previously published data about the yeast TrmB homolog Trm8-Trm82 (Leulliot et al., 2008). The tRNA core makes intermolecular contacts, while the acceptor stem and the anticodon stem protrude off the protein. Extensive protein-RNA contacts are established by the α helix α5 to the RNA backbone of the T-arm (Figure 2.7D). Further contacts are established between residues of α5, α8, and η1 to G46 and U47.

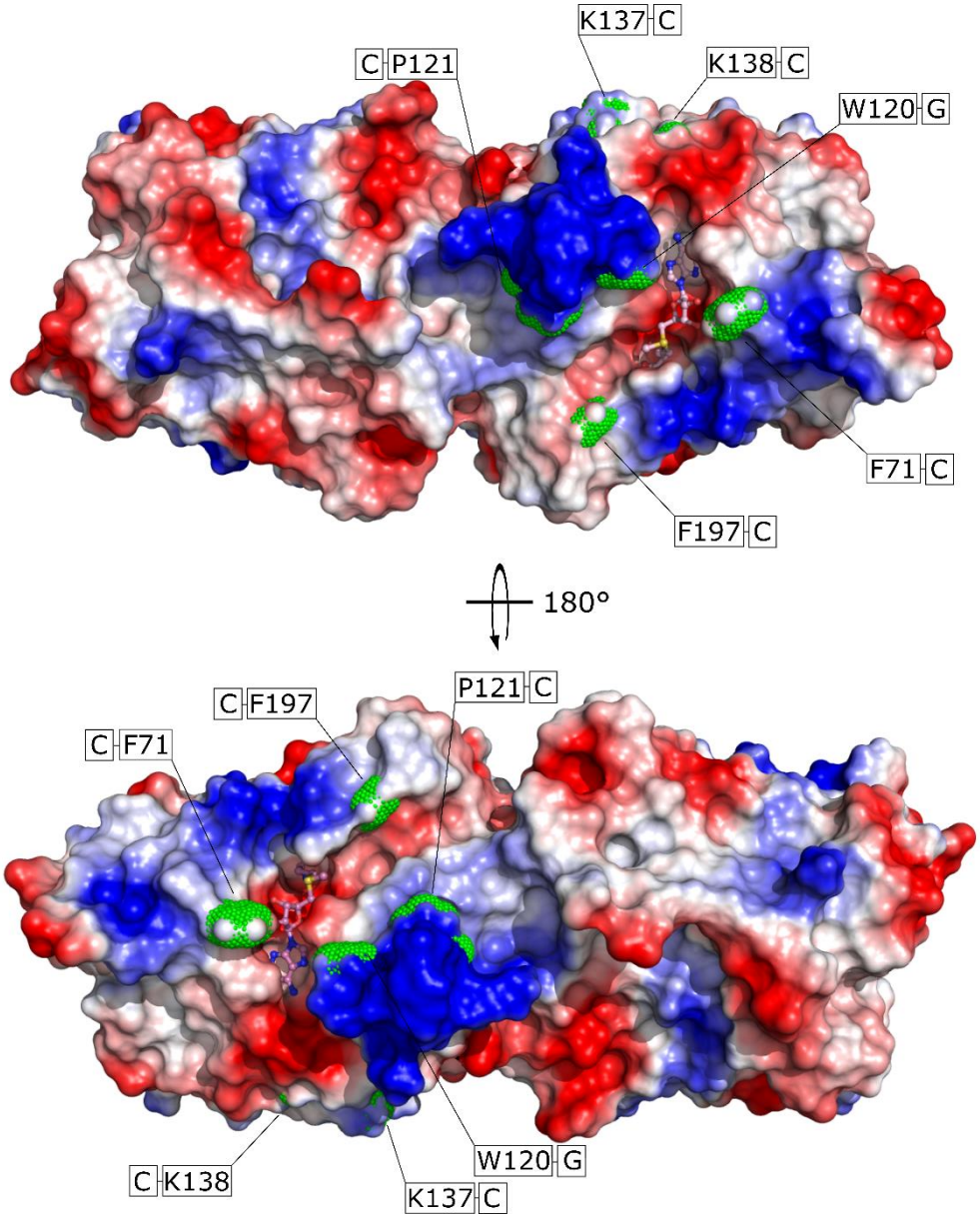

Figure 2.6: UV-Cross linking of TrmB to $tRNA^{Phe}$. Surface representation of TrmB, electrostatic potential is depicted at a contour level of ± 7 k_BT/e. SAM is shown in ball and stick mode. Residues cross-linked to $tRNA^{Phe}$ are shown as green dots. Covalent links are mapped on the protein surface and shown in black boxes.

Taken together, the TrmB-$tRNA^{Phe}$ complex model suggests that each of the TrmB subunits is able to bind a tRNA molecule. Further, the tRNA substrates are recognized via the D- and T-arm. The conserved loop region η1 of TrmB seems to stack between the variable loop and the T-arm, probably ensuring proper positioning of the tRNA molecule on the SAM binding pocket and catalytic pocket.

2.4 Discussion

The m^7G46 introducing methyltransferase TrmB is gaining attention since the discovery of its connection to the human disease microcephalic primordial dwarfism (Shaheen et al., 2015). Structural analysis of the TrmB-tRNA complex as well as biochemical investigation would give valuable insight into TrmB function. Hence, in this study, we focused on the tRNA-TrmB interaction on both, a biochemical and structural level. The TrmB/Trm8 enzyme family is structurally diverse with monomeric, homodimeric, and heterodimeric biological assemblies (Leulliot et al., 2008; Liu et al., 2008; Zegers et al., 2005). Interestingly, even though the TrmB homologues of *E. coli* and *B. subtilis* belong both to the bacterial kingdom they show differences in their biological assembly (Liu et al., 2008; Zegers et al., 2005). While *E. coli* functions as a single subunit, *B. subtilis* TrmB evolved a homodimeric assembly. Hence, the impact of homodimerization of *bs*TrmB was studied. TrmB catalysis was shown to follow negative cooperative effects by pinpointing the reaction kinetics to be described best by the Hill equation (Figure 2.2). While under standard assay conditions this effect is mildly distinct, this effect becomes more drastic when decreasing SAM concentrations. In near physiological conditions (Caudill et al., 2001; Melnyk et al., 2000), TrmB cooperativity drops from mild negative effects to a half-of-the-sites reactivity. With this, TrmB is able to ensure both substrates, SAM as well as tRNA, to bind to the same subunit and catalysis can occur. Thus, we propose a ligand based control system to ensure effective enzyme catalysis under low ligand concentrations.

However, this raises the question of whether both subunits of the TrmB homodimer are capable of binding SAM and tRNA. To shed light on this question, we solved the crystal structure of TrmB with its methyl group donor SAM and reaction product SAH (Figure 2.3). In our ligand complex structures SAM and SAH are well resolved in both subunits. As reported previously, *bs*TrmB belongs to the SAM-dependent class I methyltransferases, containing a Rossman fold core (Zegers et al., 2005). Comparison of TrmB-SAM/-SAH crystal structures with its homologs from yeast and *E. coli* shows an identical mode of binding across species. The amino group of the adenine moiety is captured by the oxygen atom of either Asp or Asn, the ribose moiety is coordinated strictly by glutamate, and the methionine moiety is coordinated by a main chain oxygen. This shows, that even though the TrmB/Trm8 protein family is divergent in their amino acid sequence, they are structurally highly similar with a conserved mode of ligand binding and therefore exhibit most likely a similar catalytic mechanism. Furthermore, we observed a repositioning of Tyr193 in the SAM-binding pocket upon ligand binding. This movement can be also seen in the yeast homologue Trm8, as well as in the human homolog METTL1. Here, Trm8 Glu261 and METTL1 Glu210 adopt the same position and side chain orientation, compared to the *B. subtilis* Tyr193.

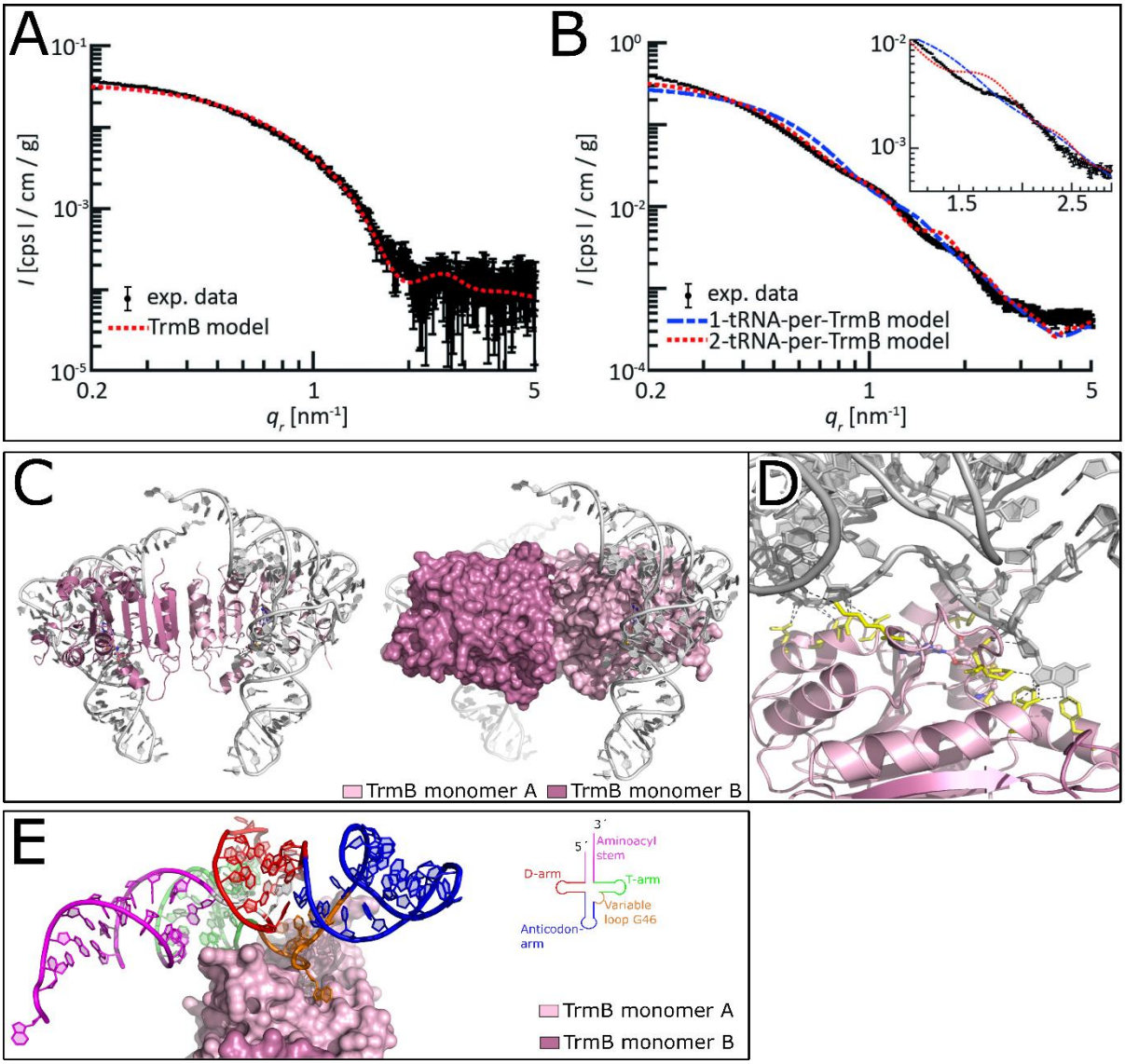

Figure 2.7: Predicted TrmB - $tRNA^{Phe}$ complex model. (A) Experimental and simulated SAXS curves of TrmB. The curve of the model is calculated from the TrmB-SAM complex crystal structure and scaled to match the experimental curve between 0.1 <= qr <= 2 nm-1. (B) Experimental SAXS curves and predicted SAXS curves from docking models. The model consisting of two tRNA molecules per TrmB homodimer (red, dotted) shows a higher agreement with the experimental data compared to the model consisting of one tRNA molecule per TrmB (blue, dashed), also seen at larger qr-values. The feature of the experimental data at qr~2.0 nm-1 is shifted to smaller qr-values in the 2-tRNA model and is not visible in the 1-tRNA model (inset). The data is plotted with Matlab (MathWorks Inc. Natick, Massachusetts, USA). (C) TrmB - $tRNA^{Phe}$ complex model is depicted as cartoon (left) with surface representation of TrmB (right). (D) Close-up view of the tRNA binding to TrmB monomer A (light pink). Residues of TrmB interacting with $tRNA^{Phe}$ are shown as sticks (yellow), hydrogen bonds are shown as dashed line. (E) TrmB-$tRNA^{Phe}$ complex model is shown with surface representation of TrmB and $tRNA^{Phe}$ highlighted by its domain architecture. The domain architecture of $tRNA^{Phe}$ is colour coded in Aminoacyl stem (purple), T-arm (green), Variable loop (orange), Aminoacyl stem (blue), and D-arm (red) with the G46 base depicted as sticks

Examining the importance of Tyr193, we exchanged Tyr193 by alanine which abolished MTase activity completely while still being able to bind tRNA, even though with 2.6 times less affinity. This provides the importance of Tyr193 during catalysis by probably correct positioning of SAM.

To address the open question of whether the homodimeric TrmB is able to bind two tRNA molecules, we performed SAXS measurements of the $tRNA^{Phe}$-TrmB complex complemented by cross-linking experiments and molecular docking approaches. The Guinier radii obtained by SAXS for TrmB (32.9 Å ± 0.4 Å) and tRNA (26.7 Å ± 0.2 Å) fit the crystallographic values of 32.5 Å (TrmB) and 29.9 Å (tRNA) well, assuming a hydration shell of 7 Å (Chen and Hub, 2014; Park et al., 2009). The final docked complex model consists of the TrmB homodimer and two tRNA molecules (one bound to each subunit Figure 2.7). Although the SAXS curves of the model and the measurements are similar, our model exhibits some misfits compared to the experimental SAXS curve. This can be explained by extensive bending of the tRNA molecule upon binding and structural rearrangement of the tRNA core during G46 base flipping. This could also explain the observed differences in the Guinier radii of the $tRNA^{Phe}$-TrmB complex of 53 Å compared to the complex model with a Guinier radius of 43 Å. Moreover, SAXS is a sensitive method able to detect small changes in length scales upon conformational rearrangements. Subsequently, such chances would lead to altered SAXS curve. Additionally, the T-arm of $tRNA^{Phe}$ comes into close vicinity of a more negatively charged area of TrmB. We assume that this negative charge may be needed to force the tRNA core to release the G46 base from base pairing and in that manner facilitate its flipping into the catalytic pocket.

The overall positioning of the tRNA on TrmB is in agreement with prior biochemical studies. In *A. aeolicus*, mutation of Lys101Ala (in *B. subtilis* Lys122) located in a conserved loop, leads to a weakened tRNA binding and a reduction in the turnover rate from 1 to 0.36 (Tomikawa et al., 2018). This indicates that this amino acid could be involved in intermolecular communication. In our complex model, Lys122 and the phosphate backbone of G10, located in the D-loop, are in close proximity to each other and might function as ruler to ensure optimal positioning of the tRNA molecule on TrmB. Additionally, mutation of the *E. coli* Arg154Ala (in *B. subtilis* Lys128) results in a loss of function of *ec*TrmB (Purta et al., 2005). In our model, Lys128 is involved in three protein-RNA contacts, positioning the tRNA over the SAM binding pocket. These examples of mutagenesis studies across different TrmB species strengthen our complex model and show the importance of the conserved loop region and η1 in catalysis.

Further, comparison of the ligand binding pockets of the TrmB-SAM and TrmB-SAH crystal structure presents hints of how pre-, and post-catalytic states could differ. In TrmB-SAH, the active sites of chain A and chain B are identical. In TrmB-SAM, the active site pocket of subunit B is narrower than the active site pocket of subunit A. This indicates, that the TrmB-SAM complex shows most likely two structurally different catalytic states, with subunit A being in the post-catalytic state and subunit B in the pre-catalytic state. Concluding that even though both subunits are topologically identical, they appear to be in chemically different states. This is reinforced by

conserved water molecules located in the catalytic pocket. While subunit A displays water molecules W_1-W_3 with even distribution across the guanine binding pocket, subunit B shows a different distribution with W_3 being positioned deep in the binding pocket whereas W_2 is located at the rim of the pocket.

Lastly, cross-linked amino acids Leu70 and Phe71 built contacts with tRNA bases C48 and U47, respectively (Figure 2.7). An extensive study about the tRNA secondary structure and the formation of hydrogen bonds within the tRNA core and anticodon stem showed the importance of both, U47 and C48 (Matsumoto et al., 2007). Upon mutation of U47A and C48A, V_{max} dropped from 1.4 µmol mg^{-1} h^{-1} to 0.28 µmol mg^{-1} h^{-1} and 1.4 µmol mg^{-1} h^{-1} to 0.04 µmol mg^{-1} h^{-1}, respectively, resulting in a reduction of the methyl acceptance activity by a decrease in V_{max}. Substitution of C48 by A results in the disruption of the G15-C48 base-pairing, which in turn results in an impaired methyl acceptance activity. This perturbation could be based on additional rearrangements of the tRNA core. Base flipping of G46 in our model lead to a rearrangement of both, U47 and C48. While U47 moves ~11 Å to the front forming hydrogen bonds with TrmB Phe71, C48 breaks the base pairing with G15 and forms additional hydrogen bonds with Phe71. If the pyrimidine C48 is substituted by the purine adenine, the interactions between A48 and Phe71 could be too strong and methyl transfer cannot be achieved (Figure S2.4).

In conclusion, we showed the cooperative activity of the TrmB homodimer with half-of-the-sites reactivity at physiological SAM concentrations. Albeit this half-of-the sites reactivity, both subunits of the TrmB homodimer are capable to bind its methyl group donor. Tyr193 is important for SAM coordination and catalysis might be mediated by conserved water molecules. Furthermore, we reported the TrmB-$tRNA^{Phe}$ complex model in which each TrmB subunit binds a tRNA molecule and protein-RNA contacts are formed by the T-arm and to a lower extent by the D-arm.

2.5 Acknowledgements

The synchrotron MX data was collected at beamline P13 operated by EMBL Hamburg at the PETRA III storage ring (DESY, Hamburg, Germany) and beamline MX 14.1 operated by the Helmholtz-Zentrum Berlin at the BESSY II storage ring (BESSY, Berlin, Germany). We would like to thank Johanna Hakanpää, Saravanan Panneerselvam, and Jan Wollenhaupt for the assistance in using the beamlines.

Disclosure of interest

The authors declare no conflict of interest.

Funding

This work was supported by the DFG (priority program SPP1784 to R.F.; SFB860 A10 to H.U.; SFB860 B10 to S.K.) and the ERC under the European 438 Union's Horizon 2020 research and innovation program CoG 439 no. 724932 (to S.K.).

2.6 Supplementary Information

tRNA complex structure of the M7G46 Methyltransferase TrmB

Blersch Katharina F.[1], Burchert Jan-Philipp[2], August Sophie C.[2], Welp Luisa[3], Neumann Piotr[1], Köster Sarah[2], Urlaub Henning[3,4], Ficner Ralf[1*]

[1] Department of Molecular Structural Biology, Institute of Microbiology and Genetics, GZMB, Georg August University Göttingen, Justus-von-Liebig Weg 11, 37077 Göttingen, Germany

[2] Institute for X-Ray Physics, Georg August University Göttingen, Friedrich-Hund-Platz 1, 37077, Göttingen, Germany

[3] Bioanalytical Mass Spectrometry Research Group, Max Planck Institute for Biophysical Chemistry, Am Faßberg 11, 37077, Göttingen, Germany

[4] Bioanalytics Group, Institute for Clinical Chemistry, University Medical Center Göttingen, 37075 Göttingen, Germany

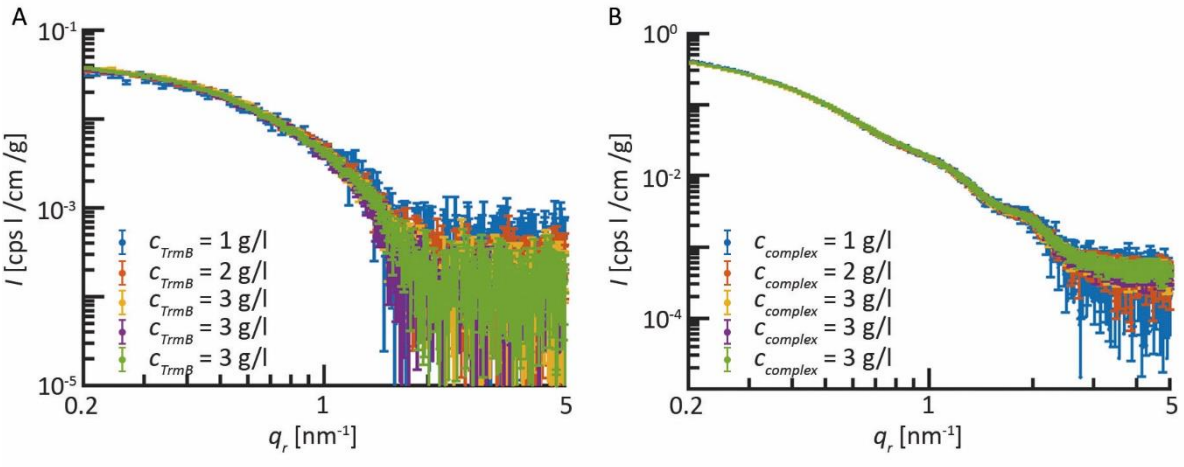

Figure S2.1: Experimental SAXS curves obtained from the concentration series of TrmB (A) and the TrmB-tRNA complex (B). Since the profiles agree with each other no interactions can be seen and thus the obtained signals purely result from form factor scattering of TrmB and its tRNA complex, respectively. The data is plotted with Matlab (MathWorks Inc. Natick, Massachusetts, USA).

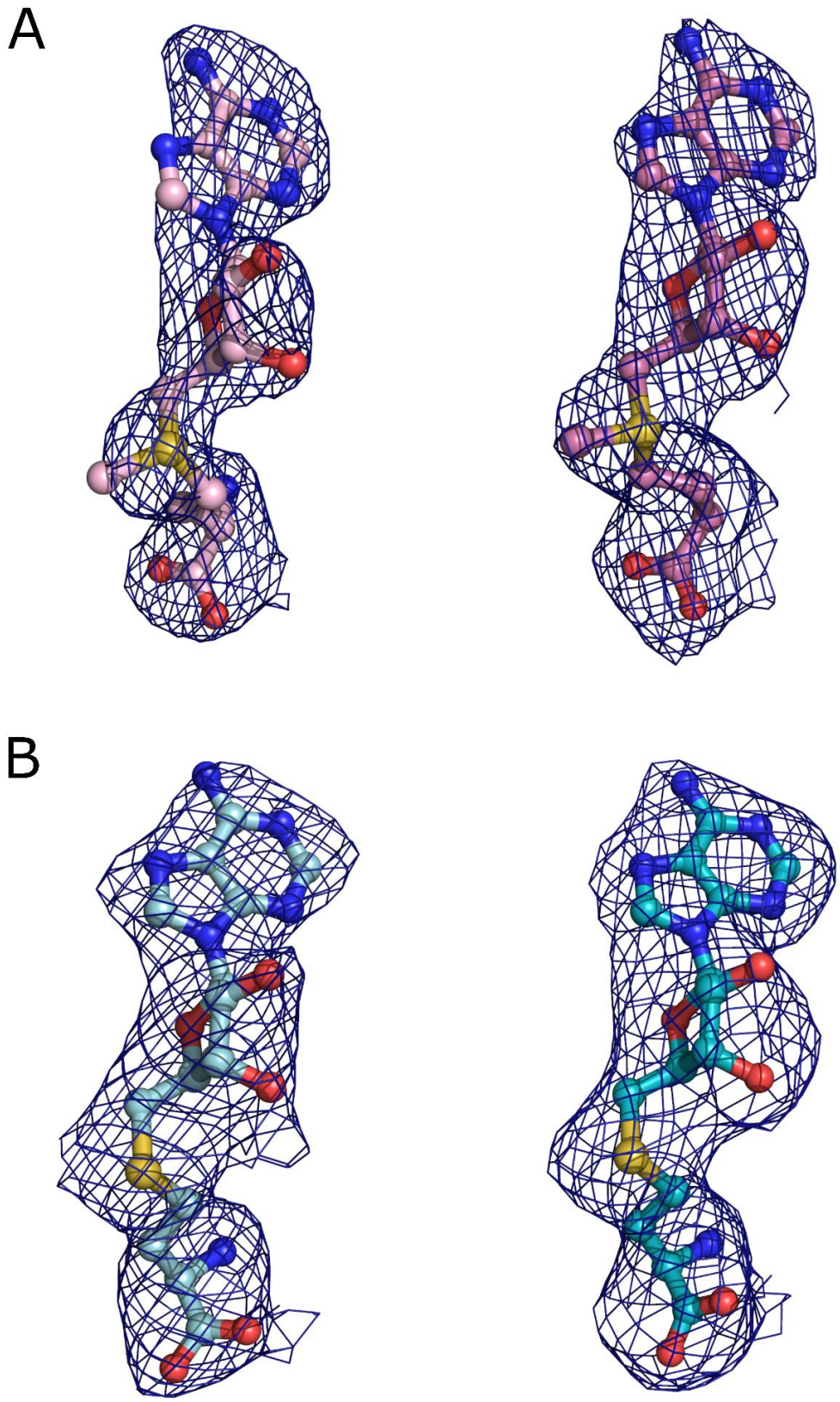

Figure S2.2: SAM and SAH are presented as ball and stick models. (A) shows the mFo-DFc electron-density OMIT map prepared by Phenix Polder contoured at 3σ level for chain A and chain B in light pink and dark pink, respectively. (B) mFo-DFc electron-density OMIT map prepared by Phenix Polder contoured at 3σ level for SAH bound to chain A and chain B coloured in light cyan and dark cyan, respectively.

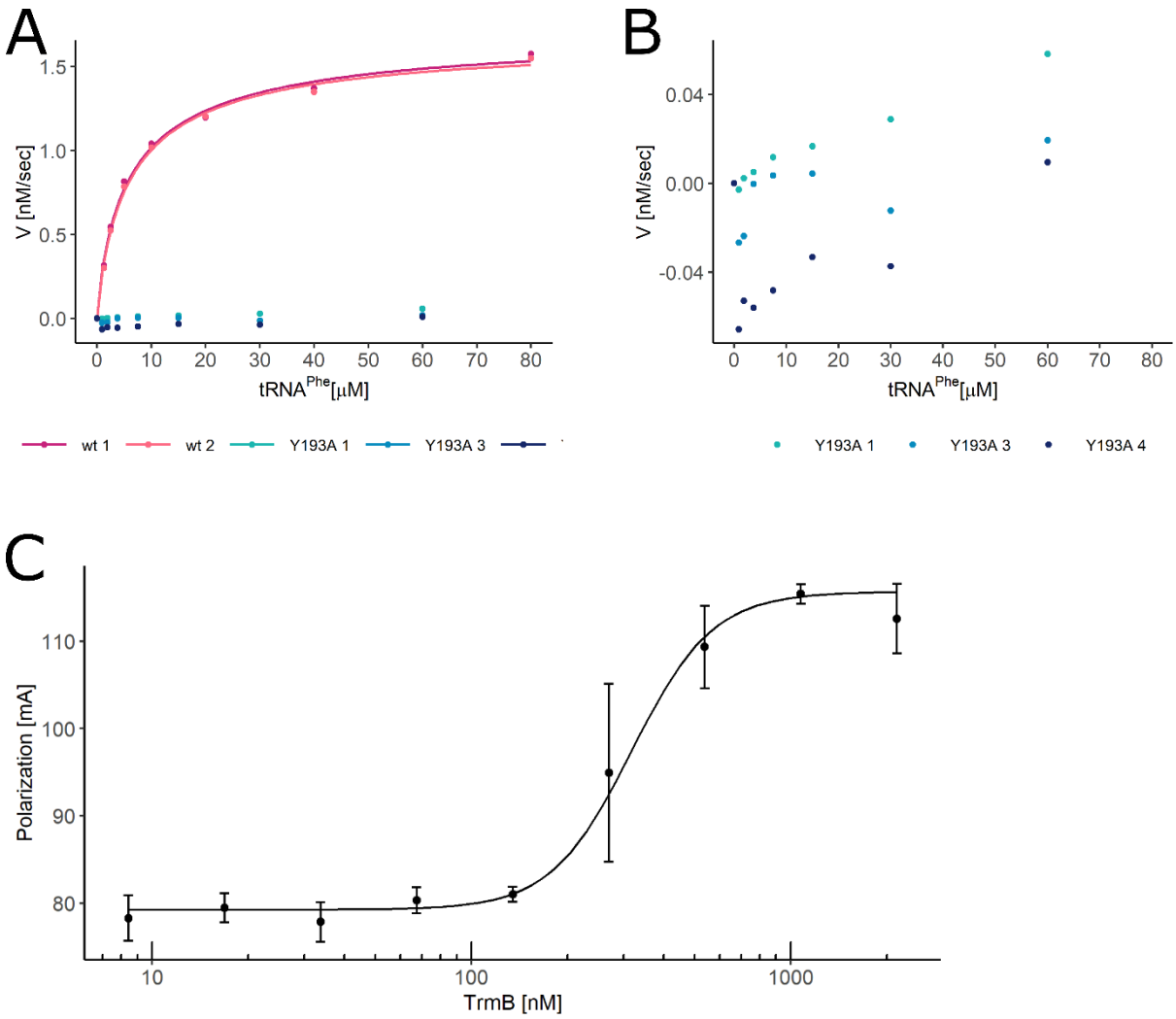

Figure S2.3: $tRNA^{Phe}$ binding and MTase activity of Y193A TrmB. (A) Methyltransferase activity assay of the Y193A TrmB mutant to in vitro transcribed $tRNA^{Phe}$. Duplicates are represented in blue and compared to the wt TrmB enzyme. (B) Fluorescence polarization based binding assay of $tRNA^{Phe}$ to Y193A TrmB mutant. Binding was measured with increasing TrmB Y193A concentrations from 0.007 to 2.1 µM.

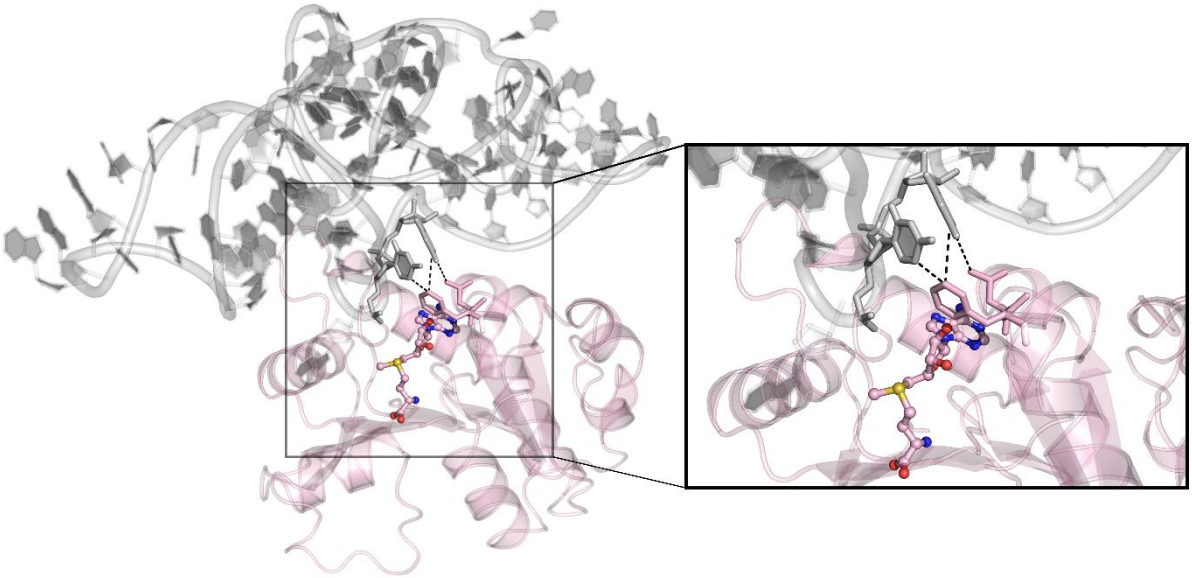

Figure S2.4: Cartoon representation of the TrmB-tRNA^{Phe} complex model. Interacting residues of the protein (pink) and RNA (grey) are presented as sticks. Polar contacts are shown as dashed lines. The inset shows a close-up view of the interacting protein residues and tRNA nucleotides.

2.7 References

Adams, P.D., Afonine, P.V., Bunkóczi, G., Chen, V.B., Davis, I.W., Echols, N., Headd, J.J., Hung, L.-W., Kapral, G.J., Grosse-Kunstleve, R.W., McCoy, A.J., Moriarty, N.W., Oeffner, R., Read, R.J., Richardson, D.C., Richardson, J.S., Terwilliger, T.C., Zwart, P.H., 2010. PHENIX: a comprehensive Python-based system for macromolecular structure solution. Acta Crystallogr D Biol Crystallogr 66, 213–221. https://doi.org/10.1107/S0907444909052925

Agris, P.F., Sierzputowska-Gracz, H., Smith, C., 1986. Transfer RNA contains sites of localized positive charge: carbon NMR studies of [13C] methyl-enriched Escherichia coli and yeast tRNAPhe. Biochemistry 25, 5126–5131. https://doi.org/10.1021/bi00366a022

Ahn, H.J., 2003. Crystal structure of tRNA(m1G37) methyltransferase: insights into tRNA recognition. The EMBO Journal 22, 2593–2603. https://doi.org/10.1093/emboj/cdg269

Alexandrov, A., 2005. tRNA m7G methyltransferase Trm8p/Trm82p: Evidence linking activity to a growth phenotype and implicating Trm82p in maintaining levels of active Trm8p. RNA 11, 821–830. https://doi.org/10.1261/rna.2030705

Barcroft, J., Hill, A.V., 1910. The nature of oxyhaemoglobin, with a note on its molecular weight. The Journal of Physiology 39, 411–428. https://doi.org/10.1113/jphysiol.1910.sp001350

Boccaletto, P., Machnicka, M.A., Purta, E., Piątkowski, P., Bagiński, B., Wirecki, T.K., de Crécy-Lagard, V., Ross, R., Limbach, P.A., Kotter, A., Helm, M., Bujnicki, J.M., 2018. MODOMICS: a database of RNA modification pathways. 2017 update. Nucleic Acids Research 46, D303–D307. https://doi.org/10.1093/nar/gkx1030

Bujnicki, J.M., 1991. Comparison of Protein Structures Reveals Monophyletic Origin of the AdoMet-Dependent Methyltransferase Family and Mechanistic Convergence Rather than Recent Differentiation of N4-Cytosine and N6-Adenine DNA Methylation. In Silico Biology 1, 334–344. https://doi.org/10.1016/0959-440X(91)90031-N

Caudill, M.A., Wang, J.C., Melnyk, S., Pogribny, I.P., Jernigan, S., Collins, M.D., Santos-Guzman, J., Swendseid, M.E., Cogger, E.A., James, S.J., 2001. Intracellular S-Adenosylhomocysteine Concentrations Predict Global DNA Hypomethylation in Tissues of Methyl-Deficient Cystathionine □-Synthase Heterozygous Mice. The Journal of Nutrition 131, 8. https://doi.org/10.1093/jn/131.11.2811

Chaudhury, S., Berrondo, M., Weitzner, B.D., Muthu, P., Bergman, H., Gray, J.J., 2011. Benchmarking and Analysis of Protein Docking Performance in Rosetta v3.2. PLoS ONE 6, e22477. https://doi.org/10.1371/journal.pone.0022477

Chen, P., Hub, J.S., 2014. Validating Solution Ensembles from Molecular Dynamics Simulation by Wide-Angle X-ray Scattering Data. Biophysical Journal 107, 435–447. https://doi.org/10.1016/j.bpj.2014.06.006

Chou, F.-C., Sripakdeevong, P., Dibrov, S.M., Hermann, T., Das, R., 2013. Correcting pervasive errors in RNA crystallography through enumerative structure prediction. Nat Methods 10, 74–76. https://doi.org/10.1038/nmeth.2262

Cianci, M., Bourenkov, G., Pompidor, G., Karpics, I., Kallio, J., Bento, I., Roessle, M., Cipriani, F., Fiedler, S., Schneider, T.R., 2017. P13, the EMBL macromolecular crystallography beamline at the low-emittance PETRA III ring for high- and low-energy phasing with variable beam focusing. J Synchrotron Rad 24, 323–332. https://doi.org/10.1107/S1600577516016465

De Bie, L.G.S., Roovers, M., Oudjama, Y., Wattiez, R., Tricot, C., Stalon, V., Droogmans, L., Bujnicki, J.M., 2003. The yggH Gene of Escherichia coli Encodes a tRNA (m7G46) Methyltransferase. Journal of Bacteriology 185, 3238–3243. https://doi.org/10.1128/JB.185.10.3238-3243.2003

Dong, A., Zeng, H., Dobrovetsky, E., Bountra, C., Weigelt, J., Arrowsmith, C.H., Edwards, A.M., Bochkarev, A., Min, Plotnikov, Wu, H., Structural Genomics Consortium (SGC), 2008. Crystal structure of human methyltransferase-like protein 1. https://doi.org/20121107150707

Emsley, P., Lohkamp, B., Scott, W.G., Cowtan, K., 2010. Features and development of *Coot*. Acta Crystallogr D Biol Crystallogr 66, 486–501. https://doi.org/10.1107/S0907444910007493

Guilhot-Gaudeffroy, A., Froidevaux, C., Azé, J., Bernauer, J., 2014. Protein-RNA Complexes and Efficient Automatic Docking: Expanding RosettaDock Possibilities. PLoS ONE 9, e108928. https://doi.org/10.1371/journal.pone.0108928

Hoburg, A., Aschhoff, H.J., Kersten, H., Manderschied, U., Gassen, H.G., 1979. Function of Modified Nucleosides 7-Methylguanosine, Ribothymidine, and 2-Thiomethyl-N6-(Isopentenyl)adenosine in Procaryotic Transfer Ribonucleic Acid. Journal of Bacteriology 140, 408–414. https://doi.org/10.1128/JB.140.2.408-414.1979

Johannsson, S., Neumann, P., Wulf, A., Welp, L.M., Gerber, H.-D., Krull, M., Diederichsen, U., Urlaub, H., Ficner, R., 2018. Structural insights into the stimulation of S. pombe Dnmt2 catalytic efficiency by the tRNA nucleoside queuosine. Sci Rep 8, 8880. https://doi.org/10.1038/s41598-018-27118-5

Juhling, F., Morl, M., Hartmann, R.K., Sprinzl, M., Stadler, P.F., Putz, J., 2009. tRNAdb 2009: compilation of tRNA sequences and tRNA genes. Nucleic Acids Research 37, D159–D162. https://doi.org/10.1093/nar/gkn772

Kabsch, W., 2010. XDS. Acta Crystallogr D Biol Crystallogr 66, 125–132. https://doi.org/10.1107/S0907444909047337

Konarev, P.V., Volkov, V.V., Sokolova, A.V., Koch, M.H.J., Svergun, D.I., 2003. PRIMUS : a Windows PC-based system for small-angle scattering data analysis. J Appl Crystallogr 36, 1277–1282. https://doi.org/10.1107/S0021889803012779

Kramer, K., Sachsenberg, T., Beckmann, B.M., Qamar, S., Boon, K.-L., Hentze, M.W., Kohlbacher, O., Urlaub, H., 2014. Photo-cross-linking and high-resolution mass spectrometry for assignment of RNA-binding sites in RNA-binding proteins. Nature Methods 11, 25. https://doi.org/10.1038/nmeth.3092

Krissinel, E., Henrick, K., 2007. Inference of Macromolecular Assemblies from Crystalline State. Journal of Molecular Biology 372, 774–797. https://doi.org/10.1016/j.jmb.2007.05.022

Leulliot, N., Chaillet, M., Durand, D., Ulryck, N., Blondeau, K., van Tilbeurgh, H., 2008. Structure of the Yeast tRNA m7G Methylation Complex. Structure 16, 52–61. https://doi.org/10.1016/j.str.2007.10.025

Liu, Q., Gao, Yang, Yang, W., Zhou, H., Gao, Yongxiang, Zhang, X., Teng, M., Niu, L., 2008. Crystallization and preliminary crystallographic analysis of tRNA m7G46 methyltransferase from Escherichia coli. Acta Crystallogr F Struct Biol Cryst Commun 64, 743–745. https://doi.org/10.1107/S1744309108020241

Machnicka, M.A., Milanowska, K., Osman Oglou, O., Purta, E., Kurkowska, M., Olchowik, A., Januszewski, W., Kalinowski, S., Dunin-Horkawicz, S., Rother, K.M., Helm, M., Bujnicki, J.M., Grosjean, H., 2012. MODOMICS: a database of RNA modification pathways—2013 update. Nucleic Acids Research 41, D262–D267. https://doi.org/10.1093/nar/gks1007

Martin, J.L., McMillan, F.M., 2002. SAM (dependent) I AM: the S-adenosylmethionine-dependent methyltransferase fold. Current Opinion in Structural Biology 12, 11. https://doi.org/10.1016/S0959-440X(02)00391-3

Matsumoto, K., Toyooka, T., Tomikawa, C., Ochi, A., Takano, Y., Takayanagi, N., Endo, Y., Hori, H., 2007. RNA recognition mechanism of eukaryote tRNA m7G46) methyltransferase (Trm8-

Trm82 complex). FEBS Letters 581, 1599–1604. https://doi.org/10.1016/j.febslet.2007.03.023

McCoy, A.J., Grosse-Kunstleve, R.W., Adams, P.D., Winn, M.D., Storoni, L.C., Read, R.J., 2007. Phaser crystallographic software. J Appl Crystallogr 40, 658–674. https://doi.org/10.1107/S0021889807021206

Melnyk, S., Pogribna, M., Pogribny, I.P., Yi, P., James, S.J., 2000. Measurement of Plasma and Intracellular S-Adenosylmethionine and S-Adenosylhomocysteine Utilizing Coulometric Electrochemical Detection: Alterations with Plasma Homocysteine and Pyridoxal 5J-Phosphate Concentrations. Clinical Chemistry 46, 8. https://doi.org/10.1093/clinchem/46.2.265

Murshudov, G.N., Skubák, P., Lebedev, A.A., Pannu, N.S., Steiner, R.A., Nicholls, R.A., Winn, M.D., Long, F., Vagin, A.A., 2011. *REFMAC* 5 for the refinement of macromolecular crystal structures. Acta Crystallogr D Biol Crystallogr 67, 355–367. https://doi.org/10.1107/S0907444911001314

Nicholls, R.A., Long, F., Murshudov, G.N., 2012. Low-resolution refinement tools in *REFMAC* 5. Acta Crystallogr D Biol Crystallogr 68, 404–417. https://doi.org/10.1107/S090744491105606X

Okamoto, H., Watanabe, K., Ikeuchi, Y., Suzuki, T., Endo, Y., Hori, H., 2004. Substrate tRNA Recognition Mechanism of tRNA (m7G46) Methyltransferase from Aquifex aeolicus. J. Biol. Chem. 279, 49151–49159. https://doi.org/10.1074/jbc.M408209200

Okamoto, S., Tamaru, A., Nakajima, C., Nishimura, K., Tanaka, Y., Tokuyama, S., Suzuki, Y., Ochi, K., 2007. Loss of a conserved 7-methylguanosine modification in 16S rRNA confers low-level streptomycin resistance in bacteria. Molecular Microbiology 63, 1096–1106. https://doi.org/10.1111/j.1365-2958.2006.05585.x

Park, S., Bardhan, J.P., Roux, B., Makowski, L., 2009. Simulated x-ray scattering of protein solutions using explicit-solvent models. The Journal of Chemical Physics 130, 134114. https://doi.org/10.1063/1.3099611

Purta, E., van Vliet, F., Tricot, C., De Bie, L.G., Feder, M., Skowronek, K., Droogmans, L., Bujnicki, J.M., 2005. Sequence-structure-function relationships of a tRNA (m7G46) methyltransferase studied by homology modeling and site-directed mutagenesis. Proteins 59, 482–488. https://doi.org/10.1002/prot.20454

Quigley, G., Rich, A., 1976. Structural domains of transfer RNA molecules. Science 194, 796–806. https://doi.org/10.1126/science.790568

R Core Team, 2017. R: A Language and Environment for Statistical Computing. R Foundation for Statistical Computing, Vienna, Austria.

Schrödinger, LLC, 2015. The PyMOL Molecular Graphics System, Version 5.0.

Schubert, H.L., Blumenthal, R.M., Cheng, X., 2003. Many paths to methyltransfer: a chronicle of convergence. Trends in Biochemical Sciences 28, 329–335. https://doi.org/10.1016/S0968-0004(03)00090-2

Shaheen, R., Abdel-Salam, G.M.H., Guy, M.P., Alomar, R., Abdel-Hamid, M.S., Afifi, H.H., Ismail, S.I., Emam, B.A., Phizicky, E.M., Alkuraya, F.S., 2015. Mutation in WDR4 impairs tRNA m7G46 methylation and causes a distinct form of microcephalic primordial dwarfism. Genome Biol 16, 210. https://doi.org/10.1186/s13059-015-0779-x

Tomikawa, C., Takai, K., Hori, H., 2018. Kinetic characterization of substrate-binding sites of thermostable tRNA methyltransferase (TrmB). J. Biochem 163, 10. https://doi.org/10.1093/jb/mvx068

Tomikawa, C., Yokogawa, T., Kanai, T., Hori, H., 2010. N 7-Methylguanine at position 46 (m7G46) in tRNA from Thermus thermophilus is required for cell viability at high temperatures

through a tRNA modification network. Nucleic Acids Research 38, 942–957. https://doi.org/10.1093/nar/gkp1059

Wang, K.-T., Desmolaize, B., Nan, J., Zhang, X.-W., Li, L.-F., Douthwaite, S., Su, X.-D., 2012. Structure of the bifunctional methyltransferase YcbY (RlmKL) that adds the m 7 G2069 and m 2 G2445 modifications in Escherichia coli 23S rRNA. Nucleic Acids Research 40, 5138–5148. https://doi.org/10.1093/nar/gks160

Weiss, J.N., 1997. The Hill equation revisited: uses and misuses. FASEB j. 11, 835–841. https://doi.org/10.1096/fasebj.11.11.9285481

Winn, M.D., Ballard, C.C., Cowtan, K.D., Dodson, E.J., Emsley, P., Evans, P.R., Keegan, R.M., Krissinel, E.B., Leslie, A.G.W., McCoy, A., McNicholas, S.J., Murshudov, G.N., Pannu, N.S., Potterton, E.A., Powell, H.R., Read, R.J., Vagin, A., Wilson, K.S., 2011. Overview of the CCP4 suite and current developments. Acta Crystallogr D Biol Crystallogr 67, 235–242. https://doi.org/10.1107/S0907444910045749

Zegers, I., Gigot, D., Bujnicki, J.M., Kosinski, J., Droogmans, L., 2005. Crystal structure of Bacillus subtilis TrmB, the tRNA (m7G46) methyltransferase. NAR 34, 10. https://doi.org/10.1093/nar/gkl116

Zhou, H., Liu, Q., Yang, W., Gao, Y., Teng, M., Niu, L., 2009. Monomeric tRNA (m7G46) methyltransferase from Escherichia coli presents a novel structure at the function-essential insertion. Proteins 76, 512–515. https://doi.org/10.1002/prot.22413

Manuscript to be submitted

Chapter 3 $tRNA^{His}$ is a substrate for human methyltransferase DNMT2

Blersch Katharina F[1], Hahn Fabienne[1], Neumann Piotr[1], Ficner Ralf[1*]

[1]Department of Molecular Structural Biology, Institute of Microbiology and Genetics, GZMB, Georg-August-University Göttingen, Justus-von-Liebig Weg 11, 37077 Göttingen, Germany

* To whom correspondence should be addressed: Ralf Ficner, Department of Molecular Structural Biology, Institute for Microbiology and Genetics, Georg-August-University Goettingen, 37077 Goettingen, Germany; rficner@uni-goettingen.de

Abstract

The DNA methyltransferase Dnmt2 belongs to the cytosine-5 methylation (m^5C) writer enzymes. Even though Dnmt2 exhibits residual DNA methyltransferase activity, higher activity levels could be observed on tRNA. Dnmt2 specifically methylates cytosine at position 38 in $tRNA^{Asp}$, $tRNA^{Gly}$, and $tRNA^{Val}$. In *Schizosaccharomyces pombe* and *Dictyostelium discoideum*, C38 methylation is strongly influenced by the adjacent queuosine (Q) modification at position 34. Q34 increases methylation efficiency of Dnmt2 and leads to a better discrimination of cognate- and near-cognate codons, thus influencing translation accuracy. Q34 is present in $tRNA^{Asp}$, $tRNA^{His}$, $tRNA^{Asn}$, and $tRNA^{Tyr}$, all containing the $G_{34}U_{35}N_{36}$ anticodon sequence. Besides $tRNA^{Asp}$, only $tRNA^{His}$ harbours at position 38 a cytosine. However, m^5C38 in $tRNA^{His}$ has not been observed. Using fluorescence polarization, we examined human Dnmt2 binding to human $tRNA^{His}$ in the unmodified (G34) and queuosinylated (Q34) form. Furthermore, applying methyltransferase activity assays, we tested the ability of human Dnmt2 to methylate $tRNA^{His}$ at position 38. We found that Dnmt2 is able to bind $tRNA^{His}$ *in vitro* and shows methyl transfer activity on $tRNA^{His}$. Additionally, Dnmt2 methyltransferase activity appears to be pH-dependent, as at pH 8.0 $tRNA^{His}$ is strongly methylated, whereas at physiological pH, $tRNA^{Asp}$ represents the better substrate for Dnmt2. We were the first to show human Dnmt2 activity on $tRNA^{His}$ and emphasizes the impact of Q on m^5C38 methylation.

Keywords: Dnmt2, queuosine, cytosine methylation, tRNA, tRNAHis

3.1 Introduction

Deoxyribonucleic acid (DNA) consists of four bases forming Watson-Crick pairs, in which adenine (A) pairs with thymine (T) and guanine (G) with cytosine (C). These Watson-Crick pairs are the base of the genetic code and can be expanded by post-transcriptional nucleotide modification in the eukaryotic, bacterial, and archaeal kingdoms of life (Carell et al., 2012). The most heavily modified nucleic acid species is transfer ribonucleic acid (tRNA) with more than 90 modifications found to date (Boccaletto et al., 2018). Depending on the position within the tRNA body, tRNA modifications exert different tasks. While modifications in the tRNA core and acceptor arm mainly modulate tertiary stability and flexibility of tRNAs, modifications within the anticodon-loop are known to affect codon-anticodon interaction and thereby have an impact on the fidelity and rate of translation (Helm, 2006; Tuorto et al., 2015).

Cytosine-5 methylation (m^5C) is a commonly found modification in DNA as an epigenetic regulator, as well as in RNA, where it is highly conserved in tRNA (reviewed in Gilbert et al., 2016; Jones, 2012; Motorin et al., 2009; Tuorto and Lyko, 2016). In tRNA, m^5C is found in the tRNA core

at positions 48, 49, and 72, and in the anticodon loop at positions 34 and 38 (Motorin et al., 2009). The lack of m^5C at these positions was found to hamper codon-anticodon interaction (Tuorto et al., 2015), tRNA folding and stability (Tuorto et al., 2012), reading frame maintenance (Urbonavicius et al., 2001), and protection from cleavage (Schaefer et al., 2010). On the other hand, the presence of m^5C38 in $tRNA^{Asp}$ promotes aminoacylation *in vitro* (Shanmugam et al., 2015) and translational accuracy (Tuorto et al., 2015). C38 methylation of $tRNA^{Asp}$ is performed by the DNA methyltransferase 2 (Dnmt2). Dnmt2 transfers the methyl group from S-adenosylmethionine (SAM) to the C5 atom of cytosine to generate 5-methylcytidine. Initially, Dnmt2 activity was thought to act as DNA methyltransferase (MTase), but turned out to be an RNA modifying enzyme with $tRNA^{Asp}$ as substrate (Goll et al., 2006). Since then, more tRNA substrates for Dnmt2 were found ($tRNA^{Val}$, $tRNA^{Gly,}$ $tRNA^{Glu}$) (reviewed Bohnsack et al., 2019; Jeltsch et al., 2017). Recent studies on *Schizosaccaromyces pombe* Dnmt2 (Pmt1) showed the dependency of $tRNA^{Asp}$ C38 methylation on prior queuosine (Q) modification (Müller et al., 2015). Q is a hypermodified nucleoside at position 34 of $tRNA^{Asp}$, $tRNA^{His}$, $tRNA^{Asn}$, and $tRNA^{Tyr}$, which share the anticodon sequence $G_{34}U_{35}N_{36}$ (reviewed Fergus et al., 2015). While prokaryotes are able to synthesize Q *de novo*, eukaryotes salvage Q from the intestinal flora as a micronutrient. The Q base queuine is a 7-deaza-guanine derivative with an additional amino-methyl side chain and a cyclopentanediol moiety (Harada and Nishimura, 1972). Q is incorporated into eukaryotic tRNAs by the tRNA-guanine-transglycosylase (TGT) via a base exchange mechanism (Romier et al., 1996). *In vitro* methylation of *S. pombe* $tRNA^{Asp}$ by Pmt1 showed that Pmt1 is not strictly dependent on prior queuosine modification, since the unmodified tRNA is also a methylation substrate. However, the *in vitro* activity of Pmt1 is stimulated in the presence of Q at position 34, suggesting a direct interaction of Dnmt2 and Q (Johannsson et al., 2018; Müller et al., 2015).

To the best of our knowledge, the question how Dnmt2 recognizes its substrate is still not answered in detail. Johannsson *et al* (2018) proposed a Dnmt2-tRNA complex model on basis of molecular docking studies coupled with experimental data of cross-linking experiments (Johannsson et al., 2018). In this model, the anticodon loop, harbouring Q34 and the methylation target C38, is placed in a groove between the large and small domain of Dnmt2, which also accommodates the methyl group donor SAM. Positive residues surrounding this pocket are thought to form the interaction site with the negatively charged tRNA backbone. Q34 is pointing toward the protein surface with the cyclopentanediol moiety facing the SAM binding area. This brings Q in close proximity to the active site and suggests a direct effect of Q on the MTase activity.

The involvement of Q on Dnmt2 activity raised the question, whether other Q-modified tRNAs containing C38 ($tRNA^{His}$ and $tRNA^{Asp}$) could act as a substrate for Dnmt2. Previous bisulfate sequencing studies on tRNAs from *S. pombe* and *D. discoideum* failed to recognize m^5C38 in $tRNA^{His}$

(Becker et al., 2012; Müller et al., 2015). Therefore, we addressed this question using *in vitro* based experiments. Applying fluorescence polarization binding assays, we tested the ability of Dnmt2 to recognize and bind the tested tRNAs $tRNA^{His}$ and $tRNA^{Asp}$. Furthermore, the impact of the hypermodified base Q was analysed using $Q_{34}tRNA^{His}$ and $Q_{34}tRNA^{Asp}$ substrates. Additionally, Dnmt2 activity was analysed using luminescence-based methyltransferase activity assays. We demonstrated the ability of human Dnmt2 to strongly bind $tRNA^{His}$ and $tRNA^{Asp}$ in their unmodified and queuosinylated form. Furthermore, we showed that Dnmt2 can methylate $tRNA^{His}$ *in vitro*, however, to low extends. Additionally, Dnmt2 methyltransferase activity demonstrated a pH-dependent activity, as $tRNA^{His}$ was strongly methylated at pH 8.0, whereas at pH 7.4 $tRNA^{Asp}$ showed higher modification levels. Lastly, we suspect two nucleotides in the tRNA anticodon stem, C32 and A37, to be important in Dnmt2 substrate recognition since they are highly conserved in Dnmt2 enzymes and showed to be in close proximity to Dnmt2.

3.2 Material and Methods

3.2.1 Expression and purification

Homo sapiens Dnmt2 (*hs*Dnmt2) was expressed and purified following Johannsson *et al* (2018). In brief, *hs*Dnmt2 was expressed from a pGEX-6P-1 expression vector as N-terminal GST-fusion protein in *Escherichia coli* BL21 (DE3) cells using autoinduction. Cell cultures were incubated at 16°C for 50 h prior harvesting and storage at -20°C. Cells were disrupted by microfluidization (M-110S Microfluidizer) with 50 mM Tris/HCl pH 7.5, 150 mM NaCl, 1M LiCl, 2 mM DTT. Cell debris was separated from soluble proteins by ultracentrifugation at 50000 g for 30 min at 4°C. The GST fusion protein GST-*hs*Dnmt2 was loaded on a Glutathione Sepharose Fast Flow column (GE Healthcare) in 50 mM Tris/HCl pH 7.5, 150 mM NaCl, 2 mM DTT and eluted with the supplementation of 30 mM reduced glutathione. After GST cleavage (1:80 w/w PreScission Protease), GST tag was removed using a Glutathione Sepharose Fast Flow column and *hs*Dnmt2 was further purified via Superdex S75 size exclusion chromatography, concentrated to 4 mg/ml and stored at -80°C until further use.

3.2.2 In vitro transcription and tRNA purification

Homo sapiens $tRNA^{Asp}$ (*hs*$tRNA^{Asp}$) was transcribed from a linearized vector in a run-off *in vitro* transcription containing T7 Polymerase, 10 mM rNTPs each, 1x HT buffer (30 mM HEPES pH 8.0, 25 mM $MgCl_2$, 10 mM DTT, 2 mM Spermidine, 0.01% Triton X-100). The reaction was incubated for 3 h at 37°C, PP_i was pelleted and the reaction was terminated by the addition of 50 mM EDTA. *hs*$tRNA^{Asp}$ was purified by ion exchange chromatography (1 ml Resource-Q GE). The *in vitro* transcription reaction was applied to the resin with IEX-A buffer (20 mM HEPES pH 7.5, 20 mM

KCl) and eluted with a linear gradient from 10-35% IEX-B buffer (20 mM HEPES pH 7.5, 2 M KCl). Fractions containing pure tRNA were pooled, ethanol precipitated, and subsequently dissolved in ddH_2O. The pure tRNA was stored at -20°C until further use. Human $tRNA^{His}$ (*hs*$tRNA^{His}$) was transcribed from oligonucleotides coding for the mature tRNA sequence (Sigma; His_forward: 5´-GGAATTCTAATACGACTCACTATAGGGCCGTGATCGTATAGTGGTTAGTACTCTGCGTTGTGGCCGCA GCAACCTCGGTTCGAATCCGAGTCACGGCACCA-3´, His_reverse: 5´-TGGTGCCGTGACTCGGATT CGAACCGAGGTTGCTGCGGCCACAACGCAGAGTACTAACCACTATACGATCACGGCCCTATAGTGAGTC GTATTAGAATTCC-3´) and purified, precipitated, and stored as described above.

3.3.3 tRNA labelling and binding

tRNA was labelled with fluorescein-5-thiosemicarbazide (Sigma Aldrich) according to Johannsson *et al* (2018). Unreacted fluorophore was removed using Zeba Spin desalting columns (Thermofisher Scientific). *hs*Dnmt2 was stepwise diluted in assay buffer in the range of 0.049 to 20 µM (20 mM Tris/HCl pH 7.5, 50 mM NaCl, 2 mM DTT). The reaction was incubated for 30 min and anisotropy was measured using a multimode microplate reader (PerkinElmer). R software, v3.x (R Core Team, 2017) was used to fit the data using the following equation $y = A_2 + (A_1 - A_2) / (1 + (x/x_0)^P)$ and the binding affinity K_d was analysed.

3.3.4 Methyltransferase assay

*hs*Dnmt2 kinetics were analysed with the MTase-Glo methyltransferase assay (Promega), following manufacturers recommendations. In brief, 1 µM Dnmt2 were mixed with 0.049 to 60 µM $G_{34}tRNA^{Asp}$, 0.039 to 40 µM $Q_{34}tRNA^{Asp}$, 0.039 to 40 µM $G_{34}tRNA^{His}$, 0.029 to 30 µM $Q_{34}tRNA^{His}$, 40 µM SAM and incubated for 30 min at RT. The reaction was stopped adding 0.5 % TFA. After the addition of the MTase-Glo reaction solution and MTase-Glo detection solution, luminescence was measured using a multimode microplate reader (PerkinElmer). Data was transformed to represent SAM consumption using a SAH standard curve. Using R, we fitted the Hill equation $v = V_{max} * x^n / (k^n+x^n)$ via the least square method which calculated the maximum velocity (V_{max}), the binding affinity (k), and the hill coefficient (n) (R Core Team, 2017).

3.3 Results

3.3.1 Human Dnmt2 is able to bind $tRNA^{His}$

Since the discovery that not only DNA but also tRNA serve as substrate for Dnmt2 (Goll et al., 2006), much effort was done to identify further Dnmt2 tRNA substrates. The increased sensitivity of methods detecting nucleotide modifications in very low amounts of isolated RNAs led to the identification of several other tRNA substrates, including $tRNA^{Glu}$, $tRNA^{Gly}$, and $tRNA^{Val}$, in

mammals, flies, fungi, and bacteria (Ehrenhofer-Murray, 2017). Cytosine methylation efficiency could be further stimulated by prior modification of the neighboring nucleoside Q (Johannsson et al., 2018; Müller et al., 2015). This raised the question, whether other tRNAs containing both, C38 and Q34, are as well substrates for Dnmt2. And if so, whether prior Q modification changes substrate affinity and methylation efficiency as reported previously for $tRNA^{Asp}$ of *S. pombe* (Johannsson et al., 2018; Müller et al., 2015).

Analysis of the four Q34 containing tRNAs showed that beside $tRNA^{Asp}$, which is known to serve as substrate for Dnmt2 *in vitro* and *in vivo*, only $tRNA^{His}$ contains at position 38 a cytosine. So far, $tRNA^{His}$ was not detected to serve as target for Dnmt2 *in vivo* (Müller et al., 2015). Therefore, we tested the ability of human Dnmt2 on binding and possibly methylating human $tRNA^{His}$ *in vitro*. We performed a fluorescence polarization (FP) binding assay as reported in Johannsson *et al.* (2018) and analyzed $tRNA^{His}$ and the well-identified substrate $tRNA^{Asp}$ in their unmodified (G34) and queuosinylated form (Q34, Figure 3.1). $tRNA^{Asp}$ and $tRNA^{His}$ were generated via *in vitro* transcription, queuosinylated at position 34 via TGT base exchange, and labelled with fluorescein. Subsequently, Dnmt2 was titrated against the labelled tRNAs and binding curves were analysed. Quantitative analysis of the FP assay revealed a sigmoidal binding curve for all four tRNA substrates. Dnmt2 is able to bind $G_{34}tRNA^{His}$ in the micro molar-range with a K_d of 0.78 ± 0.082 µM (Figure 3.1). The Q-modification lowers the dissociation constant K_d to a value of 0.597 ± 0.034 µM ($Q_{34}tRNA^{His}$). Hence, base exchange in $tRNA^{His}$ from G34 to Q34 led to an increase in binding strength. In comparison, the common Dnmt2 target $tRNA^{Asp}$ in the unmodified form binds less strong to Dnmt2 (K_d = 0.897 ± 0.043 µM; Figure 3.1). Interestingly, base exchange to Q34 led to a smaller increase in binding affinity, resulting in a K_d of 0.817 ± 0.038 µM ($Q_{34}tRNA^{Asp}$). Taken together, we showed that human Dnmt2 is able to bind $tRNA^{His}$ *in vitro*. Our experiments further corroborated published data on $tRNA^{Asp}$ binding by Dnmt2 (Johannsson et al., 2018). Additionally, we demonstrated that queuosinylation of $tRNA^{Asp}$ and $tRNA^{His}$ resulted in an increased binding strength for both $tRNA^{Asp}$ and $tRNA^{His}$.

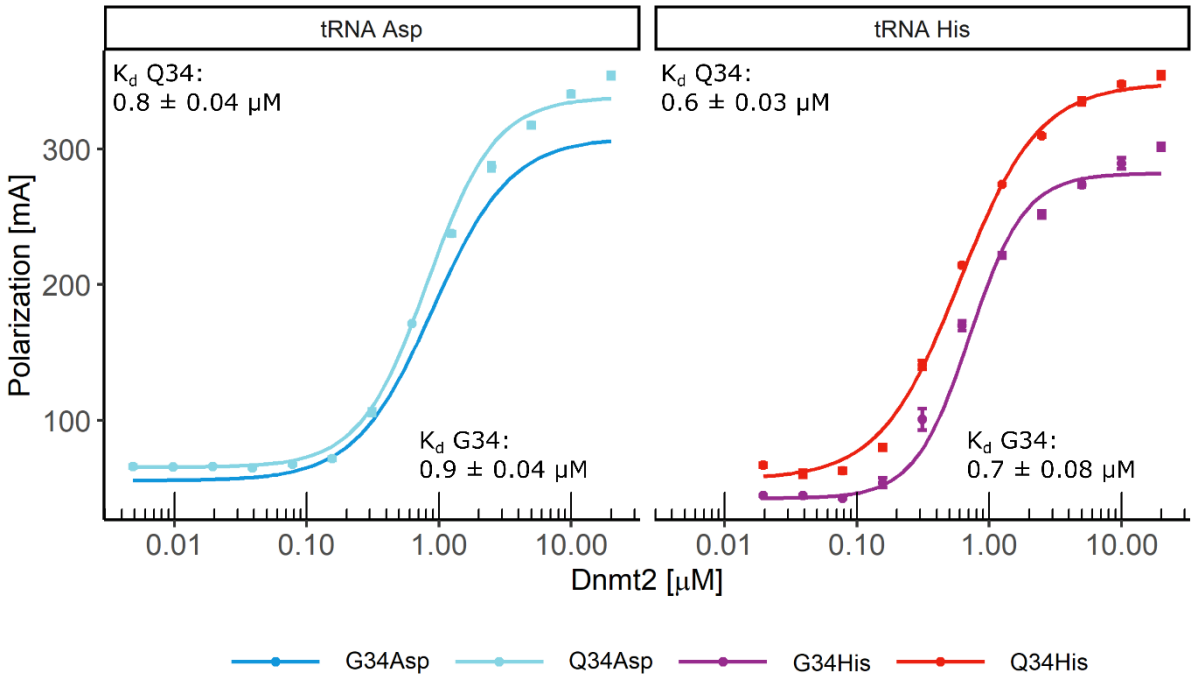

Figure 3.1: Quantitative fluorescence polarization binding assay. Comparison of binding affinities of human Dnmt2 to human G34 $tRNA^{Asp}$ (0.897 ± 0.043 µM) and Q34 $tRNA^{Asp}$ (0.817 ± 0.038 µM; left panel), and G34 (0.718 ± 0.082 µM) and Q34 $tRNA^{His}$ (0.597 ± 0.034 µM; right panel). G34 and Q34 tRNAs are indicated by colour. Measurements were performed in three indepentend experimental replicates. Results are shown as Mean ± SD with error bars of SD (n=3).

3.3.2 Dnmt2 methylates $tRNA^{His}$ in pH-dependent manner

Even though $tRNA^{His}$ is modified by Q and carries C38, *in vivo* methylation of $tRNA^{His}$ is unknown, since it has been amenable to conventional RNA bisulfate sequencing and combined RNA bisulfite treatment with next-generation sequencing (Becker et al., 2012; Müller et al., 2015). We therefore wanted to test, whether Dnmt2 is able to methylate $tRNA^{His}$ in its unmodified and queuosinylated form *in vitro*. Using the luminescence based MTase activity assay MTAse-Glo (Promega) and subsequent analysis of the data by applying the Hill equation, gave insight into the maximum velocity of the reaction (V), the binding affinity (K_m), and the Hill coefficient (n; summarized in Table 3.1). The Hill coefficient is a measure of cooperativity during catalysis and is in general thought as, values for the Hill coefficient $n < 1$ indicate negative cooperativity, $n > 1$ shows positive cooperativity, whereas values of $n = 1$ indicates independent binding in the enzymatic reaction (Weiss, 1997).

At standard assay conditions of pH 8.0, human $G_{34}tRNA^{His}$ was successfully methylated by Dnmt2 with a turnover rate k_{cat} of $0.9 * 10^3\ s^{-1} \pm 0.1 * 10^3\ s^{-1}$ with a Hill coefficient of $n=1.3 \pm 0.15$, indicating cooperativity during catalysis (Figure 3.2A, right panel). However, the methyltransferase reaction at the highest substrate concentration of 48 µM did not reach a plateau state yet and maximum luminescence was calculated to be reached at $2.2 * 10^3\ s^{-1} \pm 0.8 * 10^3\ s^{-1}$ according to the Hill

equation. G34Q base exchange decreased MTase activity to very low levels (Figure 3.2A, right panel).

To be able to compare and interpret these results, we additionally measured the previously reported Dnmt2 substrate $G_{34}tRNA^{Asp}$ and $Q_{34}tRNA^{Asp}$ for methyl acceptance activity (Figure 3.2A, left panel). $G_{34}tRNA^{Asp}$ reached a k_{cat} value of 3.2 $*10^3$ s^{-1} ± 0.1 $*10^3$ s^{-1} with n=1.0 ± 0.03. The Q modified $tRNA^{Asp}$ in turn exhibited half of the k_{cat} of 1.9 $*10^3$ s^{-1} ± 0.2 $*10^3$ s^{-1} with a Hill coefficient of n=1.0 ± 0.09. This data showed the clear ability of Dnmt2 to methylate $tRNA^{His}$ *in vitro* and strengthened previous findings of Dnmt2-mediated $tRNA^{Asp}$ methylation. However, the previously reported sigmoidal curve for Dnmt2 observed at pH 7.4 could not be observed. Therefore, all experiments were repeated at pH 7.4, the standard assay (and physiological) pH for Dnmt2 enzymes. At pH 7.4, $tRNA^{His}$ methyl group acceptance activity was very low and data could not be statistically analysed (Figure 3.2B, right panel). The conserved Dnmt2 substrate $tRNA^{Asp}$ was methylated with a k_{cat} of 2.2 $*10^3$ s^{-1} ± 0.09 $*10^3$ s^{-1} and decreased to a k_{cat} of 1.1 $*10^3$ s^{-1} ± 0.02 $*10^3$ s^{-1} upon Q modification. The Hill coefficient shifted from n=1.8 ± 0.3to n=1.2 ± 0.06 (Figure 3.2B, left panel). This indicates that the Q modified $tRNA^{Asp}$ had fewer negative cooperative effects on catalysis of Dnmt2, but results at the same time in lower turnover rates.

Table 3.1 Methyltransferase assay of human Dnmt2 with $tRNA^{His}$ and $tRNA^{Asp}$. Independent duplicate measurements were performed, analysed using the least square method to fit the Hill equation to the data and values for maximum velocity (V_{max}), binding affinity (K_d), and the Hill coefficient (n) were obtained. Standard deviation and significance for each substrate was calculated ('***' p<0.001; '**' p<0.01; '*' p<0.05).

tRNA pH 7.4	V [nM/s]	K_m [µM]	n	k_{cat} $*10^3$ [s^{-1}]	k_{cat}/K_m $*10^3$ [$\mu M^{-1} s^{-1}$]
G34 tRNA Asp	2.2 ∓ 0.09 ***	6.2 ∓ 0.6 ***	1.8 ∓ 0.3 ***	2.2 ∓ 0.09	0.4 ∓ 0.15
Q34 tRNA Asp	2.4 ∓ 0.1 ***	16.2 ∓ 1.6 ***	1.2 ∓ 0.06 ***	1.1 ∓ 0.02 ***	0.07 ∓ 0.01
G34 tRNA His	-	-	-	-	-
Q34 tRNA His	-	-	-	-	-

tRNA pH 8.0	V [nM/s]	K_m [µM]	n	k_{cat} $*10^3$ [s^{-1}]	k_{cat}/K_m $*10^3$[$\mu M^{-1} s^{-1}$]
G34 tRNA Asp	3.2 ∓ 0.1 ***	10.4 ∓ 0.6 ***	1.0 ∓ 0.03 ***	3.2 ∓ 0.1	0.3 ∓ 0.1
Q34 tRNA Asp	1.9 ∓ 0.2 ***	14.2 ∓ 4.0 **	1.0 ∓ 0.09 **	1.9 ∓ 0.2	0.1 ∓ 0.05
G34 tRNA His	2.2 ∓ 0.8 *	64.3 ∓ 32.2 ·	1.3 ∓ 0.15 ***	2.2 ∓ 0.8	0.03 ∓ 0.02
Q34 tRNA His	-	-	-	-	-

Taken together, we showed that human $tRNA^{His}$ is a substrate for human Dnmt2 *in vitro*, and that this effect is pH-dependent. Changing the pH from alkaline to physiological conditions reduced the $tRNA^{His}$ methyl group acceptance activity. Additionally, we demonstrated that Q modification has an impact in human Dnmt2 catalysis and reduces negative cooperative effects during m^5C modification, which is in agreement with studies on *S. pombe* Dnmt2 (Johannsson et al., 2018).

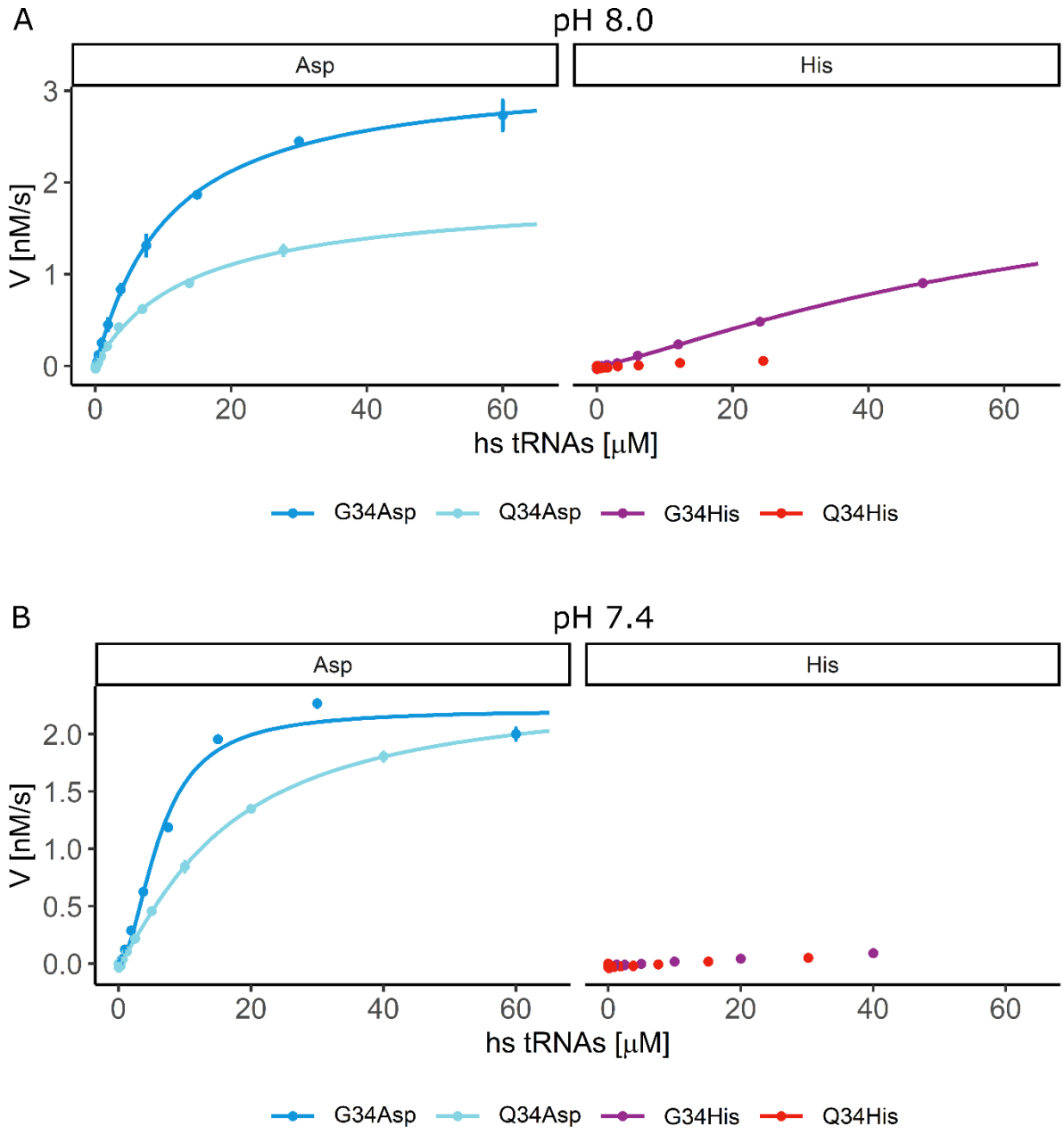

Figure 3.2: Methyltransferase activity assay of human Dnmt2 with G/Q34 $tRNA^{Asp}$ and $tRNA^{His}$ (indicated by colour) at pH 7.4 (A) and pH 8.0 (B). Measurements were performed as independent duplicates with increasing tRNA concentration. Results are shown as Mean ± SD with error bars of SD (n=2). The Hill equation was fitted to the data using the least square method. Values for V_{max}, K_d, and the Hill coefficient, as well as their statistical significance were obtained.

3.3.3 Model of $tRNA^{His}$ - Dnmt2 complex highlights putative key nucleotides for Dnmt2 substrate specificity

We showed the ability of Dnmt2 to bind and modify G34/Q34 $tRNA^{His}$. Comparison of both tRNA substrates showed that at a physiological pH $tRNA^{Asp}$ is the preferred substrate over $tRNA^{His}$. Hence, difference in the tRNA sequence must be responsible for Dnmt2 substrate discrimination. Müller and colleagues (2013) reported that nucleotides C32, C34, A37, C40 could be a major

determinant for C38 methylation by Dnmt2. Therefore, we aimed to connect experimental with computational data and evaluated this nucleotide pattern with respect to the previously published Dnmt2-tRNA complex model (Johannsson et al., 2018). Modelling protein-tRNA complexes using Rosetta is a useful tool to evaluate interactions between molecules without the existence of a crystal structure. Calculation of possible tRNA orientations on Dnmt2 and subsequent scoring by their interaction surface and energetics involved in complexation generated a few top scored complex models. Combination of these models with experimental UV cross-linking data increases the confidence of the resulting models. In this study, we re-evaluated the published complex model with respect to $tRNA^{His}$ as substrate.

We first evaluated the postulated nucleotide pattern C32, C34, A37, C40 for conservation in the known Dnmt2 tRNA substrates $tRNA^{Asp}$, $tRNA^{Glu}$, $tRNA^{Gly}$ and $tRNA^{Val}$ (Figure 3.3). Nucleotides C32 and A37 are conserved between these substrates, whereas nucleotides 34 and 40 diverge due to the exchange of C by G. Further comparison with the new Dnmt2 *in vitro* substrate $tRNA^{His}$ showed the replacement of the conserved nucleotides C32 by U and A37 by G.

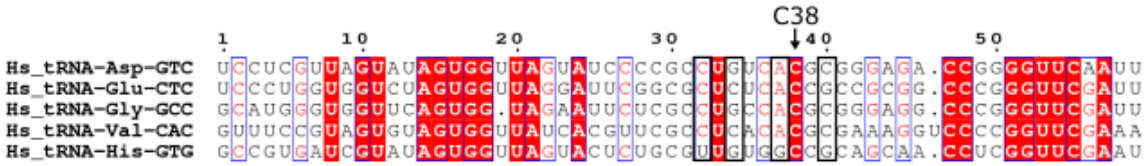

Figure 3.3: Multiple sequence alignment of annotated human Dnmt2 tRNA substrates with the addition of $tRNA^{His}$. Alignment was performed with ClustalOmega and displayed using ESPript 3.0 (Robert and Gouet, 2014). The putative nucleotide recognition pattern is highlighted with black boxes and the C38 methylation target is highlighted with an arrow.

Next, we analysed the proposed nucleotide pattern on a structural level and mapped these residues on the existing Dnmt2-tRNA complex model (Johannsson et al., 2018). The complex model showed binding of the tRNA by its anticodon stem in a negatively charged groove in the interface of the large and small domain of Dnmt2 (Figure 3.4). In this model, the proposed recognition sequence C34, A37, C40 is in close proximity with Dnmt2, except the conserved C32 which is too distant to interact with Dnmt2 directly (Figure 3.4). However, upon tRNA binding and rearrangement of the active site loop, C32 could be positioned close enough for direct interaction with Dnmt2. This close positioning of nucleotide 37 and 32 renders both nucleotides interesting positions for substrate recognition, also on a structural level.

Taken together, the proposed nucleotide recognition motive makes close contacts with Dnmt2 (Johannsson et al., 2018) and could be a determinant for Dnmt2 substrate recognition.

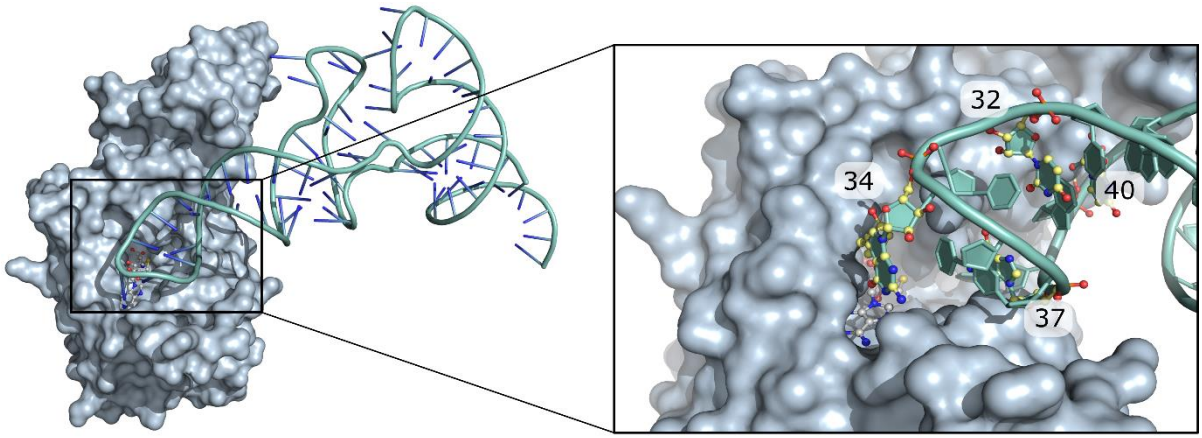

Figure 3.4: Docking model of *S. pombe* Dnmt2 with yeast $tRNA^{Asp}$ (Johannsson et al., 2018). Dnmt2 and $tRNA^{Asp}$ are presented in surface mode and as cartoon, respectively. Close-up of the anticodon-stem loop with highlighted nucleotides in ball and stick mode corresponding to the nucleotide sequence C32, C34, A37, and C40.

3.4 Discussion

In recent years, the field of RNA modification is gaining attention, since complex modification networks are elucidated through the increased sensitivity of methods detecting RNA modifications. tRNA are part of these modification networks, as their modifications can be introduced and erased in dependence on external stimuli. The realization of the dynamic nature of tRNA modifications moved tRNA modifying enzymes and the modifications themselves into the spotlight of recent research focusing on epigenetics and cancer research. Dnmt2 and its modifications are one example of enzymes and modifications, known to be part of stress response modification networks (Schaefer et al., 2010). The discovery of $tRNA^{Asp}$ as substrate for Dnmt2 (Goll et al., 2006) and the increased enzyme activity upon Q modification at position 34 (Müller et al., 2015), raised the question, whether other tRNAs containing Q34 are Dnmt2 substrates as well. This question is of special interest, since Q at the anticodon wobble position influences gene translation and prevents misreading of Asp containing proteins in human cells (Tuorto et al., 2018). Therefore, we analysed those tRNAs harbouring Q34 and C38 $tRNA^{His}$ and $tRNA^{Asp}$ for Dnmt2 binding and methyl acceptance activity.

In this study we showed the ability of human Dnmt2 to *in vitro* bind and methylate $tRNA^{His}$ in a pH-dependent manner. $tRNA^{His}$ is a member of the queuosine modified tRNAs. Our results agree with previous RNA sequencing studies that could not detect m^5C modification in $tRNA^{His}$ in *S. pombe* and *D. discoideum* at physiological pH (Müller et al., 2015). Q incorporation at position 34 resulted in both $tRNA^{Asp}$ and $tRNA^{His}$ in an increased binding affinity to Dnmt2. The dissociation constants are in the micro-molar range and are consistent with previously published data in *S.*

pombe, where Dnmt2 binds $G_{34}tRNA^{Asp}$ with a K_d of 0.96 µM (Johannsson et al., 2018). In *S. pombe* the exchange of G to Q34 led to an increase in binding strength by 0.3 µM, which could not be observed in our experiments with human Dnmt2 and $tRNA^{Asp}$. Conversion of G34 to $Q_{34}tRNA^{His}$ led to an increase in affinity of 0.12 µM, whereas $tRNA^{Asp}$ showed only slight changes of the K_d of 0.08 µM from G34 to Q34 (Figure 3.1). In human tRNAs, Q is further modified by the addition of a mannosyl moiety, resulting in mannosyl queuosine (manQ) at position 34. Previous data reported C38 methylation by Dnmt2 only in combination with manQ (Goll et al., 2006). Our data showed Dnmt2-mediated C38 modification of G34 and Q34 $tRNA^{Asp}$, leading to the conclusion that human Dnmt2 can modify Q34 tRNA in the absence of manQ. However, it would be interesting to test, whether $manQ_{34}tRNA^{Asp}$ leads to a more pronounced change in affinity as seen for *S. pombe* (Johannsson et al., 2018).

After the confirmed binding of $tRNA^{His}$ to Dnmt2, we aimed to investigated Dnmt2 MTase activity on the newly found substrate. At a slightly alkaline pH, $G_{34}tRNA^{His}$ was successfully methylated by Dnmt2 at position C38 with a k_{cat} value of 2.2 $*10^3$ s^{-1} ± 0.8 $*10^3$ s^{-1} compared to $G_{34}tRNA^{Asp}$ with a k_{cat} of 3.2 $*10^3$ s^{-1} ± 0.1 $*10^3$ s^{-1} (Figure 3.2). Given the elevated standard deviation of $tRNA^{His}$ methyltransferase reaction, human Dnmt2 methylates $tRNA^{His}$ with a comparable velocity to the common substrate $tRNA^{Asp}$. In contrast, base exchange to Q34, which was thought to increase enzyme activity, decreased methyl acceptance activity of both Dnmt2 substrates $Q_{34}tRNA^{Asp}$ and $Q_{34}tRNA^{His}$.

Dnmt2 activity seems to be further regulated in a pH-dependent manner. The MTase assays were performed at physiological conditions of pH 7.4 and at slightly alkaline conditions of pH 8.0. $tRNA^{His}$ showed high methyl acceptance activity at pH 8.0 for G34 (Figure 3.2A). At pH 7.4, measurement of $G_{34}tRNA^{His}$ and $Q_{34}tRNA^{His}$ were as low as observed for $Q_{34}tRNA^{His}$ at pH 8.0 (Figure 3.2B). Concluding, that with the lowering of the pH value, $tRNA^{His}$ changed from cognate to non-cognate tRNA. In contrast, $tRNA^{Asp}$ exhibited differences in activity between pH 7.4 and 8.0. For both $tRNA^{Asp}$ substrates, Dnmt2 turnover rates were 0.6-fold lower at pH 8.0 compared to pH 7.4. Additionally, at both assay conditions, Q-modification of $tRNA^{Asp}$ led to the decrease in turnover rate by 50%. The observed changes in substrate specificity of Dnmt2 depending on the pH might be due to changes in the physical states of $tRNA^{His}$. While at neutral pH, nucleobases do not carry electrical charges and can be protonated, at slightly alkaline conditions guanine and uracil are deprotonated (Goh et al., 2013; González-Olvera et al., 2015). This in turn disables not only G and U to form potential hydrogen bonds to C and A, respectively, but might also positively affect the active centre of Dnmt2 to be able to methylate $tRNA^{His}$. Furthermore, queuosinylation of $tRNA^{Asp}$ resulted in a lowered catalytic efficiency of human Dnmt2 for both, pH 8.0 (k_{cat}/K_m: 5.7-fold) and pH 7.4 (k_{cat}/K_m: 3-fold), contradicting results for *S. pombe* Dnmt2, where Q-modification

increased catalytic efficiency 4-fold. However, it would be important to examine the influence of manQ-tRNA^{Asp} on the catalytic efficiency of human Dnmt2, since m^{5}C$_{38}$ modification was only found in tRNA^{Asp} containing manQ34 which might increase Dnmt2 activity (Goll et al., 2006). Additionally, studies of the impact of Q-tRNA and m^{5}C$_{38}$-tRNA^{Asp} showed effects on protein translation speed. Q-deficiency in cells resulted in the accumulation of aggregates and misfolded proteins (Tuorto et al., 2018). Subsequently, the decreased catalytic efficiency of Dnmt2 on tRNA^{Asp} could represent a point of regulation.

Further, pH-dependent changes in the Hill coefficient could be observed for G to Q$_{34}$tRNA^{Asp} at pH 7.4 from n=1.8 (G34) to n=1.2 (Q34). The here reported Hill coefficients are identical to those reported earlier for *S. pombe* Dnmt2 and tRNA^{Asp} (Johannsson et al., 2018). In contrast, at alkaline pH 8.0, n values remained identical upon Q-modification and showed independent binding (n = 1.0). This indicates an influence of Q on catalysis, as shown for tRNA^{Asp} in *S. pombe* (Johannsson et al., 2018; Müller et al., 2015). However, whether cooperativity is just influenced during catalysis by Q cannot be assumed, since Q34 influenced binding of tRNAs as well. Typically, cooperativity is found in multimeric enzymes in context of allosteric ligand binding to increase or decrease affinities for a second ligand. In contrast, the authors discussed that cooperativity in monomeric enzymes is due to structural rearrangements upon substrate binding and catalysis, with the equilibrium on the site of the catalytically active conformation (Johannsson et al., 2018). Such structural rearrangements can be seen for Pro83 in the active site loop and cis-trans isomerization of this residue could result in cooperative effects. Additionally, Pro83 is in close proximity to the substrate tRNA in the complex model and could be influenced by Q, resulting in the observed decrease in cooperativity during catalysis upon Q-modification (Johannsson et al., 2018; Müller et al., 2015). Taken together, even though tRNA^{His} showed low modification levels at physiological conditions, Q34 influenced Dnmt2 activity, which was seen for both, tRNA^{His} and tRNA^{Asp}. Furthermore, cooperativity and affinity of Dnmt2 changes with the use of buffer differing in their pH. However, these are preliminary results and further biochemical analyses need to be performed in order to understand the impact of Q on MTase activity, especially of tRNA^{His}.

Lastly, we examined our data in a structural context. In recent years, tRNA mutation studies tried to pinpoint recognition motifs on the tRNA molecule by exchanging parts of cognate tRNAs with non-cognate tRNAs. For example, two nucleotides of the variable region of murine tRNA^{Glu} (non-cognate tRNA) were inserted to murine tRNA^{Asp} (cognate tRNA), resulting in a decrease of Dnmt2 methyltransferase activity (Shanmugam et al., 2015). These experiments showed that small changes in the tRNA sequence can alter substrate recognition. Müller *et al.* (2013) reported the nucleotide pattern C32, C34, A37, C40 as a possible RNA recognition determinant. Comparison of known Dnmt2 substrates with the tRNA^{His} nucleotide sequence, showed differences at conserved

positions C32 and A37 (Figure 3.3). Both nucleotides are in close proximity to Dnmt2 in the Dnmt2-tRNA^{Asp} complex model by Johannsson *et al*. (2018) (Figure 3.4). Interaction of Dnmt2 with C32 and A37 might enable Dnmt2 to discriminate between substrate and non-substrate tRNAs. The questions, whether Dnmt2 activity on tRNA^{His} is just an artefact seen in *in vitro* experiments, remains open and needs to be addressed. Binding and methyltransferase activity assays with U32C and G37A tRNA^{His} would be useful to validate if these positions are in fact recognition determinants for Dnmt2.

3.5 Conclusion

In this study we examined substrate specificity of human Dnmt2. We showed the ability of Dnmt2 to bind tRNA^{His} and tRNA^{Asp} in their unmodified and Q-modified form. In cell free conditions, we could show the direct influence of Q34 on binding affinities, where tRNA^{His} showed higher affinities towards Dnmt2 than tRNA^{Aps} and base exchange from G34 to Q34 increased binding strength. Further methyltransferase activity assays demonstrated the ability of Dnmt2 to modify tRNA^{His} and tRNA^{Asp}. In contrast to the strengthened binding, Q decreases the methylation velocity for tRNA^{His} and tRNA^{Asp}. Furthermore, we applied the Hill equation to analyse the obtained data which gave an additional value describing cooperativity during catalysis. tRNA^{Asp} showed a decrease of the hill coefficient upon Q34 modification at pH 7.4. This describes a direct influence of Q34 on human Dnmt2 C38 methyltransferase activity by positioning Q34 to the active site. Comparison of the tRNA^{His} nucleotide sequence with reported Dnmt2 tRNA substrate sequences revealed differences in tRNA^{His} at conserved nucleotide positions C32 and A37. These nucleotides are positioned close to Dnmt2 in the tRNA-Dnmt2 complex model. Using our experimental and structural data, we condensed the reported nucleotide pattern to nucleotides C32 and A37 which could be used as determinants for Dnmt2 substrate specificity. Taken together, we show the ability of human Dnmt2 to methylate tRNA^{His} in a Q-dependent and pH-dependent manner. We further suspect two nucleotides located in the anticodon stem to drive substrate specificity of Dnmt2.

3.6 Acknowledgements

Human tRNA-guanine-transglycosylase (TGT) was kindly provided by Sven Johannsson.

3.7 References

Becker, M., Müller, S., Nellen, W., Jurkowski, T.P., Jeltsch, A., Ehrenhofer-Murray, A.E., 2012. Pmt1, a Dnmt2 homolog in Schizosaccharomyces pombe, mediates tRNA methylation in response to nutrient signaling. Nucleic Acids Research 40, 11648–11658. https://doi.org/10.1093/nar/gks956

Boccaletto, P., Machnicka, M.A., Purta, E., Piątkowski, P., Bagiński, B., Wirecki, T.K., de Crécy-Lagard, V., Ross, R., Limbach, P.A., Kotter, A., Helm, M., Bujnicki, J.M., 2018. MODOMICS: a database of RNA modification pathways. 2017 update. Nucleic Acids Research 46, D303–D307. https://doi.org/10.1093/nar/gkx1030

Bohnsack, K., Höbartner, C., Bohnsack, M., 2019. Eukaryotic 5-methylcytosine (m5C) RNA Methyltransferases: Mechanisms, Cellular Functions, and Links to Disease. Genes 10, 102. https://doi.org/10.3390/genes10020102

Carell, T., Brandmayr, C., Hienzsch, A., Müller, M., Pearson, D., Reiter, V., Thoma, I., Thumbs, P., Wagner, M., 2012. Structure and Function of Noncanonical Nucleobases. Angew. Chem. Int. Ed. 51, 7110–7131. https://doi.org/10.1002/anie.201201193

Ehrenhofer-Murray, A., 2017. Cross-Talk between Dnmt2-Dependent tRNA Methylation and Queuosine Modification. Biomolecules 7, 14. https://doi.org/10.3390/biom7010014

Fergus, C., Barnes, D., Alqasem, M., Kelly, V., 2015. The Queuine Micronutrient: Charting a Course from Microbe to Man. Nutrients 7, 2897–2929. https://doi.org/10.3390/nu7042897

Gilbert, W.V., Bell, T.A., Schaening, C., 2016. Messenger RNA modifications: Form, distribution, and function. Science 352, 1408–1412. https://doi.org/10.1126/science.aad8711

Goh, G.B., Knight, J.L., Brooks, C.L., 2013. pH-Dependent Dynamics of Complex RNA Macromolecules. J. Chem. Theory Comput. 9, 935–943. https://doi.org/10.1021/ct300942z

Goll, M.G., Kirpekar, F., Maggert, K.A., Yoder, J.A., Hsieh, C.-L., Zhang, X., Golic, K.G., Jacobsen, S.E., Bestor, T.H., 2006. Methylation of tRNA Asp by the DNA Methyltransferase Homolog Dnmt2. Science 311, 395–398. https://doi.org/10.1126/science.1120976

González-Olvera, J.C., Martínez-Reyes, J., González-Jasso, E., Pless, R.C., 2015. Determination of pKa values for deprotonable nucleobases in short model oligonucleotides. Biophysical Chemistry 206, 58–65. https://doi.org/10.1016/j.bpc.2015.07.001

Harada, F., Nishimura, S., 1972. Possible anticodon sequences of tRNAHis, tRNAAsn, and tRNAAsp from Escherichia coli. Universal presence of nucleoside O in the first position of the anticodons of these transfer ribonucleic acid. Biochemistry 11, 301–308. https://doi.org/10.1021/bi00752a024

Helm, M., 2006. Post-transcriptional nucleotide modification and alternative folding of RNA. Nucleic Acids Research 34, 721–733. https://doi.org/10.1093/nar/gkj471

Jeltsch, A., Ehrenhofer-Murray, A., Jurkowski, T.P., Lyko, F., Reuter, G., Ankri, S., Nellen, W., Schaefer, M., Helm, M., 2017. Mechanism and biological role of Dnmt2 in Nucleic Acid Methylation. RNA Biology 14, 1108–1123. https://doi.org/10.1080/15476286.2016.1191737

Johannsson, S., Neumann, P., Wulf, A., Welp, L.M., Gerber, H.-D., Krull, M., Diederichsen, U., Urlaub, H., Ficner, R., 2018. Structural insights into the stimulation of S. pombe Dnmt2 catalytic efficiency by the tRNA nucleoside queuosine. Sci Rep 8, 8880. https://doi.org/10.1038/s41598-018-27118-5

Jones, P.A., 2012. Functions of DNA methylation: islands, start sites, gene bodies and beyond. Nat Rev Genet 13, 484–492. https://doi.org/10.1038/nrg3230

Motorin, Y., Lyko, F., Helm, M., 2009. 5-methylcytosine in RNA: detection, enzymatic formation and biological functions. Nucleic Acids Research 38, 1415–1430. https://doi.org/10.1093/nar/gkp1117

Müller, M., Hartmann, M., Schuster, I., Bender, S., Thüring, K.L., Helm, M., Katze, J.R., Nellen, W., Lyko, F., Ehrenhofer-Murray, A.E., 2015. Dynamic modulation of Dnmt2-dependent tRNA methylation by the micronutrient queuine. Nucleic Acids Res 43, 10952–10962. https://doi.org/10.1093/nar/gkv980

Müller, S., Windhof, I.M., Maximov, V., Jurkowski, T., Jeltsch, A., Forstner, K.U., Sharma, C.M., Graf, R., Nellen, W., 2013. Target recognition, RNA methylation activity and transcriptional regulation of the Dictyostelium discoideum Dnmt2-homologue (DnmA). Nucleic Acids Research 41, 8615–8627. https://doi.org/10.1093/nar/gkt634

R Core Team, 2017. R: A Language and Environment for Statistical Computing. R Foundation for Statistical Computing, Vienna, Austria.

Robert, X., Gouet, P., 2014. Deciphering key features in protein structures with the new ENDscript server. Nucleic Acids Research 42, W320–W324. https://doi.org/10.1093/nar/gku316

Romier, C., Reuter, K., Suck, D., Ficner, R., 1996. Crystal structure of tRNA-guanine transglycosylase: RNA modification by base exchange. The EMBO Journal 15, 2850–2857. https://doi.org/10.1002/j.1460-2075.1996.tb00646.x

Schaefer, M., Pollex, T., Hanna, K., Tuorto, F., Meusburger, M., Helm, M., Lyko, F., 2010. RNA methylation by Dnmt2 protects transfer RNAs against stress-induced cleavage. Genes & Development 24, 1590–1595. https://doi.org/10.1101/gad.586710

Shanmugam, R., Fierer, J., Kaiser, S., Helm, M., Jurkowski, T.P., Jeltsch, A., 2015. Cytosine methylation of tRNA-Asp by DNMT2 has a role in translation of proteins containing poly-Asp sequences. Cell Discov 1, 15010. https://doi.org/10.1038/celldisc.2015.10

Tuorto, F., Herbst, F., Alerasool, N., Bender, S., Popp, O., Federico, G., Reitter, S., Liebers, R., Stoecklin, G., Gröne, H., Dittmar, G., Glimm, H., Lyko, F., 2015. The tRNA methyltransferase Dnmt2 is required for accurate polypeptide synthesis during haematopoiesis. EMBO J 34, 2350–2362. https://doi.org/10.15252/embj.201591382

Tuorto, F., Legrand, C., Cirzi, C., Federico, G., Liebers, R., Müller, M., Ehrenhofer-Murray, A.E., Dittmar, G., Gröne, H., Lyko, F., 2018. Queuosine-modified tRNAs confer nutritional control of protein translation. EMBO J 37. https://doi.org/10.15252/embj.201899777

Tuorto, F., Liebers, R., Musch, T., Schaefer, M., Hofmann, S., Kellner, S., Frye, M., Helm, M., Stoecklin, G., Lyko, F., 2012. RNA cytosine methylation by Dnmt2 and NSun2 promotes tRNA stability and protein synthesis. Nat Struct Mol Biol 19, 900–905. https://doi.org/10.1038/nsmb.2357

Tuorto, F., Lyko, F., 2016. Genome recoding by tRNA modifications. Open Biol. 6, 160287. https://doi.org/10.1098/rsob.160287

Urbonavicius, J., Qian, Q., Durand, J.M., Hagervall, T.G., Björk, G.R., 2001. Improvement of reading frame maintenance is a common function for several tRNA modifications. EMBO J 20, 4863–4873. https://doi.org/10.1093/emboj/20.17.4863

Weiss, J.N., 1997. The Hill equation revisited: uses and misuses. FASEB j. 11, 835–841. https://doi.org/10.1096/fasebj.11.11.9285481

Manuscript to be submitted

Chapter 4 Structural analysis of the tRNA-modifying ribosyltransferase-isomerase QueA

Katharina F. Blersch[1], Piotr Neumann[1], Ralf Ficner[1*]

[1] Department of Molecular Structural Biology, Institute of Microbiology and Genetics, GZMB, Georg-August-University Goettingen, Justus-von-Liebig Weg 11, 37077 Goettingen, Germany

* To whom correspondence should be addressed: Ralf Ficner, Department of Molecular Structural Biology, Institute for Microbiology and Genetics, Georg-August-University Goettingen, 37077 Goettingen, Germany; rficner@uni-goettingen.de

Abstract

The enzyme S-adenosylmethionine:tRNA ribosyltransferase isomerase (QueA) catalyses the penultimate step in the queuosine (Q) biosynthesis pathway. QueA transfers in an unprecedented reaction mechanism the ribosyl moiety of S-adenosylmethionine (SAM) to the 7-aminomehtyl group of $preQ_1$ (7-aminomethyl-7-deazaguanine) with subsequent rearrangement to form epoxyqueuosine (oQ-tRNA). Q plays an important role in the virulent phenotype of *Shigella* bacteria, causative for bacillary dysentery and reason for thousands of deaths in developing countries. Enzymes part of the Q-biosynthesis were subjected to structure-based drug design to treat shigellosis. QueA represents a suitable target for structure-based drug design, since there is no homologue in humans. In this study, the crystal structure of *Bacillus subtilis* QueA was determined. The full length QueA model, including loop regions not resolved in the presented crystal structure, was obtained applying the loop modelling application utilizing weak electron density map. Lastly, molecular docking experiments of the full length QueA model with a tRNA substrate gave valuable insight into a putative QueA-tRNA complex. The reported full length QueA structure enabled the identification of a putative SAM-binding pocket which forces SAM to bind in a bent conformation leading to the exposure of its ribosyl moiety. The model of QueA-tRNA complex implicates binding of the tRNA molecule by its anticodon stem with the positioning of $preQ_1$-34 in front of the SAM-binding pocket. The proposed model of QueA-tRNA gives valuable insight into QueA activity and provides a model for initial computer based fragment screening in order to perform structure-based drug design against *Shigella* bacteria.

Keywords: QueA, tRNA, Queuosine, RNA modification, structure-based drug design

4.1 Introduction

The complex genetic code is stored in deoxyribonucleic acid (DNA) built by only four nucleosides, the building blocks of life. These four nucleosides are the canonical pyrimidines deoxyadenosine (dA), deoxyguanine (dG), and the purines deoxycytosine (dC), and deoxythymidine (dT) with the corresponding ribonucleosides A, G, C, and uracil (U) in ribonucleic acid (RNA) (Dahm, 2008). Expansion of the genetic code is achieved by the addition of a vast variety of chemical modifications to the canonical nucleosides (Carell et al., 2018). The largest fraction and diversity of these modifications is found in transfer RNA (tRNA) with over 90 modification found to date (Boccaletto et al., 2018). Differing in their complexity, modifications can mean the simple addition of a methyl- or alkyl-group, or can be the result of a multienzyme modification machinery to achieve, in the most drastic cases, a complete base exchange. One member of the latter

modifications and so called hypermodifications is the nucleotide queuosine (Q). Q is a 7-deazaguanosine derivative containing an aminomethyl-cyclopentandiol side chain (Emmerich et al., 1985; Katze et al., 1984). Q and its derivatives occur only at position 34 (the wobble position) in the anticodon of bacterial and eukaryotic tRNAs, encoding for the amino acids tyrosine, aspartate, asparagine, and histidine. Each of these tRNAs harbour the anticodon sequence $G_{34}U_{35}N_{36}$, where N can be any nucleotide. The enzyme S-adenosylmethionine:tRNA ribosyltransferase isomerase (QueA) catalyses the penultimate step in Q biosynthesis (Slany, 1993). QueA transfers in an unprecedented reaction mechanism the ribose moiety of S-adenosylmethionine (SAM) to the Q precursor 7-aminomethyl-7-deazaguanine ($preQ_1$), which is the only known example of using SAM as a ribosyl donor in an enzymatic reaction. The QueA catalysed ribosyl transfer results in nitrogen substitution of the $preQ_1$ exocyclic aminomethyl group with an epoxy-dihydroxy-cyclopentenly moiety, yielding epoxyqueuosine (oQ) (Kinzie et al., 2000; Van Lanen and Iwata-Reuyl, 2003). In a final step catalysed by QueG, the epoxide is reduced to the mature queuosine (Payne et al., 2015). Although Q is found in bacteria and eukaryotes, Q-biosynthesis is confined to eubacteria. Eukaryotes salvage Q as dietary nutrient or from the intestinal flora, and incorporate it via the tRNA-guanine transglycosylase (TGT) (Reuter et al., 1991). In contrast to the TGT catalysed base exchange mechanism, the reaction mechanism of QueA is still poorly understood. Steady-state kinetics resulted in a theoretical catalytic mechanism, where the reaction starts with the deprotonation of C-5´ of SAM (Van Lanen and Iwata-Reuyl, 2003). This in turn results in the opening of the ribose ring under elimination of adenine. Subsequently, the C-4´ of the intermediate vinyl sulfonium is attacked by the $preQ_1$ amine, resulting in the formation of the epoxycarbocycle and elimination of the methionine moiety. In agreement with this mechanism, QueA catalysis follows a fully ordered sequential kinetic mechanism, where $preQ_1$-tRNA binds first, then SAM second, followed by the product releasing in the order, adenine first, methionine second, and oQ-tRNA last (Van Lanen and Iwata-Reuyl, 2003). The proposed active centre is located in a “strand-loop-helix” segment (residues 244-258 and 287-305, nomenclature according to *Thermatoga maritima*) and an additional loop region (325-330 according to *T. maritima*) (Mathews et al., 2005). These segments contain conserved residues closely located to the hypothetical ligand binding pocket. Further, conserved residues were identified as putative ligand-binding residues and attributed to Gly248, Thr249, Thr250, Arg253, Thr289, Asn290, His292, Leu298, Phe326, and Ser327. These reports give valuable insight into the QueA enzyme, however, we still lack knowledge about the exact catalytic mechanism, SAM binding, and tRNA recognition. Over 20 years ago, Durand and colleagues identified a connection of Q modification with the virulence of *Shigella* bacteria, causative agent of bacillary dysentery (Durand et al., 2000). Deletion of the *tgt* gene in *Shigella flexneri* leads to the modulated translation of VirF, the most upstream regulatory protein

necessary for virulence, and loss of virulence (Durand et al., 2000). This renders the Q-biosynthesis pathway an interesting target to design drugs against shigellosis on a structural basis. First efforts were made using crystal structures of TGT to design inhibitors (Brenk et al., 2004; Romier et al., 1996). However, in contrast to TGT, which contains homologues in humans, QueA has no counterpart and should present itself a more suitable target for structure-based drug design.

This encouraged us to determine the crystal structure of QueA by means of X-ray crystallography. Even though the presented structure showed medium highest resolution limit, it comprises more residues when compared to already determined QueA structures. Due to the presence of conserved amino acids in the unresolved loop regions, loop modelling approach, as implemented in ROSETTA, gave insight into the full length QueA structure. Analysis of the QueA model surface revealed a cavity which could be assigned as putative SAM-binding pocket. SAM is only able to bind to this pocket upon bending, which in turn forces the molecule to expose its ribosyl moiety that is supposed to be transferred. Additional molecular docking experiments of full length QueA and tRNA showed binding of the tRNA by its anticodon stem. The target preQ1-34 was located in front of the putative SAM-binding pocket. Subsequently, the complex model led us to the proposition of residues His225, Arg258, and Glu227 to be important for the initial step and residues Thr179, Thr254, or Thr255 to be important for the second enzymatic driven stem during catalysis.

4.2 Material and Methods

4.2.1 Expression and purification of QueA

Bacillus subtilis QueA (QueA) was amplified from genomic *Bacillus subtilis* str. 168 DNA and cloned into the expression vector pGEX-6P-1 using 5´ BamHI and 3´ XhoI restriction sites, introducing an N-terminal GST affinity tag. The expression vector was introduced into *Escherichia coli* BL21(DE3) cells and cultivated until an optical density OD_{600} of 0.8. QueA expression was induced with the addition of 0.5 mM Isopropyl β-D-1-thiogalactopyranoside (IPTG), and cell cultures were incubated at 37°C for 4 h prior to harvesting and storage at -20°C. Cells were disrupted by microfluidization (M-110S Microfluidizer) with 50 mM Tris/HCl pH 8.5, 2 mM DTT, cell debris was separated from soluble proteins by ultracentrifugation at 20000 g for 30 min, and 4°C. GST-QueA was applied to Glutathione Sepharose Fast Flow column (GE Healthcare) in 50 mM Tris/HCl pH 8.5, 100 mM NaCl, 2 mM DTT, residual nucleotides bound to the enzyme were removed with 2 M $LiCl_2$, and GST-QueA was subsequently eluted with the supplementation of 20 mM reduced glutathione. After GST-cleavage (1:50 w/w PreScission Protease), the GST tag was removed using a

Glutathione Sepharose Fast Flow column (GE) and further purified via Superdex 200 size exclusion chromatography. Fractions containing pure QueA protein were pooled, concentrated to 14 mg/ml and stored at -80°C until further use.

4.2.2 In vitro transcription and tRNA purification

Bacillus subtilis $tRNA^{Asn}$ ($tRNA^{Asn}$) was transcribed from a linearized vector in a run-off *in vitro* transcription. The transcription reaction contained T7 Polymerase, 10 mM rNTPs each, 1x HT buffer (30 mM HEPES pH 8.0, 25 mM $MgCl_2$, 10 mM DTT, 2mM spermidine, 0.01% Triton X-100) and was incubated for 3 h at 37°C. PP_i was pelleted and the reaction was stopped upon addition of 50 mM EDTA. $tRNA^{Asn}$ was purified by ion exchange chromatography (1 mL Resource-Q GE), applied to the resin with IEX-A buffer (20 mM HEPES pH 7.4, 50 mM KCl) and eluted in a linear gradient with IEX-B buffer (20 mM HEPES pH 7.4, 2 M KCl). Fractions containing pure tRNA were pooled, ethanol precipitated, dissolved in ddH_20, and stored at -20°C until further use. *B. subtilis* $tRNA^{Tyr}$ anticodon stem-loop ($tRNA^{Tyr}$ ASL) was transcribed from oligonucleotides coding for the mature tRNA sequence (Sigma: $tRNA^{Tyr}$ ASL_forward: 5´-AGTGAATTCTAATACGACTCACTATAGGGGCGG-3´, and $tRNA^{Tyr}$ ASL_reverse: 5´-TAGGGATCCGCGGATTTAC AGTCCGCCCC-3´) and purified, precipitated, and stored as described for $tRNA^{Asn}$.

4.2.3 Complex assembly and purification

Equimolar concentrations of $tRNA^{Tyr}$ ASL/$tRNA^{Asn}$ and QueA were mixed with 10x excess amount of SAM, incubated for 30 min on ice, and applied to Superdex 200 size exclusion chromatography column. Elution fractions were analysed by SDS-PAGE and Urea-PAGE and complex containing fractions pooled, concentrated, and stored at -80°C.

4.2.4 Crystallization

The QueA-tRNA complex was crystallized using sitting drop vapour diffusion. QueA:$tRNA^{Tyr}$ ASL:SAM were used in the ration 1:1.2:10 and adjusted to 2 mg/ml, and incubated 30 min at 4°C. 1 volume complex was mixed with 2 volumes of crystallization solution 0.1 M MOPS/HEPES-Na pH 7.5, 0.03 M $MgCl_2$, 0.03 M $CaCl_2$, 10% PEG 20k, 20% PEG 550 MME (buffer condition from the Morpheus Screen, Protomnis). Crystals were obtained after 3-7 days at 293 K and harvested using nylon cryo loops and subsequently stored at 77 K. No additional cryo protection was required.

4.2.5 Data collection, molecular replacement and refinement

X-ray data were collected at MX-14.1 (BESSY, Berlin). Diffraction images were indexed, integrated and scaled using the XDS-package (Kabsch, 2010). The QueA structure was solved using molecular replacement method by PHASER (McCoy et al., 2007) implemented in the CCP4 suite (Winn et al., 2011) and the QueA apo structure used as the search model (PDB ID: 1YY3). Structure refinement was performed in iterative steps using Refmac (Murshudov et al., 2011) implemented in the CCP4 suite and subsequent manual adjustments in Coot (Emsley et al., 2010). Crystallographic data and refinement statistics were summarized in table 4.1 Figures were prepared using PyMOL (Schrödinger, LLC, 2015).

4.2.6 Modelling of full length QueA

Modelling of loop regions (residues 170 to 175 and 212 to 223), which were not present in the reported crystal structure, have been performed in ROSETTA utilizing tools developed for structure determination in density and employing CCD (Cyclic coordinate descent) algorithm (Mandell et al., 2009; Stein and Kortemme, 2013). Over a 1000 of models have been generated and scored based on an agreement to a weak electron density map calculated using phenix.refine from PHENIX suite (Adams et al., 2010). The atomic models with completed loop regions have been scored based on an in Rosetta implemented energy term describing the fit to map as well as an overall score and number of contacts. The top 20 scored models have been manually inspected and three of those, which did not form interactions with neighbouring molecules in the asymmetric unit, have been selected.

4.2.7 Molecular docking

The top three full length QueA models from the ROSETTA remodelling were used to perform molecular docking. Initially a blind docking run was performed using the ClusPro web server (Vajda et al., 2017). QueA was set as ligand and the tRNA molecule as receptor. *Saccharomyces cerevisiae* $tRNA^{Asp}$ (PDB ID: 2TRA) was used as tRNA model. Prior docking, modified nucleotides were replaced by their corresponding canonical nucleotides. The QueA modification target G34 is supposed to tightly interact with QueA and was subsequently set as point of attraction. Furthermore, based on the identification of the putative SAM-binding pocket and superposition with the co-crystallized complex structure of *Thermatoga maritima* QueA (PDB ID: 1VKY), a group of three residues on QueA as further points of attraction: 255, 258, 304 have been set. Three of the resulting models were used to perform high resolution refinement using RosettaDock (Chaudhury et al., 2011; Guilhot-Gaudeffroy et al., 2014). During the high resolution docking, Rosetta performed rigid body adjustments of both docking parties followed by model optimization (1000 decoys).

The resulting decoys have been first sorted by *I_sc* score (representing the energy of the interactions across the interface) and the most favourable 100 models have been manually inspected and validated. Modelling of the flipped G34 nucleotide was performed in Coot (Emsley et al., 2010). Figures were prepared using PyMOL (Schrödinger, LLC, 2015).

Table 4.1: Crystallographic data and refinement statistics

Crystallographic data	**bsQueA**
Beamline	MX-14.1 BESSY, Berlin
Wavelength (Å)	0.9184
Resolution range (Å)	47.40 - 3.18 (3.43-3.18)
Unique reflections	16105
Redundancy	24.7 (25.8)
Completeness (%)	99.9 (100)
Space group	$P42_12$
a, b, c (Å)	99.99, 99.99, 149.22
α, β, γ (deg)	90, 90, 90
R_{meas} (%)	28.9 (237.59)
I/σ (I)	12.73 (1.83)
$CC_{1/2}$	99.8 (71.2)
Wilson B $(Å)^2$	96.65
Refinement statistics	
R_{work}/R_{free}	0.28/0.30
No. of atoms	5169
Average B-factor $(Å)^2$	88.7
Root mean square deviation	
Bonds Å	0.003
Angles (°)	0.655
Ramachandran plot	
Favoured (%)	90.14
Allowed (%)	8.61
Outlier (%)	1.25

4.3 Results

4.3.1 Crystal structure of *Bacillus subtilis* QueA

The QueA crystal structure was solved by means of molecular replacement (using PDB ID:1YY3) and refined to 3.18 Å resolution with R/R_{free} 27.9%/30.3%. The enzyme shows the typical topology of an extended structure separated in two domains (Figure 4.1A). The smaller domain folds into a β-barrel consisting of 6 β-strands (β1 to 6s for small). The large domain consists of a central β-sheet comprising seven beta strands (l large domain) flanked by six α-helices (α1-6l), forming a αβα sandwich topology. Strands β5, β7, and β4 form a small β-sheet, of which the latter is partially shared with the central β-sheet. Together with α-helix 4l, these structures form the interface to the small domain. As described previously, the small domain is inserted into the large domain between strand β3l and helix α2l (Grimm et al., 2006; Mathews et al., 2005). The connecting loops between the large and small domain are not fully resolved and amino acids 171-175 (molecule A) and 170-174 (molecule B) between α2s and α2l and 212-221 (molecule A) and 213-223 (molecule B) between β5l and α4l could not be modelled and are most likely disordered in the crystal (Figure 4.1A, dashed lines). Albeit the lower resolution of the here reported model compared to available structures from *B. subtilis* QueA (PDB ID: 1YY3; 2.88 Å) and *T. maritima* QueA (PDB ID: 1VKY; 2.0 Å) (Grimm et al., 2006; Mathews et al., 2005), this model is more complete in terms of percentage of build residues and gives more insight into the QueA structure. B-factors are low in the central β-sheet of the large domain and in the β-barrel of the small domain, they are elevated in the loop regions connecting both domains, with three-times higher values at the ends of the last resolved amino acids of the missing loops. These high B-factors indicated increased mobility of these regions in the crystal lattice, leading to the lack of traceable electron density for two loops. Even though QueA was co-crystallized with anticodon stem-loop (ASL) of $tRNA^{Tyr}$ and SAM, neither of these substrates could be identified in the electron density map. Molecule A and molecule B are structurally very similar as indicated by an RMSD (root mean square deviation) of 0.956 Å. The observed similarity results from applying non-crystallographic positional restraints between the two copies of QueA occupying the asymmetric unit. Bacterial QueA enzymes show high sequence conservation with most conserved amino acids being located in a groove between the large and small domain (Figure 4.1B). An additional patch of conserved residues was mapped on the surface of the small domain facing the aforementioned cavity. The groove opposing site harbours predominantly not well conserved amino acids.

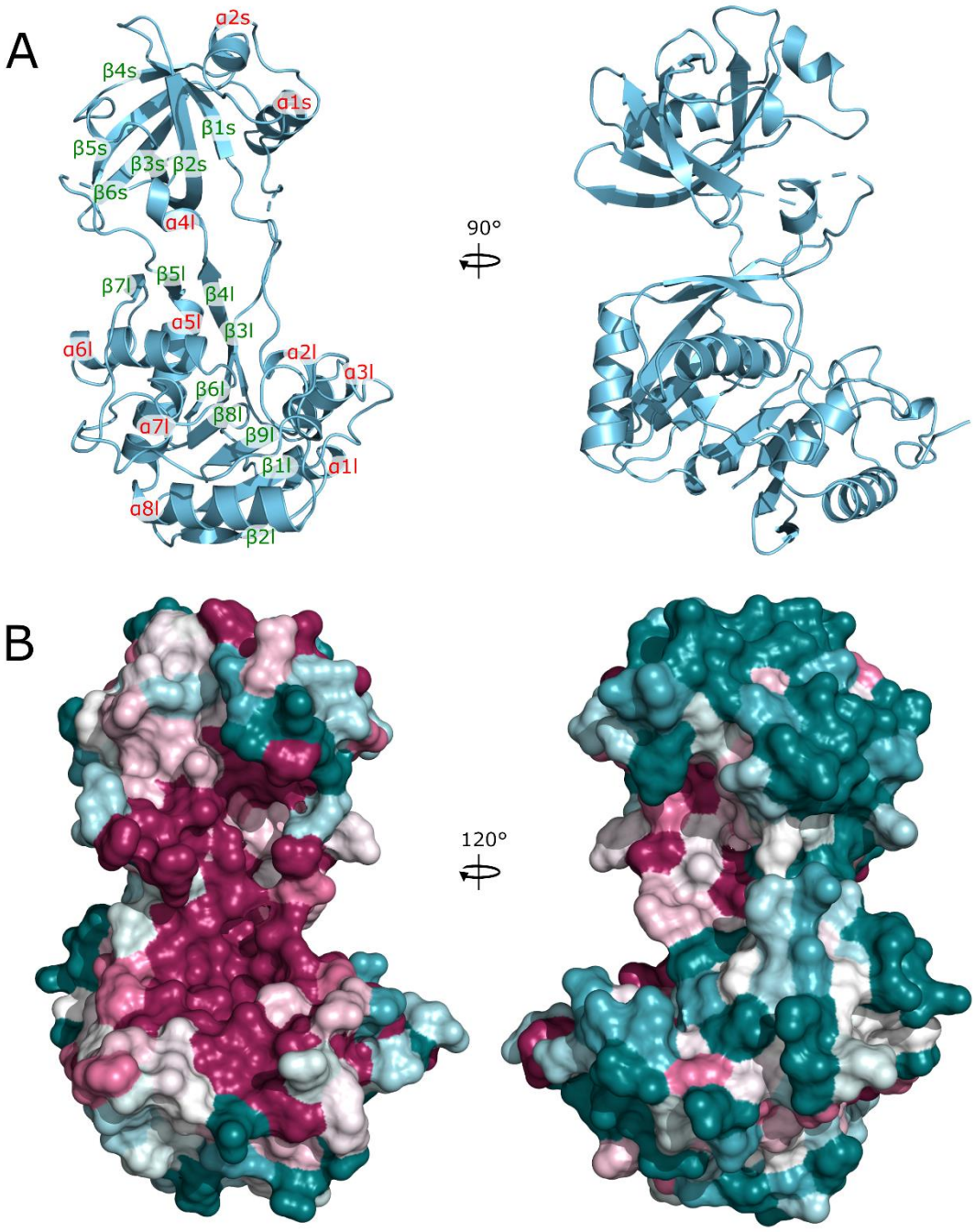

Figure 4.1: Crystal structure of *Bacillus subtilis* QueA at 3.18 Å resolution. (A) QueA is shown in cartoon mode at two orientations revealing the overall architecture (large and small domain). Secondary structure elements are marked and colour coded according to α-helices (red) and β-strands (green). (B) Surface representation of QueA ramp coloured by sequence conservation from high (magenta) to low conservation (dark green) as calculated with ConSurf (Ashkenazy et al., 2016). The cleft between large and small domain shows high sequence conservation, whereas the side opposite the cleft of QueA reveals large sequence variations.

4.3.2 QueA forms stable complex with full length tRNA and the ASL alone

In general, crystallization of a recombinantly obtained enzyme is an indication of its proper folding. However, in order to assure that the crystals of apo QueA have been obtained due to (i) pH, (ii) used crystallisation conditions or (iii) crystal packing and (iiii) not because of enzyme misfolding and malfunction, the ability of purified QueA to bind tRNA was analysed. Therefore, we tested QueA-tRNA complex formation using both full length $tRNA^{Asn}$ and $tRNA^{Tyr}$ ASL (Figure 4.2). According to preceding studies, the QueA-tRNA complex is formed in a sequential fashion. Hence, G34-tRNA was added to QueA first, followed by SAM. After an incubation time of 30 min on ice, we applied the putative complex to a size exclusion chromatography column. Analysis of fractions corresponding to the elution peaks showed the formation of stable complexes for both tRNA substrates. Taken together, the QueA enzyme prepared in this study is able to bind $tRNA^{Tyr}$ ASL as well as the full length $tRNA^{Asn}$. Stable complexes were obtained in a SAM-dependent manner and were stable during size exclusion chromatography. Hence, we can conclude that the QueA structure presented here is based on a properly folded and active protein.

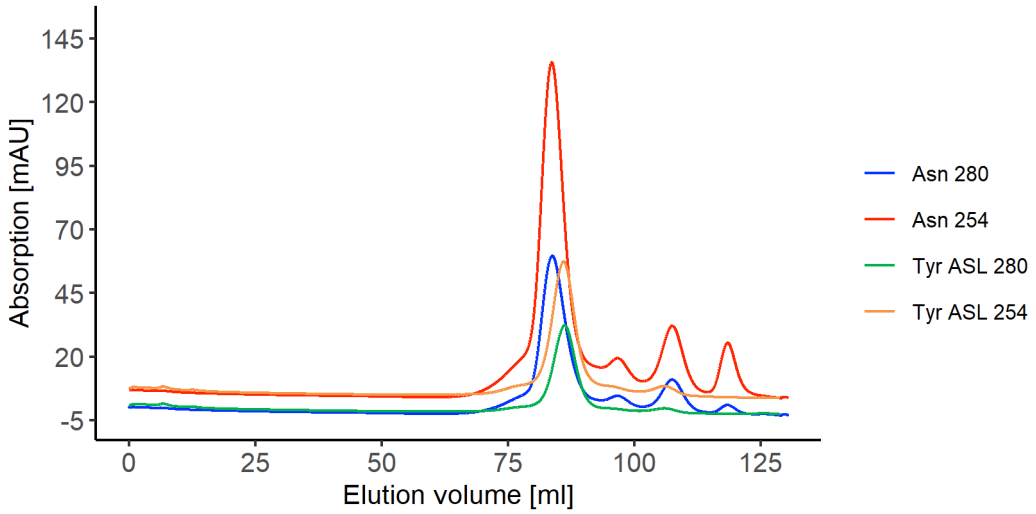

Figure 4.2: Size exclusion chromatography of QueA-$tRNA^{Tyr}$ anticodon stem loop (ASL) and QueA-$tRNA^{Asn}$ complexes. The ternary complex was assembled and subjected to a Superdex 200 size exclusion chromatography column (GE). Stable complexes were observed for both tRNA substrates: $tRNA^{Asn}$ and $tRNA^{Tyr}$ anticodon stem-loop (ASL), differing in their elution volumes.

4.3.3 Modelling of full lengths QueA

To get full insight into the QueA structure, ROSETTA tools for structure rebuilding and determination using electron density map restraints have been used to model the missing residues in the crystal structure (Mandell et al., 2009; Stein and Kortemme, 2013). Two stretches of amino acid 170 to 175 and 212 to 223

have been modelled utilising the 2mFo-DFc electron density map calculated based on the determined QueA crystal structure. In this modelling approach, ROSETTA utilizes even a very weak electron density map both as spatial restraints as well as for scoring function due to incorporation of additional energy terms assessing the agreement between model and map. We generated 10.000 decoys and the best 100 poses, selected based on calculated score, were examined for feasible orientations of these modelled loop regions. Decoys lacking helix 4l (Figure 4.1A), which is resolved in the crystal structure, were excluded. The loop comprising residues 212 to 223 and connecting helix α4l with β5l was modelled in many different orientations, from wrapping over the central groove to pointing completely to the side of QueA. The loop connecting α2l and α2s comprising residues 170 to 175 remained unstructured and formed in most decoys a straight connection between the small and large domain. Subsequently, two models were chosen in which the modelled loop connecting helix α4l with β5l adopted two spatially different orientations and was not involved in any clashes with neighbouring molecules in the crystal lattice (Figure 4.3A).

Surface representation of the full length QueA model showed a cavity in the groove between the large and small domain (Figure 4.3B). Both edges of this cavity protrude deeper into the enzyme, of which the right end of this cavity is larger than the left end. Superposition of the full length QueA model with the crystal structure of *T. maritima* QueA complexed with an unknown ligand (UNL) (Mathews et al., 2005) placed the UNL molecule in the right (deeper and larger) site of the cavity (Figure 4.3B). This rendered the described cavity a possible binding area for the ribosyl-donor SAM. However, this cavity cannot accommodate SAM in its extended conformation. Hence, we searched the Protein Data Bank (PDB; Berman et al., 2000) for other SAM conformations and found several bent conformers, such as the one present in the following structures: the 16S rRNA methyltransferase (Gregory et al., 2009), MnmC bifunctional protein (Kim and Almo, 2013), and 16S rRNA G527 methyltransferase (Macmaster et al., 2010) (with the PDB IDs: 3MTE, 3SGL, and 3G8B, respectively). Subsequently, we used SAM found in the latter one and manually docked it in the putative SAM-binding pocket, so that the ring structure of the UNL aligns with the adenine moiety of SAM (Figure 4.3B). The identified cavity accommodates the SAM molecule completely and forces it to expose the ribosyl group that is supposed to be transferred to the $preQ_1$-tRNA. This strengthens our hypothesis of the location of the SAM-binding pocket. Furthermore, analysis of the electrostatic surface potential of QueA revealed positive charges within the putative SAM-binding pocket (Figure 4.3C). This positively charged area expands toward the small domain. The central groove opposing site showed predominantly negative charges with strictly negative patches on the sides of QueA. The distribution of positively charged patches on the QueA surface led to the hypothesis of the plausible tRNA binding mode in which the tRNA molecule binds via its anticodon stem-loop in an upright position with the G34 reaching into the SAM-binding pocket.

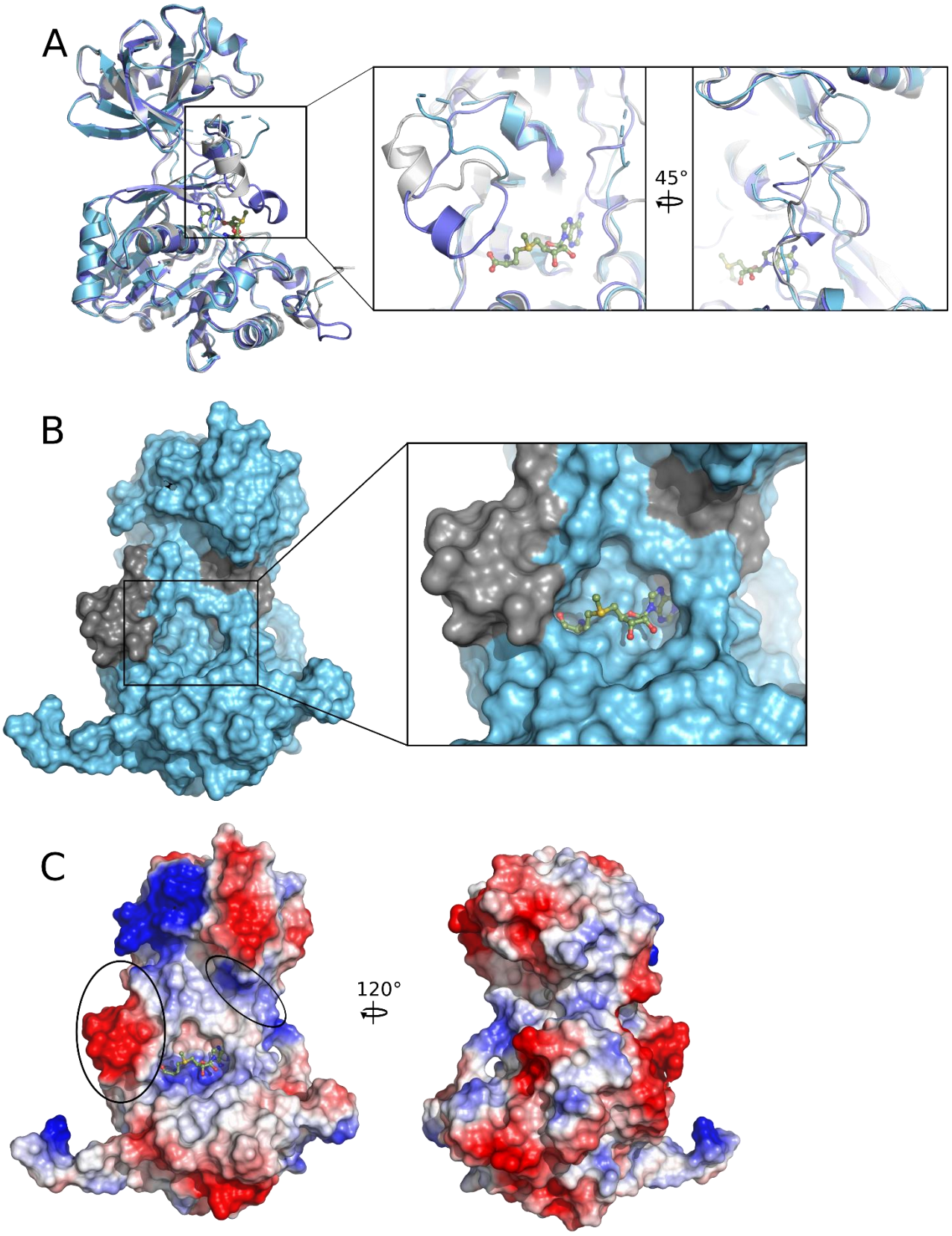
A
45°
B
C
120°

Figure 4.3: QueA structure with modelled loop regions, representing a full QueA model. (A) Comparison of the QueA crystal structure (light blue) with two alternative loop models, model 1 (grey), and model 2 (dark blue). QueA structures are presented in cartoon mode with SAM presented as ball-and-stick model. Close-up views of the loop modelled QueA structures including amino acids 170 to 175 and 212 to 223. (B) Surface representation of a modelled full length QueA (model 1) highlighting a deep cavity between small and large domain (left). Modelled loops are presented in grey. On the right side, close-up view of a putative bound SAM molecule, exposing its ribosyl moiety. (C) Electrostatic surface potential of QueA loop model 1 is depicted at a contour level of ± 6 k_BT/e. SAM is shown in ball and stick mode. The QueA model displays positive patches in the putative SAM binding pocket and at the small domain facing the front side of QueA. Modelled loops are indicated by black circles.

Taken together, modelling of the QueA full length structure showed high flexibility of loop 212 to 223. In contrast, in most decoys the loop 170 to 175 formed a straight connection between the small and large domain. Surface analysis of two representative models revealed a cavity within the central groove. Placement of SAM in this cavity requires a bent ligand conformation resulting in exposing the ribosyl group to the solvent. Electrostatic potential surface analysis of QueA revealed positively charged patches reaching from the central groove (including the SAM-binding pocket) to the small domain.

4.3.4 Molecular docking of $tRNA^{Asp}$ with QueA homology model

Crystallization of tRNA-protein complexes is a challenging task and attempts to obtain the QueA-tRNA binary complex have failed so far. Therefore, we aimed to get a model of the QueA-tRNA complex using molecular docking, since much progress has been done in the field of *in silico* prediction and predicted models are getting increasingly more accurate. For modelling of the QueA-tRNA complex, we used the aforementioned full length QueA model, including the loop regions containing conserved residues which are lacking in the crystal structure. Initial blind docking was performed using the ClusPro web server (Kozakov et al., 2017). Prerequisite for molecular docking is the definition of receptor and ligand molecules. The ClusPro server allows tRNA molecules to be set as receptor only, leading to the definition of the QueA as ligand. Additional spatial restraints in the form of receptor-ligand attractions (tRNA G34 – QueA 255, 258, 304) were set to define the interaction site of the tRNA molecule with QueA (Kozakov et al., 2017, 2013; Vajda et al., 2017). ClusPro divides one docking run into three computational steps. First, a rigid body docking run samples a myriad of conformations. Second, the docked conformers are clustered by means of root-mean-square deviation (RMSD) and the 1000 lowest energy structures are generated. This aims to find the largest cluster which represents the most likely complex model. And third, the selected models are refined using energy minimization. During the rigid body modelling, the resulting models are scored into four sets, balanced, electrostatic-favoured, hydrophobic-favoured, and van der Waals + electrostatics. Models not fitting in these categories are termed others, for which the probability of resembling the native complex is less than 50% (Kozakov et al., 2017). Next, up to 30 clusters are generated of which 10 are finally

chosen for scoring. The resulting models are scored according to their electrostatic interactions and desolvation contributions. Subsequently, three models calculated by Cluspro were chosen to perform high resolution docking using Rosetta. Rosetta adds hydrogens to the complete model and performs rigid body alterations of both components followed by minimization. During the latter step, Rosetta adjusts protein side chains to ensure satirical correctness of the resulting model. Rosetta generated over 10.000 decoys which were scored by their *I_sc* (interface score) score. The best model has been selected based on the *I_sc* score and was further evaluated (Figure 4.4A). In this model, the tRNA molecule interacts with QueA via its anticodon stem loop (ASL). Protein-tRNA contacts in this model are made by amino acids Gly76, Ala77, Tyr153, Gln157, Asp159, Asp160, Lys161, Thr210, and Phe211 located at the front face of the small domain of QueA with the tRNA ASL. Further interactions are made by Asn223 and Ser303 with the anticodon of the tRNA molecule. Interaction of the tRNA with QueA in these two distant positions (Figure 4.4A) might ensure proper orientation and stabilization of the protein-RNA complex. The remaining part of the RNA (elbow and acceptor stem) points away from QueA (Figure 4.4). The QueA interaction interface consists of mainly positively charged resides pointing towards the negatively charged sugar-phosphate backbone of the tRNA molecule. According to our model, the modification target preQ1$_{34}$ (in this model unmodified G34 and superimposed with preQ$_1$) binds in a small cavity in front of the putative SAM-binding site with the 7-aminomethyl moiety protruding into this cavity towards SAM. The amine of the 7-aminomethyl group is coordinated by Ser303 and the 7-deazaguanine is coordinated via π-stacking with Phe333 (Figure 4.4C). The aromatic nature of residue 333 is conserved across QueA enzymes and is either presented as Phe or Trp amino acid. The SAM-binding pocket is surrounded by conserved amino acids. Especially His225, Arg258, and Glu227 are of interest, because they are in close proximity to the C5´ Atom of SAM (Arg258: 3.0Å, His255: 2.9Å in a bent conformation) where the proposed reaction mechanism starts with the deprotonation of C5´ (Figure 4.4B). Furthermore, prerequisite for the elimination of adenine from SAM is the protonation of the adenine N3 or N7, leading to the breakage of the N-C glycosidic bond (Kinzie et al., 2000). In our model, residues Thr179, Thr254, or Thr255 are close to either positions and highly conserved among other QueAs.

Taken together, using a molecular docking approach we propose a model of the complex between the full length QueA enzyme, completed by modelling using ROSETTA tools, and the target tRNA^{Asp}. In this model, QueA binds its tRNA substrate via the anticodon stem. Positive patches on the QueA surface are exposed to the negatively charged sugar-phosphate backbone of the tRNA. The modification target base preQ$_1$ is coordinated by π-stacking with Phe333 and polar contacts to Ser303, with the 7-aminomethyl group pointing towards the ribosyl moiety of SAM. Based on this model, we proposed residues His225, Arg258,

and Glu227 to be important for the initial deprotonation of the C' 5 of SAM and residues Thr170, Thr254, or Thr255 to protonate the SAM adenine moiety to fulfil catalysis.

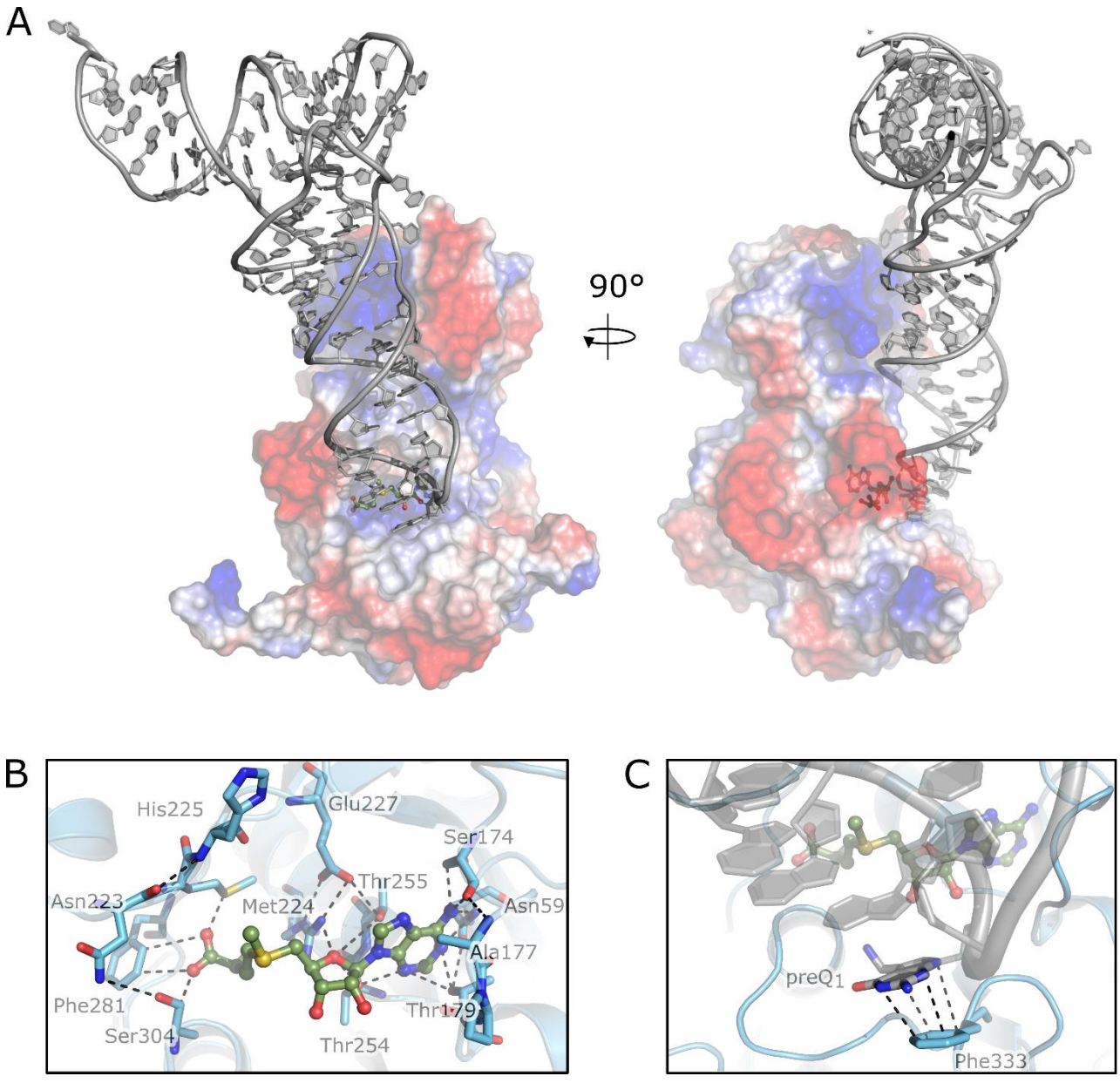

Figure 4.4: QueA-tRNA complex model. The full length QueA (model 1) was used to initially dock tRNA (PDB ID: 2TRA) using the ClusPro web server (Kozakov et al., 2017). (A) The QueA model 1 is displayed in two orientations in surface mode ramp coloured according the electrostatic potentials (± 6 k_BT/e), the tRNA molecule is shown in cartoon mode (grey), and SAM is depicted as ball and stick (green). The tRNA molecule makes contacts with QueA by its anticodon stem loop and a positively charged patch located at the front side of the small domain of QueA, possibly stabilizing the tRNA-QueA complex. (B) Close-up view of the bound SAM molecule. Residues involved in SAM coordination are marked and hydrogen bonds indicated by dashed lines. (C) The close-up view of tRNA bound to QueA. The $preQ_1$-34 base is coordinated by Phe333 via π-stacking (indicated by dashed lines).

4.4 Discussion

The unique enzyme S-adenosylmethionine:tRNA ribosyltransferase isomerase (QueA) catalyses the penultimate step in the queuosine (Q) biosynthesis pathway (Grimm et al., 2006; Kinzie et al., 2000; Mathews et al., 2005; Van Lanen and Iwata-Reuyl, 2003). Q is a key player in *Shigella* bacteria driving the expression of virulence factors (Durand et al., 2000). *Shigella* infection is causative for bacterial dysentery and reason for thousands of deaths in developing countries (Louise K. Francois Watkins and Grace D. Appiah, 2019). Inhibition of Q leads to the loss of the virulent phenotype of *Shigella* and rendered the Q biosynthesis pathway an interesting target for structure-based drug design (Brenk et al., 2004; Romier et al., 1996). The enzyme tRNA-guanine transglycosylase (TGT) is the upstream enzyme of QueA and was subjected to fragment-based drug discovery campaigns to find structure based inhibitors (Grädler, 2001). However, in contrast to TGT, QueA has no homologue in humans, rendering this enzyme a more suitable target. Even though Q biosynthesis is well understood, QueA activity is still enigmatic as it utilizes the ribosyl moiety of SAM to modify its tRNA substrate, which is the first description of the use of the ribosyl moiety of SAM in enzymatic reactions. To address QueA activity and substrate recognition, we solved the crystal structure of *Bacillus subtilis* QueA determined to 3.1 Å (Figure 4.1A) and modelled loop regions missing in the crystal structure. This full length QueA model was further subjected to perform molecular docking to gain insight in complex formation. And lastly, we propose key residues important for catalysis of QueA.

QueA enzymes showed high sequence conservation all over the enzyme surface with dense clusters of conserved amino acids between the large and small domain and on the side of the small domain facing the central groove (Figure 4.1B). However, due to these many conserved areas, it is difficult to infer catalytically important amino acids, as well as residues important for tRNA binding, solely based on sequence alignments. Since approaches utilizing model rebuilding in combination with homology modelling get increasingly accurate, we performed loop modelling including weak electron density map as additional restraints to obtain a full length QueA model (Mandell et al., 2009; Stein and Kortemme, 2013). The resulting models were scored according to an internally calculated ROSETTA score and manually inspected using Pymol (Figure 4.3A) (Schrödinger, LLC, 2015). One of the modelled loops (212 to 223) is most likely crucial for tRNA binding. The last resolved secondary structure feature proceeding this loop region is the α-helix 4 located in the small domain. The existence of this helix was set as a prerequisite for all decoys with a modelled loop to be further considered. Hence, decoys lacking helix 4 were rejected. Subsequently, two representative conformations including two distinct spatial conformations of loop 212 to 223 were selected

and further analysed (Figure 4.3A). Inspection of the enzyme surface showed a deep cavity as part of the central groove (Figure 4.3B). Comparison of the full length QueA model with the *T. maritima* QueA (PDB ID: 1YVK) revealed the co-localization of the co-crystallized unknown ligand (UNL) with this newly identified cavity. Here, the UNL was placed in the right end of the cavity and aligned with the adenine of the manually placed SAM. Furthermore, this cavity is formed by positively charged amino acids and led us to the proposition of a putative SAM-binding pocket (Figure 4.3B and C). SAM only fits to this cavity in a bent conformation, forcing SAM to expose its ribosyl moiety. This bent conformation is typically found in knotted SAM-dependent enzymes and to a lesser extend in unknotted enzymes (Perlinska et al., 2020).

Due to the lack of tRNA-QueA complex crystal structures, we performed molecular docking experiments with the full length QueA model. Initial blind docking was performed using the ClusPro web server (Kozakov et al., 2017; Vajda et al., 2017). Docking of the QueA-tRNA complex was performed with the QueA model (crystal structure with modelled amino acids missing in the structure) and a tRNA crystal structure. Due to the rigidity of crystal structures, which might not completely represent the solvated conformation, the ClusPro server implemented thresholds to tolerate protein-RNA clashes. Therefore, ClusPro uses a scoring method in which docked conformations which do not have the lowest energies, are taken into account, since they might be closer to the native structure (Kozakov et al., 2017). It is to be assumed that upon complexation the protein undergoes conformational changes, as comparison of QueA crystal structures showed rotational movement of the small domain and loop modelling confirmed the flexible nature of the loop comprising of residues 212 to 223. Since the QueA-tRNA complex model predicted by molecular docking is based on the rigid body assembly formation, the native complex most probably shows differences in its conformation. In the reported tRNA-QueA complex model, the tRNA molecule binds solely via its anticodon stem (Figure 4.5C), which is in agreement with previous biochemical studies showing the ability of QueA to bind tRNAs consisting only of their ASL and exhibit similar enzymatic kinetics (Van Lanen and Iwata-Reuyl, 2003). More strikingly, comparison of the QueA-tRNA complex model with the *Escherichia coli* 2-thiouridylase MnmA shows similar tRNA binding strategies (Numata et al., 2006). Albeit MnmA and QueA are biochemical unrelated, MnmA architecture is similar to QueA consisting of several domains, including a large and two small domains (Figure 4.5A). The large domain harbours a central β-sheet, one of the two small domains consists of a β-barrel domain, and the other small domain represents the catalytic domain. The MnmA-tRNA crystal structure shows similar tRNA binding seen in the reported QueA-tRNA^{Asp} complex model. The three domains of MnmA form a positively charged central cleft surrounded by negatively charged residues on the remaining protein surface (Figure 4.5A). Protein-RNA contacts are established by the anticodon arm and D-stem with the central groove of MnmA. These interactions fulfil a common feature

found in protein-RNA complexes. The positively charged RNA sugar-phosphate backbone forces the interacting protein molecule to expose mostly positively charged residues in the interacting surface to enable RNA-binding. The establishment of electrostatic interactions help to stabilize protein-RNA complexes (Chen and Lim, 2008). This holds true for the QueA-tRNA complex model, where an extensive positively charged patch is found in the central groove extending toward the small domain (Figure 4.5C). Binding of the tRNA molecule to the central groove of QueA and MnmA further fulfil a key feature in protein-RNA interactions, where the interaction area of the protein shows a concave form, since the surface of RNA molecules are convex (Bahadur et al., 2008). Last but not least, although protein-RNA complexes typically exhibit large interaction interfaces, protein-tRNA complexes show fewer direct hydrogen bonds and in general a smaller interaction interface (Ellis et al., 2006). In general, the MnmA-tRNA complex interface area spans 1327.1 $Å^2$ with a hydrophobic interface indicated by a ΔG of -22.5 kcal/mol (Krissinel and Henrick, 2007). In general, the MnmA surface spans 16808.3 $Å^2$, of which 4% are buried upon complex formation. In comparison, the QueA-$tRNA^{Asp}$ complex model exhibits a protein-RNA interface area of 1131.0 $Å^2$ with a ΔG of -24.4 kcal/mol. Upon complexation, 6.8% of the total QueA surface (15638.7 $Å^2$) becomes inaccessible to the solvent (Krissinel and Henrick, 2007). Furthermore, MnmA-tRNA and QueA-tRNA form 32 and 4 hydrogen bonds, respectively. These results are in agreement with a comprehensive report analysing protein-nucleic acid complex formation (Bahadur et al., 2008). tRNA-protein complexes show the largest shift from accessible surface to buried surface area of 1660 $Å^2$, compared to protein-duplex RNA complexes (1270 $Å^2$), protein-single-strand complexes (880 $Å^2$), and protein-protein interactions (0 $Å^2$). The number of hydrogen bonds per interface varies from 25 (tRNA-protein), 24 (duplex RNA-protein), 15 (single strand-protein), to 10 hydrogen bonds per interface found in protein-protein complexes (Bahadur et al., 2008). The low number of 4 hydrogen bonds found in the QueA-$tRNA^{Asp}$ complex model can be explained by the use of crystal structures for QueA and $tRNA^{Asp}$ in the docking experiment. Complex formation most probably leads to structural rearrangements of amino acid side chains, enabling the tRNA molecule to tightly fit to the protein cavity. The closer contact of both molecules subsequently leads to the formation of more hydrogen bonds. However, besides the differences in hydrogen bonds, the QueA-tRNA complex model displays similar solvation energies and interface areas, corroborating the likelihood of the presented QueA-tRNA complex model to display the biological assembly.

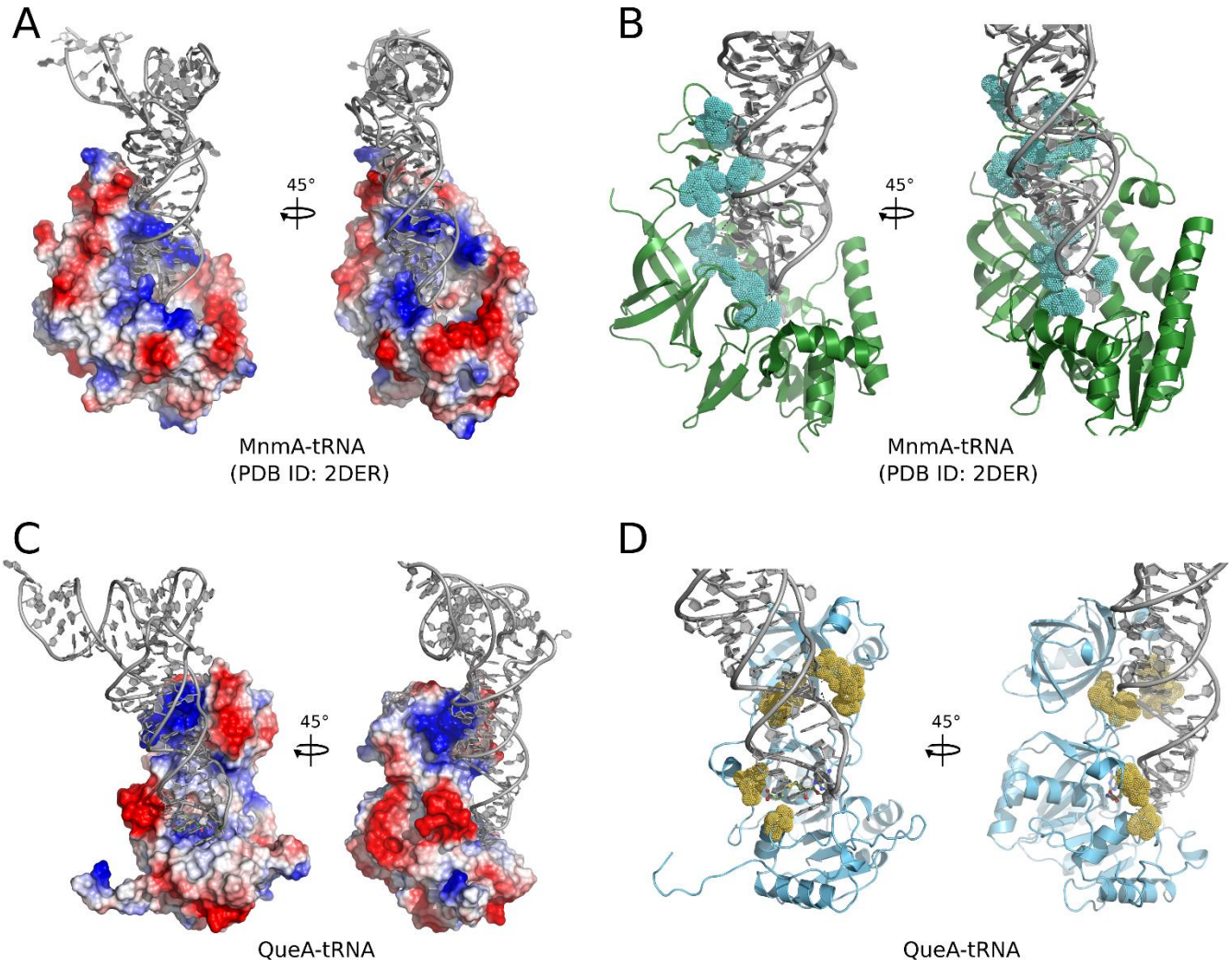

Figure 4.5: Comparison of the QueA-tRNA^{Asp} complex model with the crystal structure of MnmA-tRNA. (A) MnmA-tRNA complex crystal structure is presented in two orientations (PDB ID: 2DER). The tRNA molecule is displayed as cartoon and MnmA surface indicates the electrostatic potential from ± 7 k_BT/e. (B) MnmA crystal structure is shown as cartoon (green). Protein-RNA contacts are shown as dots (blue). (C) The QueA-tRNA complex model is shown as cartoon (tRNA) and the QueA electrostatic potential is ramp coloured from ± 6 k_BT/e. (D) QueA is shown as cartoon (blue) with RNA-protein contacts displayed as dots (yellow).

Taken together, the reported QueA-tRNA^{Asp} complex model shows biding of the tRNA molecule solely by its anticodon arm. Protein-RNA contacts are established between the small domain with the base of the anticodon arm and the central groove with the anticodon. The interface area, solvation energies, and percentage of buried interface area upon complex formation is in the range of determined protein-tRNA complexes, hence the complex model satisfies tRNA-protein interaction principles. Further, the QueA-tRNA complex model is supported by the MnmA-tRNA crystal structure which shows highly similar tRNA binding strategies.

4.5 Conclusion

Here we present the most complete structural model of a QueA enzyme. Utilising modelling approaches, a QueA full length structure was obtained, enabling to infer the putative SAM-binding pocket. A plausible QueA-tRNA complex model was obtained by applying molecular docking of the full length QueA model with a tRNA substrate. In this model the tRNA molecule binds by its anticodon stem and the modified base $preQ_1$ is located in front of the SAM-binding pocket. Furthermore, on basis of this model we proposed important residues for the initial enzymatic driven catalytic step to be His225, Arg228, and Glu285. Future studies addressing these residues by mutagenesis and subsequent activity assays would be interesting to validate the presented model. Lastly, the QueA full length model including the putative SAM-binding pocket can be the base of first *in silico* based fragment screening as starting point for structure-based drug design, as knowledge of a full length protein is prerequisite for a computational based inhibitor screening.

4.6 References

Adams, P.D., Afonine, P.V., Bunkóczi, G., Chen, V.B., Davis, I.W., Echols, N., Headd, J.J., Hung, L.-W., Kapral, G.J., Grosse-Kunstleve, R.W., McCoy, A.J., Moriarty, N.W., Oeffner, R., Read, R.J., Richardson, D.C., Richardson, J.S., Terwilliger, T.C., Zwart, P.H., 2010. PHENIX: a comprehensive Python-based system for macromolecular structure solution. Acta Crystallogr D Biol Crystallogr 66, 213–221. https://doi.org/10.1107/S0907444909052925

Ashkenazy, H., Abadi, S., Martz, E., Chay, O., Mayrose, I., Pupko, T., Ben-Tal, N., 2016. ConSurf 2016: an improved methodology to estimate and visualize evolutionary conservation in macromolecules. Nucleic Acids Res 44, W344–W350. https://doi.org/10.1093/nar/gkw408

Bahadur, R.P., Zacharias, M., Janin, J., 2008. Dissecting protein–RNA recognition sites. Nucleic Acids Research 36, 2705–2716. https://doi.org/10.1093/nar/gkn102

Berman, H.M., Westbrook, J., Feng, Z., Gilliland, G., Bhat, T.N., Weissig, H., Shindyalov, I.N., Bourne, P.E., 2000. The Protein Data Bank. Nucleic Acids Research 28, 235–242. https://doi.org/10.1093/nar/28.1.235

Boccaletto, P., Machnicka, M.A., Purta, E., Piątkowski, P., Bagiński, B., Wirecki, T.K., de Crécy-Lagard, V., Ross, R., Limbach, P.A., Kotter, A., Helm, M., Bujnicki, J.M., 2018. MODOMICS: a database of RNA modification pathways. 2017 update. Nucleic Acids Research 46, D303–D307. https://doi.org/10.1093/nar/gkx1030

Brenk, R., Meyer, E.A., Reuter, K., Stubbs, M.T., Garcia, G.A., 2004. Crystallographic Study of Inhibitors of tRNA-guanine Transglycosylase Suggests a New Structure-based Pharmacophore for Virtual Screening. Journal of Molecular Biology 55–75. https://doi.org/10.1016/j.jmb.2004.02.019

Carell, T., Kurz, M.Q., Müller, M., Rossa, M., Spada, F., 2018. Non-canonical Bases in the Genome: The Regulatory Information Layer in DNA. Angew. Chem. Int. Ed. 57, 4296–4312. https://doi.org/10.1002/anie.201708228

Chaudhury, S., Berrondo, M., Weitzner, B.D., Muthu, P., Bergman, H., Gray, J.J., 2011. Benchmarking and Analysis of Protein Docking Performance in Rosetta v3.2. PLoS ONE 6, e22477. https://doi.org/10.1371/journal.pone.0022477

Chen, Y.C., Lim, C., 2008. Predicting RNA-binding sites from the protein structure based on electrostatics, evolution and geometry. Nucleic Acids Research 36, e29. https://doi.org/10.1093/nar/gkn008

Dahm, R., 2008. Discovering DNA: Friedrich Miescher and the early years of nucleic acid research. Hum Genet 122, 565–581. https://doi.org/10.1007/s00439-007-0433-0

Durand, J.M.B., Dagberg, B., Uhlin, B.E., Bjork, G.R., 2000. Transfer RNA modification, temperature and DNA superhelicity have a common target in the regulatory network of the virulence of Shigella flexneri: the expression of the virF gene. Mol Microbiol 35, 924–935. https://doi.org/10.1046/j.1365-2958.2000.01767.x

Ellis, J.J., Broom, M., Jones, S., 2006. Protein-RNA interactions: Structural analysis and functional classes. Proteins 66, 903–911. https://doi.org/10.1002/prot.21211

Emmerich, B., Zubrod, E., Weber, H., Maubach, P.A., Kersten, H., Kersten, W., 1985. Relationship of Queuine-lacking Transfer RNAs to the Grade of Malignancy in Human Leukemias and Lymphomas 45, 8.

Emsley, P., Lohkamp, B., Scott, W.G., Cowtan, K., 2010. Features and development of *Coot*. Acta Crystallogr D Biol Crystallogr 66, 486–501. https://doi.org/10.1107/S0907444910007493

Grädler, U. et al, 2001. A New Target for Shigellosis: Rational Design and Crystallographic Studies of Inhibitors of tRNA-guanine Transglycosylase. Journal of Molecular Biology 306, 455–467. https://doi.org/10.1006/jmbi.2000.4256

Gregory, S.T., Demirci, H., Belardinelli, R., Monshupanee, T., Gualerzi, C., Dahlberg, A.E., Jogl, G., 2009. Structural and functional studies of the Thermus thermophilus 16S rRNA methyltransferase RsmG. RNA 15, 1693–1704. https://doi.org/10.1261/rna.1652709

Grimm, C., Ficner, R., Sgraja, T., Haebel, P., Klebe, G., Reuter, K., 2006. Crystal structure of Bacillus subtilis S-adenosylmethionine:tRNA ribosyltransferase-isomerase. Biochemical and Biophysical Research Communications 351, 695–701. https://doi.org/10.1016/j.bbrc.2006.10.096

Guilhot-Gaudeffroy, A., Froidevaux, C., Azé, J., Bernauer, J., 2014. Protein-RNA Complexes and Efficient Automatic Docking: Expanding RosettaDock Possibilities. PLoS ONE 9, e108928. https://doi.org/10.1371/journal.pone.0108928

Kabsch, W., 2010. XDS. Acta Crystallogr D Biol Crystallogr 66, 125–132. https://doi.org/10.1107/S0907444909047337

Katze, J.R., Gunduz, U., Smith, D.L., Cheng, C.S., McCloskey, J.A., 1984. Evidence that the nucleic acid base queuine is incorporated intact into tRNA by animal cells. Biochemistry 23, 1171–1176. https://doi.org/10.1021/bi00301a022

Kim, J., Almo, S.C., 2013. Structural basis for hypermodification of the wobble uridine in tRNA by bifunctional enzyme MnmC. BMC Struct Biol 13, 5. https://doi.org/10.1186/1472-6807-13-5

Kinzie, S.D., Thern, B., Iwata-Reuyl, D., 2000. Mechanistic Studies of the tRNA-Modifying Enzyme QueA: A Chemical Imperative for the Use of AdoMet as a "Ribosyl" Donor. Org. Lett. 2, 1307–1310. https://doi.org/10.1021/ol005756h

Kozakov, D., Beglov, D., Bohnuud, T., Mottarella, S.E., Xia, B., Hall, D.R., Vajda, S., 2013. How good is automated protein docking?: Automated Protein Docking. Proteins 81, 2159–2166. https://doi.org/10.1002/prot.24403

Kozakov, D., Hall, D.R., Xia, B., Porter, K.A., Padhorny, D., Yueh, C., Beglov, D., Vajda, S., 2017. The ClusPro web server for protein–protein docking. Nat Protoc 12, 255–278. https://doi.org/10.1038/nprot.2016.169

Krissinel, E., Henrick, K., 2007. Inference of Macromolecular Assemblies from Crystalline State. Journal of Molecular Biology 372, 774–797. https://doi.org/10.1016/j.jmb.2007.05.022

Louise K. Francois Watkins, Grace D. Appiah, 2019. Chapter 4 Travel-Related Infectious Diseases-Shigellosis. URL https://www.cdc.gov/travel/yellowbook/2020/travel-related-infectious-diseases/shigellosis

Macmaster, R., Zelinskaya, N., Savic, M., Rankin, C.R., Conn, G.L., 2010. Structural insights into the function of aminoglycoside-resistance A1408 16S rRNA methyltransferases from antibiotic-producing and human pathogenic bacteria. Nucleic Acids Research 38, 7791–7799. https://doi.org/10.1093/nar/gkq627

Mandell, D.J., Coutsias, E.A., Kortemme, T., 2009. Sub-angstrom accuracy in protein loop reconstruction by robotics-inspired conformational sampling. Nat Methods 6, 551–552. https://doi.org/10.1038/nmeth0809-551

Mathews, I., Schwarzenbacher, R., McMullan, D., Abdubek, P., Ambing, E., Axelrod, H., Biorac, T., Canaves, J.M., Chiu, H.-J., Deacon, A.M., DiDonato, M., Elsliger, M.-A., Godzik, A., Grittini, C., Grzechnik, S.K., Hale, J., Hampton, E., Han, G.W., Haugen, J., Hornsby, M., Jaroszewski, L., Klock, H.E., Koesema, E., Kreusch, A., Kuhn, P., Lesley, S.A., Levin, I., Miller, M.D., Moy, K., Nigoghossian, E., Ouyang, J., Paulsen, J., Quijano, K., Reyes, R., Spraggon, G., Stevens, R.C., van den Bedem, H., Velasquez, J., Vincent, J., White, A., Wolf, G., Xu, Q., Hodgson, K.O., Wooley, J., Wilson, I.A., 2005. Crystal structure of S-adenosylmethionine:tRNA ribosyltransferase-isomerase (QueA) from Thermotoga maritima at 2.0 Å resolution reveals a new fold. Proteins 59, 869–874. https://doi.org/10.1002/prot.20419

McCoy, A.J., Grosse-Kunstleve, R.W., Adams, P.D., Winn, M.D., Storoni, L.C., Read, R.J., 2007. Phaser crystallographic software. J Appl Crystallogr 40, 658–674. https://doi.org/10.1107/S0021889807021206

Murshudov, G.N., Skubák, P., Lebedev, A.A., Pannu, N.S., Steiner, R.A., Nicholls, R.A., Winn, M.D., Long, F., Vagin, A.A., 2011. *REFMAC* 5 for the refinement of macromolecular crystal structures. Acta Crystallogr D Biol Crystallogr 67, 355–367. https://doi.org/10.1107/S0907444911001314

Numata, T., Ikeuchi, Y., Fukai, S., Suzuki, T., Nureki, O., 2006. Snapshots of tRNA sulphuration via an adenylated intermediate. Nature 442, 419–424. https://doi.org/10.1038/nature04896

Payne, K.A.P., Fisher, K., Sjuts, H., Dunstan, M.S., Bellina, B., Johannissen, L., Barran, P., Hay, S., Rigby, S.E.J., Leys, D., 2015. Epoxyqueuosine Reductase Structure Suggests a Mechanism for Cobalamin-dependent tRNA Modification. J. Biol. Chem. 290, 27572–27581. https://doi.org/10.1074/jbc.M115.685693

Perlinska, A.P., Stasiulewicz, A., Nawrocka, E.K., Kazimierczuk, K., Setny, P., Sulkowska, J.I., 2020. Restriction of S-adenosylmethionine conformational freedom by knotted protein binding sites. PLoS Comput Biol 16, e1007904. https://doi.org/10.1371/journal.pcbi.1007904

Reuter, K., Slany, R., Ullrich, F., Kersten, H., 1991. Structure and organization of Escherichia coli genes involved in biosynthesis of the deazaguanine derivative queuine, a nutrient factor for eukaryotes. J. Bacteriol. 173, 2256–2264. https://doi.org/10.1128/jb.173.7.2256-2264.1991

Romier, C., Reuter, K., Suck, D., Ficner, R., 1996. Crystal structure of tRNA-guanine transglycosylase: RNA modification by base exchange. The EMBO Journal 15, 2850–2857. https://doi.org/10.1002/j.1460-2075.1996.tb00646.x

Schrödinger, LLC, 2015. The PyMOL Molecular Graphics System, Version 5.0.

Slany, R.K., 1993. A New Function of S-Adenosylmethionine: The Ribosyl Moiety of AdoMet Is the Precursor of the Cyclopentenediol Moiety of the tRNA Wobble Base Queuinet. Biochemistry 7811–7817. https://doi.org/10.1021/bi00081a028

Stein, A., Kortemme, T., 2013. Improvements to Robotics-Inspired Conformational Sampling in Rosetta. PLoS ONE 8, e63090. https://doi.org/10.1371/journal.pone.0063090

Vajda, S., Yueh, C., Beglov, D., Bohnuud, T., Mottarella, S.E., Xia, B., Hall, D.R., Kozakov, D., 2017. New additions to the ClusPro server motivated by CAPRI: Development of the ClusPro Server. Proteins 85, 435–444. https://doi.org/10.1002/prot.25219

Van Lanen, S.G., Iwata-Reuyl, D., 2003. Kinetic Mechanism of the tRNA-Modifying Enzyme S-Adenosylmethionine:tRNA Ribosyltransferase-Isomerase (QueA). Biochemistry 42, 5312–5320. https://doi.org/10.1021/bi034197u

Winn, M.D., Ballard, C.C., Cowtan, K.D., Dodson, E.J., Emsley, P., Evans, P.R., Keegan, R.M., Krissinel, E.B., Leslie, A.G.W., McCoy, A., McNicholas, S.J., Murshudov, G.N., Pannu, N.S., Potterton, E.A., Powell, H.R.,

Read, R.J., Vagin, A., Wilson, K.S., 2011. Overview of the CCP4 suite and current developments. Acta Crystallogr D Biol Crystallogr 67, 235–242. https://doi.org/10.1107/S0907444910045749

Chapter 5 Discussion and Outlook

Cells have only a limited number of biological macromolecules. Chemical modification of these macromolecules is used to enlarge their physiological role, as well as to efficiently regulate their function. Covalent modifications are introduced to proteins, sugars, lipids, DNA, and RNA (Wang et al., 2019). However, the largest variety of modifications is found in RNA with more than 100 different types of modifications (Boccaletto et al., 2018). During the last decade, tRNA modifications have come into prominence due to the fundamental finding that tRNAs are not merely a shuttle service during translation, but have rather direct functional effects on cellular processes, such as gene expression or in human diseases (Delaunay and Frye, 2019; Frye et al., 2018; Gu et al., 2014; Jonkhout et al., 2017; Pereira et al., 2018). These modifications vary in their complexity from simple methylations to sophisticated multi-step modifications found for instance for queuosine. The overall aim of this thesis was to investigate the tRNA modifying enzymes TrmB, Dnmt2, and QueA on a structural and biochemical level. The studied enzymes introduce methyl groups, as well as a more elaborate reaction mechanisms resulting in the transfer of a ribosyl moiety. Common to those three enzymes is the modification of tRNA molecules, however, on different positions within the tRNA body. In addition to the detailed discussions in chapters 2-4, the following discussion will focus on a general aspect of the subsequent modifications and future perspectives of the tRNA modification field.

The second chapter of this thesis investigated the methyltransferase TrmB. Biochemical data revealed a half-of-the site reaction mechanism of the homodimeric enzyme at near physiological SAM concentrations (Figure 2.2). However, in principle, both subunits are capable of binding the methyl group donor SAM and post-catalytic product SAH, as seen in the respective crystal structures (Figure 2.3). Furthermore, SAXS experiments revealed a 2:2 TrmB-tRNA stoichiometry, in which each TrmB subunit is complexed with one tRNA molecule (Figure 2.7). The TrmB-SAM/SAH complex crystal structures enabled to identify the active site pocket of *Bacillus subtilis* TrmB (Figure 2.3). Analysis of the active site pocket and conserved water molecules within this pocket showed that even though both TrmB subunits are topologically identical, they are in chemically different states (Figure 2.5). The presented results connected biochemical data of a half-of-the sites reactivity with structural data of the pre- and post-catalytic methyl group donor SAM and SAH. In the following, the TrmB-tRNA^{Phe} complex model is compared to the yeast Trm8/Trm82-tRNA complex model (Leulliot et al., 2008) to further infer TrmB activity.

The third chapter focused on the methyltransferase Dnmt2. Recently, Dnmt2 activity was shown to be stimulated by prior modification of the tRNA^{Asp} substrate with queuosine (Johannsson et al., 2018; Müller et al., 2015). Analyses of substrate specificity of human Dnmt2 showed the

modulated activity of human $tRNA^{His}$ and human $tRNA^{Asp}$ upon queuosinylation (Figure 3.2). However, this activity was demonstrated to be pH dependent. In the following paragraphs, pH sensitivity and modulated Dnmt2 activity in the context of stress response will be discussed.

The last chapter investigated the unique enzyme QueA. So far, only incomplete structures of QueA without the ribosyl group donor are available. The reported crystal structure (Figure 4.1) and full length QueA model (Figure 4.3) enabled to locate the SAM-binding pocket and putative active site residues (Figure 4.4). Furthermore, molecular docking of the full length QueA model with $tRNA^{Asp}$ resulted in the proposition of a QueA-$tRNA^{Asp}$ complex model (Figure 4.4). On basis of this model, the relevance of QueA as target in computer aided drug design approaches will be discussed herein.

5.1 tRNA binding is not conserved in the TrmB/Trm8 enzyme family

Members of the TrmB/Trm8 enzyme family differ in their nucleotide sequence with a sequence identity of < 20%. On the other hand, crystal structures of TrmB/Trm8 family members revealed high structural conservation with a root mean square deviation of RMSD = 1.19 Å for *B. subtilis* TrmB and yeast Trm8 (Figure 2.3 and Leulliot et al., 2008; Zegers, 2006) and RMSD = 1.49 Å for *B. subtilis* TrmB and *E. coli* TrmB (Figure 2.3 and Q. Liu et al., 2008; Zegers, 2006). However, albeit the structural conservation, the TrmB/Trm8 enzyme family differ in their biological assembly (Leulliot et al., 2008; Q. Liu et al., 2008; Zegers, 2006). While the *E. coli* homologue represents the simplest possible arrangement forming a monomer (Q. Liu et al., 2008), the *B. subtilis* (TrmB) (Zegers, 2006), yeast (Trm8/Trm82) (Leulliot et al., 2008), and human (METTL1/WDR4) homologues (Dong et al., 2008) arrange in a complex way. Trm8/Trm82 and METTL1/WDR4 form a heterodimer with Trm82 and WDR4 representing the non-catalytic subunits. TrmB in contrast assembles in a homodimeric form. Of all known crystal structures, neither crystallization attempts succeeded in co-crystallization of tRNAs.

The TrmB/Trm8 protein family contains only a few conserved residues. Most of these residues are involved in SAM biding and part of the putative catalytic centre, as in the case of Asp118 (Purta et al., 2005; Tomikawa et al., 2018). Some of the conserved amino acids are located at the ends of secondary structure elements, possibly introducing unstructured loop regions. The remaining residues are part of the conserved η1 region and were shown to interact with tRNA in the TrmB-$tRNA^{Phe}$ complex model (Figure 2.7), as well as in the yeast Trm8/Trm82 complex model (Leulliot et al., 2008). Both TrmB-$tRNA^{Phe}$ (Figure 2.7) and Trm8/Trm82-$tRNA^{Phe}$ complex models were obtained from SAXS experiments. The structural arrangements of both complex models showed differences in the orientation of the tRNA substrate on TrmB/Trm8 (Figure 5.1B). In the TrmB-

$tRNA^{Phe}$ complex model, the tRNA anticodon-stem loop (ASL) pointed in the direction of the methionine moiety (Figure 5.1B, the tRNA ASL pointing to the left) and the tRNA elbow pointed in the direction of the adenine moiety of SAM (Figure 5.1B, tRNA ASL pointing to the right). In contrast, analysis of the yeast Trm8/Trm82-$tRNA^{Phe}$ complex model (Leulliot et al., 2008) shows that the tRNA substrate is rotated by 180° with respect to the TrmB-$tRNA^{Phe}$ complex model. This orients the tRNA ASL in the direction of the adenine moiety and the tRNA elbow in the direction of the methionine moiety of SAM. In both positions, the G46 base of the tRNA substrate was able to break hydrogen bonds and flip out, into the G46 binding pocket of TrmB/Trm8. However, superposition of the Trm8/Trm82 heterodimer with the TrmB-$tRNA^{Phe}$ complex model revealed clashes of the $tRNA^{Phe}$ complex acceptor stem with the yeast regulatory subunit Trm82 (Figure 5.1B). Adopting the TrmB-$tRNA^{Phe}$ complex model orientation, $tRNA^{Phe}$ protrudes deep into Trm82. In contrast, $tRNA^{Phe}$ bound to Trm8 reveals no interaction points with Trm82 (Leulliot et al., 2008).

This raises the question whether the presented complex models are correct, or if TrmB/Trm8 enzymes have converged during evolution and developed distinct tRNA recognition mechanisms. To support the reported TrmB-$tRNA^{Phe}$ complex model (Figure 2.7), mass-spectrometry analyses of cross-linked protein-RNA complexes were performed. Six protein-RNA cross-links induced by UV irradiation were identified by means of mass-spectrometry (Figure 2.6). Of these six cross-links, Lys137 and Lys138 are of special interest (Figure 5.1A). Both residues are located above the adenine moiety of SAM. The respective residues in yeast Trm8 are Ser and Glu. In contrast to Lys137/138 which were found to interact with tRNA, Trm8 Ser and Glu interact directly with Trm82. Subsequently, complexation of TrmB-$tRNA^{Phe}$ with the tRNA orientation according to the Trm8/Trm82-$tRNA^{Phe}$ complex model would prevent Lys137/138 from interacting with the tRNA substrate and cross-links would not be established. However, this is unlikely due to the formation of covalent bonds induced by UV irradiation and the necessity of the protein and RNA molecules to be in close association. Additionally, the Lys137/138 cross-links were found in all biological replicates (Figure 2.6). This might indicate that even though the TrmB/Trm8 enzyme family is structurally conserved, the mode of tRNA binding is different. This leads to the conclusion that during evolution heterodimerization of Trm8/Trm82 forced the enzyme to bind its tRNA substrate in a different way. Additionally, this hypothesis is strengthened by biochemical studies showing differences in substrate specificity. While eukaryotic TrmB enzymes recognize their tRNA substrate by the T- and D-arm (Trm8/Trm82 recognizes tRNA by the D-arm and T-arm Matsumoto et al., 2007b), eubacterial TrmB enzymes distinguish cognate form non-cognate TrmB by its T-arm (*A. aeolicus* TrmB; Okamoto et al., 2004). Concluding, that the establishment of a catalytic and regulatory subunit of Trm8/Trm82 changed the protein-RNA interaction interface, resulting in the need of an altered substrate binding pattern. Hence, heterodimerization of the

yeast Trm8/Trm82 enzyme possibly forced Trm8/Trm82 to evolve a more restrictive substrate recognition mechanism compared to the monomeric *E. coli* TrmB and homodimeric *B. subtilis* TrmB.

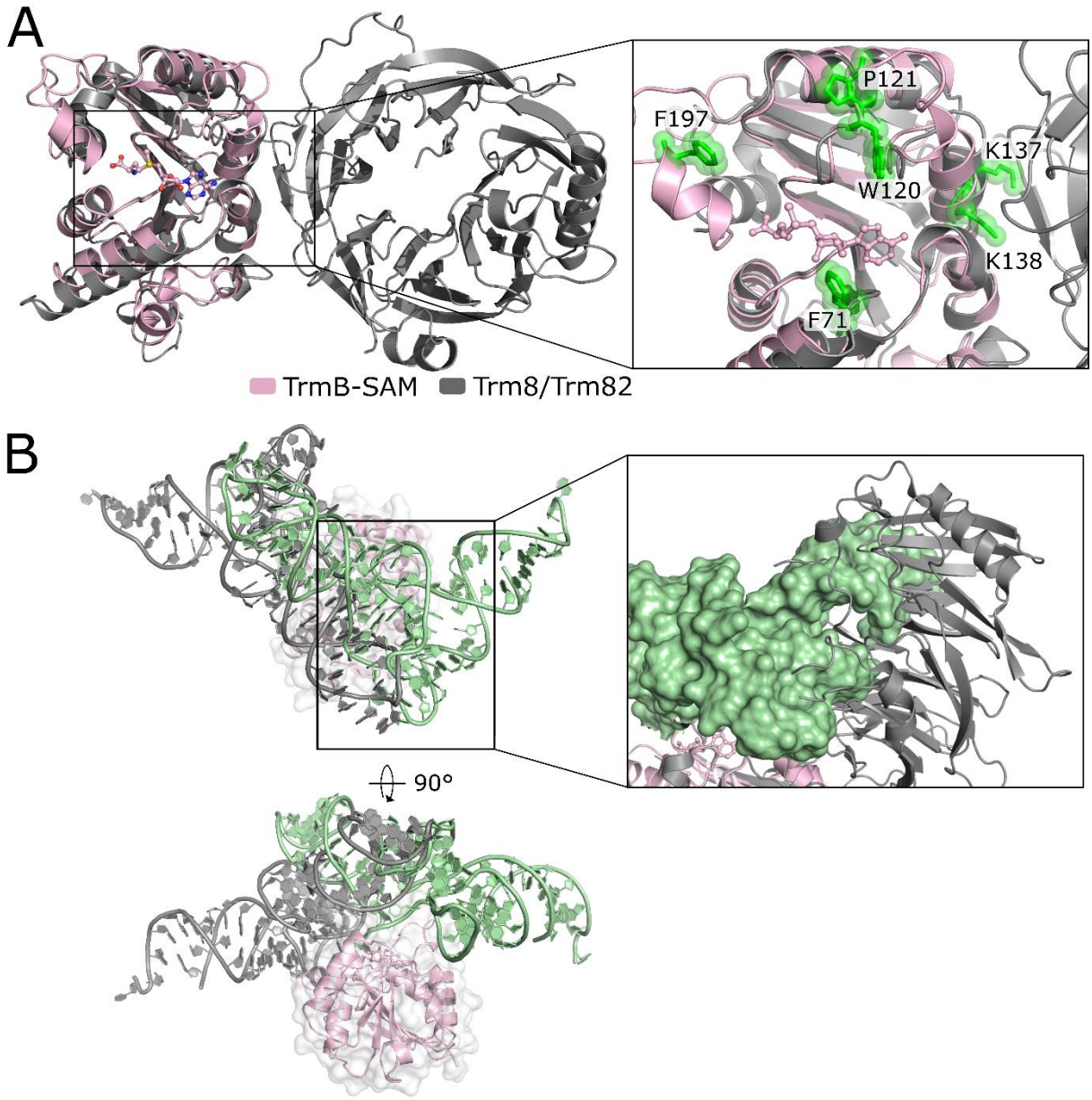

Figure 5.1: *B. subtilis* and yeast TrmB/Trm8-tRNA^{Phe} complex models. (A) Superposition of Trm8/Trm82 (Leulliot et al., 2008) (grey) with TrmB (light pink) both represented as cartoon, bound SAM molecule is shown in ball and stick mode. Zoomed in view of TrmB/Trm8 (right) with highlighted UV cross-links of TrmB-tRNA^{Phe} depicted as sticks and spheres (green). (B) Comparison of TrmB/Trm8-tRNA^{Phe} complex models with respect to the position of the substrate tRNA shown as cartoon and depicted at two orientations. TrmB is presented as cartoon (light pink) with a transparent surface. Yeast tRNA^{Phe} (grey) in the Trm8/Trm82 complex model is rotated by 90° with respect to the *B. subtilis* tRNA^{Phe} (green). Zoomed-in view of yeast Trm82 and *B. subtilis* tRNA^{Phe} surface.

The identification of different binding patterns in the heterodimeric Trm8/Trm82-tRNA^{Phe} enzymes (Leulliot et al., 2008) and homodimeric TrmB-tRNA^{Phe} enzymes (Chapter 2) gives

valuable insights for further investigations of these enzymes in diseases. Even though the TrmB/Trm8 enzyme family is structurally conserved, they developed different tRNA binding strategies. The presented TrmB-tRNA^{Phe} complex model (Figure 2.7) might serve as study model for bacterial TrmB enzymes. In general, even though the yeast TrmB-tRNA complex model and the in this thesis presented TrmB-tRNA^{Phe} complex model show distinct tRNA binding modes, both complex models can be used to analyse the TrmB enzymatic mechanism, since amino acids present in the active site pocket are highly conserved.

5.2 pH-dependent Dnmt2 activity and possible roles in stress response

A key point during posttranscriptional modification is the specific recognition of correct and rejection of incorrect substrates by the respective RNA modifying enzyme. However, in many cases, substrate recognition remains enigmatic, since crystallization of protein-tRNA complexes are recalcitrant to crystallographic analysis. In chapter 3, changes in substrate specificity of human Dnmt2 was shown by means of biochemical methods. tRNA^{Asp} is the commonly known Dnmt2 substrate so far. Recently, Dnmt2 was found to be stimulated upon queuosine modification at position 34 in the wobble position (Johannsson et al., 2018; Müller et al., 2015). During the course of this thesis, tRNA^{His} was found to be tightly bound (Figure 3.1) and methylated by human Dnmt2 (Figure 3.2). These changes in substrate specificity were found to be pH-dependent (Figure 3.2). Such altered enzyme activity could indicate a connection to stress response pathways. Indeed, Goll *et al.* (2006) discussed the level of Dnmt2 conservation across different taxa. The high conservation implied positive selection of Dnmt2, which results in increasing Dnmt2 fitness under different stress conditions. For example, the lack of the m^{5}C38 modification leads to an increased production of tRNA fragments that would be otherwise inhibited. These tRNA fragments in turn can interfere with mRNAs and thus, can lead to translational defects (Schaefer et al., 2010). Additionally, cultivation of *S. pombe* cells in minimal medium resulted in a methylation level of tRNA$^{Asp\ (GUC)}$ to approximately 6% (in the absence of queuosine). In the presence of queuosine, the methylation level of Q34tRNA$^{Asp(GUC)}$ increased to 100% (Müller et al., 2015). This shows a link between nutrient sensing and Dnmt2 methylation activity. Thus, nutrient sensing in starvation conditions can lead to the activation of signalling pathways via the lack of Dnmt2-dependent modification and therefore increased production of tRNA fragments.

Additionally, due to the high pH sensitivity of most enzymes, pH homeostasis is critical to living cells. Within HeLa cells, pH values were approximated for the Golgi apparatus, cytoplasm, and mitochondria to be 6.6, 7.4, and 8.0, respectively (Casey et al., 2010; Theillet et al., 2014). Beside the high abundance of RNA modifying enzymes in the cytosol, there are several enzymes

associated with mitochondria. Two of in total seven enzymes belonging to the NOL1/NOP2/SUN domain (NSUN) protein family that install m^5C modifications are localized to the mitochondria and modify mt-$tRNA^{Met}$ and mt-12S rRNA (reviewed in Bohnsack et al., 2019; Haag et al., 2016). tRNA methylation has been implied in the regulation of tRNA folding and stability. Misfolded or less stable tRNAs might have an impact on the rate and fidelity of protein synthesis, especially under stress conditions or during aging (Schaefer and Lyko, 2010). Hence, it could be possible that Dnmt2, as part of stress response networks, is able to methylate $tRNA^{His}$ *in vivo* under certain environmental conditions and as result of stress induced re-location of Dnmt2 to more alkaline environments.

Furthermore, Dnmt2 is able to localize to stress granules and RNA processing bodies as a consequence of external stimuli, such as oxidative stress, heat shock, low pH, and more surprisingly upon viral infection (Dev et al., 2017; Schaefer et al., 2010). Studies on different human cell lines and mouse lung fibroblasts revealed a dynamic shuttling of Dnmt2 between the nucleus and cytoplasm. In the latter, Dnmt2 displays a non-uniform distribution, with local accumulations into cytoplasmic foci (Thiagarajan et al., 2011). Furthermore, upon virus infection, predominantly nuclear Dnmt2 re-localises into cytoplasmic stress granules (Dev et al., 2017). These stress granules belong to cytoplasmic foci and RNA-processing bodies and show themselves dynamicity in their location, as they have been identified in the cytosol as well as in the nucleus. Special to foci is that they bring in different cytoplasmic and nucleic RNA species, typically after cellular stress and translational arrest, where these RNA species are to be sorted either for storage or degradation. Showing that beyond stress induced Dnmt2 activity on tRNAs, Dnmt2 can be further regulated via re-localization within the cell to be part of an RNA processing machinery during stress.

The preliminary results obtained for human Dnmt2 activity on human G34/Q34-$tRNA^{His}$ should be confirmed by further investigating the pH-dependency of Dnmt2. Due to the re-localization of Dnmt2 as a consequence of different stress stimuli, the reported pH-dependency of Dnmt2 activity could in fact have a biological role. To gain more insight into Dnmt2 substrate specificity, protein-tRNA complex crystal structures would be highly desirable. Crystallization trials to obtain a crystal structure of full length tRNA in complex with Dnmt2 failed so far. Dnmt2 was shown to interact mainly with the tRNA anticodon stem/loop (Jeltsch et al., 2017; Johannsson et al., 2018) and should suffice for proper interactions. Hence, crystallization of the Dnmt2-$tRNA^{Asp}$ anticodon stem loop complex could increase the success rate of complex crystallization due to the smaller size of the tRNA substrate.

5.3 Significance of QueA-tRNA^{Asp} complex model for drug design

Increasing numbers of antimicrobial resistances in combination with the unattended development of new antimicrobials, raise the need for alternative drugs against bacterial infections (*WHO. Antimicrobial resistance (WHO Fact sheet).*, 2018). An alternative approach to drug design would be to identify key proteins for bacterial infection and to specifically design inhibitors for those proteins. These inhibitors could result in the inactivity or death of the bacterium and would help to overcome and circumvent microbial resistances (Ferreira and Andricopulo, 2014).

The fourth chapter focused on QueA catalysing the penultimate step in Q biosynthesis. So far, only incomplete structures of QueA were available (Grimm et al., 2006; Mathews et al., 2005). As part of the Q biosynthesis and the role of Q in the virulent phenotype of *Shigella flexneri*, it is highly desirable to obtain a complete QueA structure. The presented QueA crystal structure (Figure 4.1) was used to perform loop modelling to obtain a full length QueA structure model (Figure 4.3). This model enabled the localization of the SAM-binding pocket, hence the putative active site (Figure 4.3). With the hypothesized location of the active site pocket, the reported QueA model represents an interesting starting point for structure-based drug design to tackle shigellosis.

5.3.1 *S. flexneri* infection cycle and inhibition of pathogenicity

QueA is involved in the pathogenic phenotype of *Shigella flexneri*. *Shigella* bacteria are highly infectious as its infective dose is as low as 10 to 100 organisms (DuPont et al., 1989; Louise K. Francois Watkins and Grace D. Appiah, 2019). The infection cycle starts by the attack of epithelial cells in the intestines. To do so, *Shigella* produces virulence factors called "invasins" (Jennison and Verma, 2004; Philpott et al., 2000). Together with proteins present on the epithelial cells, they form a complex allowing penetration and proliferation of the bacteria in the infected cells. Basis of the virulence phenotype is the transcription factor *VirF*. In order for *VirF* to be efficiently transcribed, it takes Q-modified tRNAs. If Q-modified tRNAs are not present, translation of *VirF* is inefficient. Hence, *Shigella* is unable to produce enough invasins and the pathogenic potential is reduced.

Usually, bacterial diseases can be treated with antibiotics. However, *Shigella* bacteria are prone to develop resistances and are already resistant to most antibiotics (Ranjbar and Farahani, 2019). Additionally, due to the elimination of naturally occurring bacteria in the intestinal flora, antibiotics could lead to diarrheal symptoms during *Shigella* infection and could cause severe dehydration in patients. Therefore, therapeutics specifically tackling the suppression of the pathogenic phenotype of *Shigella* would be advantageous. So far, only the QueA upstream enzyme TGT was subjected to structure-based drug design. In contrast to TGT, QueA has no equivalent in

humans, which renders QueA a better druggable target than TGT. TGT inhibition can be achieved at two different steps during catalysis. First, a sufficiently large molecule mimicking the tRNA can prevent binding of the tRNA substrate to TGT. Second, binding of $preQ_1$ can be stalled by blocking the $preQ_1$ binding site in the catalytic pocket (Grädler, 2001; Hörtner et al., 2007). So far, this approach was not used to design inhibitors for QueA, since no full length QueA model was available and the active site was not defined.

5.3.2 Crystallographic based drug design

Structural based approaches have been increasingly powerful tools in the field of drug development. Crystallography-based screening can provide initial lead compounds for elaborate drug campaigns. Typical fragments used for co-crystallization or soaking experiments are small molecules between 110-250 Da in size, used in high concentrations (Badger, 2012). The crystal structures of bound fragments enable direct analysis of the binding landscape for potential fragment expansion, merging, or linking (Patel et al., 2014). Additionally, crystallography-based fragment screening allows the detection of ligands with low binding affinities from sub-nanomolar to millimolar range, with the only limitation represented by the resolution limit. Ideally, protein crystals should diffract to high resolution better than 2.5 Å (Patel et al., 2014). Even though this technique is not as fast as high throughput biochemical screening methodologies, it still allows screening of large compound libraries, the reduction of false positives, and highly credible fragment hits (Leach et al., 2006), which is of high value to speed up experimental screening subsequently.

The QueA-$tRNA^{Asp}$ complex model (Figure 4.4) gave first valuable insights into substrate binding of QueA. Even though QueA crystal structures have been determined to resolutions up to 2 Å viable for structure-based drug design (Figure 4.1, Grimm et al., 2006; Mathews et al., 2005), important parts of the QueA structure remain unresolved so far (Grimm et al., 2006; Mathews et al., 2005). Importantly, these unresolved regions of QueA contain conserved residues which could be part of the active centre and involved in catalysis. The here presented full length QueA model (Figure 4.3) based on the crystal structure (Figure 4.1) with homology modelled loops is a good starting point to investigate possible biding sites on QueA to design drugs.

However, a crystallography-based structural approach for QueA seems difficult due to several reasons. First, obtaining a full length QueA crystal structure could not be obtained yet even though crystallization conditions have been improved (Figure 4.1). Second, even though QueA was co-crystallized and soaked with several compounds including SAM, SAH, adenine, and methionine to high concentrations, a complex structure of QueA with these compounds could not be obtained (Figure 4.1, Grimm et al., 2006; Mathews et al., 2005). Hence, a different approach to crystallography-based drug design would be a promising approach. Aside X-ray based

approaches, nuclear magnetic resonance could be applied to yield structure-inhibitor complexes without the need of protein crystals that are well-diffracting. However, a more promising strategy combines experimental with computational methods. Fragment libraries are virtually screened against receptor molecules (known crystal structures), subsequently increasing hit rates compared to classical high throughput screening (Nicola and Abagyan, 2009). Computational analysis includes molecular docking of fragments to receptors followed by scoring the quality of fit of the compound. Scoring functions can be e.g. physics-based, empirical, and knowledge-based (Li et al., 2019). Subsequently, lead compounds can be used in *in vitro* biochemical assays to test its inhibition potential. Using the full length QueA model, these approaches could give first insights into the feasibility of QueA inhibition.

Inhibition strategies for TGT were shown to target either tRNA or $preQ_1$ interactions (Grädler, 2001; Hörtner et al., 2007). Both approaches could also apply to inhibit QueA. The QueA-$tRNA^{Asp}$ complex model (Figure 4.4) showed two major interaction sites of the tRNA substrate with QueA in the (i) proposed catalytic pocket, and (ii) with the small domain. Blocking of these positions with molecules large enough to disrupt electrostatic interactions of QueA with its substrate tRNA could stall QueA activity. Conducting protein-RNA cross-linking experiments would further increase our knowledge about direct protein-RNA contacts and additionally validate the proposed QueA-$tRNA^{Asp}$ complex model. The second method tackles the binding of $preQ_1$ to the active site. Analogous to this approach is blocking of the QueA active site and to prevent SAM from binding, hence ribosyl transfer would be stopped. However, the proposed active site needs to be further analysed. Mutagenesis of the putative active site residues with subsequent activity assays would increase knowledge about QueA activity. Therefore, SAM turnover could be measured by means of mass spectrometry testing the amount of released adenine and methionine. Continuing in the scenario of blocking the active site, a highly specific molecule is needed that is able to block either one or both sides of the SAM-biding pocket (Figure 4.3). However, mimicking SAM binding can be a challenging task, since SAM contains an adenine moiety which is among others part of the ubiquitous molecule adenosine triphosphate (ATP) needed in many essential biochemical mechanisms of all cells. To overcome this issue, inhibitors mimicking ATP often consist of a peptide fragment conjugated with an adenosine or a nonhydrolyzable ATP derivative (Winiewska-Szajewska et al., 2019). Importantly, specificity of such inhibitors is not determined by the adenine moiety, but rather by the conjugated peptide fragment. The QueA-$tRNA^{Asp}$ complex model showed the binding of the $preQ_1$34 base to a pocket in front of the SAM-binding pocket (Figure 4.4). Subsequently, inhibitors could be designed in a way that they not only bind to one side of the SAM-binding pocket, but also reach into the $preQ_1$34-binding pocket. Hence, such inhibitors would not only prevent SAM from binding, but also disrupt $preQ_1$34 coordination by QueA. Taken together, the in this thesis reported QueA-$tRNA^{Asp}$ complex model could be a good

starting point for structure-based fragment engineering to inhibit QueA activity and tackle shigellosis.

5.3.3 Current developments in drugging *Shigella spp*.

So far, only the treatment of Shigellosis was discussed. However, due to the occurrence of severe shigellosis cases in developing countries, prevention of infections poses the major goal. Several approaches to develop a vaccine against *Shigella spp.* have been attempted. These include, among others, the administration of subunit vaccines (clinical trials showed strong serum antibody responses; Ashkenazi et al., 1999; Cohen et al., 1996), acetone-killed *S. flexneri* (unable to protect from infection; Formal et al., 1965), heat-killed *S. flexneri* (100% protective in rabbit model; Chakrabarti et al., 2007), and non-invasive live vaccines (up to 85% efficacy but must be administered every six months in high doses; Meitert et al., 1984). Even though some vaccine strategies have been shown to be safe in animal models and humans, and were promising in initial human clinical trials, complete protection against *Shigella* infection could not be reached yet. Therefore, future vaccine developments will focus on vaccine cocktails, as seen for influenza vaccination, to protect against a variety of *Shigella* serotypes (Ranjbar and Farahani, 2019). In conclusion, using structural and computational approaches to find potential compounds to inhibit QueA activity combined with the development of vaccines could help to prevent *Shigella* infection and treat putative infections without the risk of obtaining resistant bacteria.

Chapter 6 References

Agris, P.F., Sierzputowska-Gracz, H., Smith, C., 1986. Transfer RNA contains sites of localized positive charge: carbon NMR studies of [13C] methyl-enriched Escherichia coli and yeast tRNAPhe. Biochemistry 25, 5126–5131. https://doi.org/10.1021/bi00366a022

Alexandrov, A., 2005. tRNA m7G methyltransferase Trm8p/Trm82p: Evidence linking activity to a growth phenotype and implicating Trm82p in maintaining levels of active Trm8p. RNA 11, 821–830. https://doi.org/10.1261/rna.2030705

Alexandrov, A., Chernyakov, I., Gu, W., Hiley, S.L., Hughes, T.R., Grayhack, E.J., Phizicky, E.M., 2006. Rapid tRNA Decay Can Result from Lack of Nonessential Modifications. Molecular Cell 21, 87–96. https://doi.org/10.1016/j.molcel.2005.10.036

Alexandrov, A., Martzen, M.R., Phizicky, E.M., 2002. Two proteins that form a complex are required for 7-methylguanosine modification of yeast tRNA. RNA 8, 1253–1266. https://doi.org/10.1017/S1355838202024019

Ashkenazi, S., Passwell, J.H., Harlev, E., Miron, D., Dagan, R., Farzan, N., Ramon, R., Majadly, F., Bryla, D.A., Karpas, A.B., Robbins, J.B., Schneerson, R., the Israel Pediatric Shigella Study Group, 1999. Safety and Immunogenicity of *Shigella sonnei* and *Shigella flexneri* 2a O-Specific Polysaccharide Conjugates in Children. J INFECT DIS 179, 1565–1568. https://doi.org/10.1086/314759

Badger, J., 2012. Crystallographic Fragment Screening, in: Tari, L.W. (Ed.), Structure-Based Drug Discovery, Methods in Molecular Biology. Humana Press, Totowa, NJ, pp. 161–177. https://doi.org/10.1007/978-1-61779-520-6_7

Bandarian, V., Drennan, C.L., 2015. Radical-mediated ring contraction in the biosynthesis of 7-deazapurines. Current Opinion in Structural Biology 35, 116–124. https://doi.org/10.1016/j.sbi.2015.11.005

Berman, H.M., Westbrook, J., Feng, Z., Gilliland, G., Bhat, T.N., Weissig, H., Shindyalov, I.N., Bourne, P.E., 2000. The Protein Data Bank. Nucleic Acids Research 28, 235–242. https://doi.org/10.1093/nar/28.1.235

Betat, H., Long, Y., Jackman, J.E., Mörl, M., 2014. From End to End: tRNA Editing at 5'- and 3'-Terminal Positions. Int. J. Mol. Sci. 24. https://doi.org/10.3390/ijms151223975

Boccaletto, P., Machnicka, M.A., Purta, E., Piątkowski, P., Bagiński, B., Wirecki, T.K., de Crécy-Lagard, V., Ross, R., Limbach, P.A., Kotter, A., Helm, M., Bujnicki, J.M., 2018. MODOMICS: a database of RNA modification pathways. 2017 update. Nucleic Acids Research 46, D303–D307. https://doi.org/10.1093/nar/gkx1030

Bohnsack, K., Höbartner, C., Bohnsack, M., 2019. Eukaryotic 5-methylcytosine (m5C) RNA Methyltransferases: Mechanisms, Cellular Functions, and Links to Disease. Genes 10, 102. https://doi.org/10.3390/genes10020102

Boland, C., Hayes, P., Santa-Maria, I., Nishimura, S., Kelly, V.P., 2009. Queuosine Formation in Eukaryotic tRNA Occurs via a Mitochondria-localized Heteromeric Transglycosylase. Journal of Biological Chemistry 284, 18218–18227. https://doi.org/10.1074/jbc.M109.002477

Bujnicki, J.M., 1991. Comparison of Protein Structures Reveals Monophyletic Origin of the AdoMet-Dependent Methyltransferase Family and Mechanistic Convergence Rather than Recent Differentiation of N4-Cytosine and N6-Adenine DNA Methylation. In Silico Biology 1, 334–344. https://doi.org/10.1016/0959-440X(91)90031-N

Cantara, W.A., Crain, P.F., Rozenski, J., McCloskey, J.A., Harris, K.A., Zhang, X., Vendeix, F.A.P., Fabris, D., Agris, P.F., 2011. The RNA Modification Database, RNAMDB: 2011 update. Nucleic Acids Res 39, D195-201. https://doi.org/10.1093/nar/gkq1028

Cao, G., Li, H.-B., Yin, Z., Flavell, R.A., 2016. Recent advances in dynamic m6A RNA modification. Open Biology 6, 8. https://doi.org/10.1098/rsob.160003

Cao, T., Rajasingh, S., Samanta, S., Dawn, B., Bittel, D.C., Rajasingh, J., 2018. Biology and clinical relevance of noncoding sno/scaRNAs. Trends in Cardiovascular Medicine 28, 81–90. https://doi.org/10.1016/j.tcm.2017.08.002

Carell, T., Brandmayr, C., Hienzsch, A., Müller, M., Pearson, D., Reiter, V., Thoma, I., Thumbs, P., Wagner, M., 2012. Structure and Function of Noncanonical Nucleobases. Angew. Chem. Int. Ed. 51, 7110–7131. https://doi.org/10.1002/anie.201201193

Carell, T., Kurz, M.Q., Müller, M., Rossa, M., Spada, F., 2018. Non-canonical Bases in the Genome: The Regulatory Information Layer in DNA. Angew. Chem. Int. Ed. 57, 4296–4312. https://doi.org/10.1002/anie.201708228

Cartlidge, R.A., Knebel, A., Peggie, M., Alexandrov, A., Phizicky, E.M., Cohen, P., 2005. The tRNA methylase METTL1 is phosphorylated and inactivated by PKB and RSK in vitro and in cells. EMBO J 24, 1696–1705. https://doi.org/10.1038/sj.emboj.7600648

Casey, J.R., Grinstein, S., Orlowski, J., 2010. Sensors and regulators of intracellular pH. Nat Rev Mol Cell Biol 11, 50–61. https://doi.org/10.1038/nrm2820

Catalanotto, C., Cogoni, C., Zardo, G., 2016. MicroRNA in Control of Gene Expression: An Overview of Nuclear Functions. IJMS 17, 1712. https://doi.org/10.3390/ijms17101712

Cavarelli, J., Moras, D., 1993. Recognition of tRNAs by aminoacyl-tRNA synthetases. The FASEB Journal 7, 79–86. https://doi.org/10.1096/fasebj.7.1.8422978

Chakrabarti, M., Bhattacharya, J., Bhattacharya, M., Nair, G., Bhattacharya, S., Mahalanabis, D., 2007. Killed oral Shigella vaccine made from Shigella flexneri 2a protects against challenge in the rabbit model of shigellosis. Acta Paediatrica 88, 161–165. https://doi.org/10.1111/j.1651-2227.1999.tb01075.x

Chan, P.P., Lowe, T.M., 2016. GtRNAdb 2.0: an expanded database of transfer RNA genes identified in complete and draft genomes. Nucleic Acids Res 44, D184–D189. https://doi.org/10.1093/nar/gkv1309

Chen, Y., Sierzputowska-Gracz, H., Guenther, R., Everett, K., Agris, P.F., 1993. 5-Methylcytidine is required for cooperative binding of magnesium(2+) and a conformational transition at the anticodon stem-loop of yeast phenylalanine tRNA. Biochemistry 32, 10249–10253. https://doi.org/10.1021/bi00089a047

Cohen, D., Ashkenazi, S., Green, M., Lerman, Y., Slepon, R., Robin, G., Orr, N., Taylor, D.N., Sadoff, J.C., Chu, C., Shiloach, J., Schneerson, R., Robbins, J.B., 1996. Safety and immunogenicity of investigational Shigella conjugate vaccines in Israeli volunteers. Infection and immunity 64, 4074–4077. https://doi.org/10.1128/IAI.64.10.4074-4077.1996

Dahm, R., 2008. Discovering DNA: Friedrich Miescher and the early years of nucleic acid research. Hum Genet 122, 565–581. https://doi.org/10.1007/s00439-007-0433-0

De Bie, L.G.S., Roovers, M., Oudjama, Y., Wattiez, R., Tricot, C., Stalon, V., Droogmans, L., Bujnicki, J.M., 2003. The yggH Gene of Escherichia coli Encodes a tRNA (m7G46) Methyltransferase. Journal of Bacteriology 185, 3238–3243. https://doi.org/10.1128/JB.185.10.3238-3243.2003

Delaunay, S., Frye, M., 2019. RNA modifications regulating cell fate in cancer. Nat Cell Biol 21, 552–559. https://doi.org/10.1038/s41556-019-0319-0

Dev, R.R., Ganji, R., Singh, S.P., Mahalingam, S., Banerjee, S., Khosla, S., 2017. Cytosine methylation by DNMT2 facilitates stability and survival of HIV-1 RNA in the host cell during infection. Biochemical Journal 474, 2009–2026. https://doi.org/10.1042/BCJ20170258

Dong, A., 2001. Structure of human DNMT2, an enigmatic DNA methyltransferase homolog that displays denaturant-resistant binding to DNA. Nucleic Acids Research 29, 439–448. https://doi.org/10.1093/nar/29.2.439

Dong, A., Zeng, H., Dobrovetsky, E., Bountra, C., Weigelt, J., Arrowsmith, C.H., Edwards, A.M., Bochkarev, A., Min, Plotnikov, Wu, H., Structural Genomics Consortium (SGC), 2008. Crystal structure of human methyltransferase-like protein 1. https://doi.org/20121107150707

DuPont, H.L., Levine, M.M., Hornick, R.B., Formal, S.B., 1989. Inoculum Size in Shigellosis and Implications for Expected Mode of Transmission. Journal of Infectious Diseases 159, 1126–1128. https://doi.org/10.1093/infdis/159.6.1126

Durand, J.M., Okada, N., Tobe, T., Watarai, M., Fukuda, I., Suzuki, T., Nakata, N., Komatsu, K., Yoshikawa, M., Sasakawa, C., 1994. vacC, a virulence-associated chromosomal locus of Shigella flexneri, is homologous to tgt, a gene encoding tRNA-guanine transglycosylase (Tgt) of Escherichia coli K-12. Journal of Bacteriology 176, 4627–4634. https://doi.org/10.1128/JB.176.15.4627-4634.1994

Edmonds, C.G., Crain, P.F., Gupta, R., Hashizume, T., Hocart, C.H., Kowalak, J.A., Pomerantz, S.C., Stetter, K.O., McCloskey, J.A., 1991. Posttranscriptional modification of tRNA in thermophilic archaea (Archaebacteria). Journal of Bacteriology 173, 3138–3148. https://doi.org/10.1128/JB.173.10.3138-3148.1991

Emmerich, B., Zubrod, E., Weber, H., Maubach, P.A., Kersten, H., Kersten, W., 1985. Relationship of Queuine-lacking Transfer RNAs to the Grade of Malignancy in Human Leukemias and Lymphomas 45, 8.

Endres, L., Dedon, P.C., Begley, T.J., 2015. Codon-biased translation can be regulated by wobble-base tRNA modification systems during cellular stress responses. RNA Biology 12, 603–614. https://doi.org/10.1080/15476286.2015.1031947

Fabrega, C., Shen, V., Shuman, S., Lima, C.D., 2004. Structure and Mechanism of mRNA Cap (Guanine-N7) Methyltransferase. Molecular Cell 77–89. https://doi.org/10.1016/S1097-2765(03)00522-7

Ferreira, R., Andricopulo, A., 2014. Structure-Based Drug Design to Overcome Drug Resistance: Challenges and Opportunities. CPD 20, 687–693. https://doi.org/10.2174/13816128200514021416194 9

Fish, L., Zhang, S., Yu, J., Culbertson, B., Zhou, A.Y., Goga, A., Goodarzi, H., 2018. Cancer cells exploit an orphan RNA to drive metastatic progression. Nat Med 24, 1743–1751. https://doi.org/10.1038/s41591-018-0230-4

Formal, S.B., LaBrec, E.H., Palmer, A., Falkow, S., 1965. Protection of Monkeys Against Experimental Shigellosis with Attenuated Vaccines. Journal of Bacteriology 90, 63–68. https://doi.org/10.1128/JB.90.1.63-68.1965

Frazer, J.M., Yang, W.-K., 1972. Isoaccepting transfer ribonucleic acids in liver and brain of young and old BC3F1 mice. Archives of Biochemistry and Biophysics 153, 610–618. https://doi.org/10.1016/0003-9861(72)90380-3

Frye, M., Harada, B.T., Behm, M., He, C., 2018. RNA modifications modulate gene expression during development. Science 361, 1346–1349. https://doi.org/10.1126/science.aau1646

Garcia, G.A., Kittendorf, J.D., 2005. Transglycosylation: A mechanism for RNA modification (and editing?). Bioorganic Chemistry 33, 229–251. https://doi.org/10.1016/j.bioorg.2005.01.001

Goll, M.G., Bestor, T.H., 2005. EUKARYOTIC CYTOSINE METHYLTRANSFERASES. Annu. Rev. Biochem. 74, 481–514. https://doi.org/10.1146/annurev.biochem.74.010904.153721

Goll, M.G., Kirpekar, F., Maggert, K.A., Yoder, J.A., Hsieh, C.-L., Zhang, X., Golic, K.G., Jacobsen, S.E., Bestor, T.H., 2006. Methylation of tRNA Asp by the DNA Methyltransferase Homolog Dnmt2. Science 311, 395–398. https://doi.org/10.1126/science.1120976

Goodman, H.M., Abelson, J., Landy, A., Brenner, S., Smith, J.D., 1968. Amber Suppression: a Nucleotide Change in the Anticodon of a Tyrosine Transfer RNA. Nature 217, 1019–1024. https://doi.org/10.1038/2171019a0

Grädler, U. et al, 2001. A New Target for Shigellosis: Rational Design and Crystallographic Studies of Inhibitors of tRNA-guanine Transglycosylase. Journal of Molecular Biology 306, 455–467. https://doi.org/10.1006/jmbi.2000.4256

Gregson, J.M., Crain, P.F., Edmonds, C.G., Gupta, R., Hashizume, T., Phillipson, D.W., McCloskey, J.A., 1993. Structure of the archaeal transfer RNA nucleoside G*-15 (2-amino-4,7-dihydro- 4-oxo-7-beta-D-ribofuranosyl-1H-pyrrolo[2,3-d]pyrimidine-5-carboximi dam ide (archaeosine)). Journal of Biological Chemistry 268, 10076–10086. https://doi.org/10.1016/S0021-9258(18)82174-3

Grimm, C., Ficner, R., Sgraja, T., Haebel, P., Klebe, G., Reuter, K., 2006. Crystal structure of Bacillus subtilis S-adenosylmethionine:tRNA ribosyltransferase-isomerase. Biochemical and Biophysical Research Communications 351, 695–701. https://doi.org/10.1016/j.bbrc.2006.10.096

Gu, C., Begley, T.J., Dedon, P.C., 2014. tRNA modifications regulate translation during cellular stress. FEBS Letters 588, 4287–4296. https://doi.org/10.1016/j.febslet.2014.09.038

Gutierrez, A., 2004. Evolution of dnmt-2 and mbd-2-like genes in the free-living nematodes Pristionchus pacificus, Caenorhabditis elegans and Caenorhabditis briggsae. Nucleic Acids Research 32, 6388–6396. https://doi.org/10.1093/nar/gkh982

Guzzi, N., 2020. Novel insights into the emerging roles of tRNA-derived fragments in mammalian development. RNA BIOLOGY 17, 1214–1222. https://doi.org/10.1080/15476286.2020.1732694

Haag, S., Sloan, K.E., Ranjan, N., Warda, A.S., Kretschmer, J., Blessing, C., Hübner, B., Seikowski, J., Dennerlein, S., Rehling, P., Rodnina, M.V., Höbartner, C., Bohnsack, M.T., 2016. NSUN3 and ABH1 modify the wobble position of mt-tRNA Met to expand codon recognition in mitochondrial translation. EMBO J 35, 2104–2119. https://doi.org/10.15252/embj.201694885

Hanukoglu, I., 2015. Proteopedia: Rossmann fold: A beta-alpha-beta fold at dinucleotide binding sites. Wiley Online Library 4. https://doi.org/10.1002/bmb.20849

Harada, F., Nishimura, S., 1972. Possible anticodon sequences of tRNAHis, tRNAAsn, and tRNAAsp from Escherichia coli. Universal presence of nucleoside O in the first position of the anticodons of these transfer ribonucleic acid. Biochemistry 11, 301–308. https://doi.org/10.1021/bi00752a024

Hayes, P., Fergus, C., Ghanim, M., Cirzi, C., Burtnyak, L., McGrenaghan, C.J., Tuorto, F., Nolan, D.P., Kelly, V.P., 2020. Queuine Micronutrient Deficiency Promotes Warburg Metabolism and Reversal of the Mitochondrial ATP Synthase in Hela Cells. Nutrients 12, 871. https://doi.org/10.3390/nu12030871

Helm, M., 2006. Post-transcriptional nucleotide modification and alternative folding of RNA. Nucleic Acids Research 34, 721–733. https://doi.org/10.1093/nar/gkj471

Helm, M., Brulé, H., Degoul, F., Cepanec, C., Leroux, J.P., Giegé, R., Florentz, C., 1998. The presence of modified nucleotides is required for cloverleaf folding of a human mitochondrial tRNA. Nucleic Acids Res 26, 1636–1643. https://doi.org/10.1093/nar/26.7.1636

Helm, M., Giege, R., Florentz, C., 1999. A Watson-Crick Base-Pair-Disrupting Methyl Group (m1A9) Is Sufficient for Cloverleaf Folding of Human Mitochondrial tRNALys. Biochemistry 38, 13338–13346. https://doi.org/10.1021/bi991061g

Hermann, A., Schmitt, S., Jeltsch, A., 2003. The Human Dnmt2 Has Residual DNA-(Cytosine-C5) Methyltransferase Activity. J. Biol. Chem. 278, 31717–31721. https://doi.org/10.1074/jbc.M305448200

Hörtner, S.R., Ritschel, T., Stengl, B., Kramer, C., Schweizer, W.B., Wagner, B., Kansy, M., Klebe, G., Diederich, F., 2007. Potent Inhibitors of tRNA-Guanine Transglycosylase, an Enzyme Linked to the Pathogenicity of theShigella Bacterium: Charge-Assisted Hydrogen Bonding. Angew. Chem. Int. Ed. 46, 8266–8269. https://doi.org/10.1002/anie.200702961

Hou, Y.M., 1997. Discriminating among the discriminator bases of tRNAs. Chem Biol 4, 93–96. https://doi.org/10.1016/s1074-5521(97)90252-0

Ibba, M., Söll, D., 2000. AMINOACYL-tRNA SYNTHESIS 36. https://doi.org/10.1146/annurev.biochem.69.1.617

Iwata-Reuyl, D., 2003. Biosynthesis of the 7-deazaguanosine hypermodified nucleosides of transfer RNA. Bioorganic Chemistry 31, 24–43. https://doi.org/10.1016/S0045-2068(02)00513-8

Jeltsch, A., Ehrenhofer-Murray, A., Jurkowski, T.P., Lyko, F., Reuter, G., Ankri, S., Nellen, W., Schaefer, M., Helm, M., 2017. Mechanism and biological role of Dnmt2 in Nucleic Acid Methylation. RNA Biology 14, 1108–1123. https://doi.org/10.1080/15476286.2016.1191737

Jeltsch, A., Nellen, W., Lyko, F., 2006. Two substrates are better than one: dual specificities for Dnmt2 methyltransferases. Trends in Biochemical Sciences 31, 306–308. https://doi.org/10.1016/j.tibs.2006.04.005

Jennison, A.V., Verma, N.K., 2004. *Shigella flexneri* infection: pathogenesis and vaccine development. FEMS Microbiol Rev 28, 43–58. https://doi.org/10.1016/j.femsre.2003.07.002

Johannsson, S., Neumann, P., Wulf, A., Welp, L.M., Gerber, H.-D., Krull, M., Diederichsen, U., Urlaub, H., Ficner, R., 2018. Structural insights into the stimulation of S. pombe Dnmt2 catalytic efficiency by the tRNA nucleoside queuosine. Sci Rep 8, 8880. https://doi.org/10.1038/s41598-018-27118-5

Jonkhout, N., Tran, J., Smith, M.A., Schonrock, N., Mattick, J.S., Novoa, E.M., 2017. The RNA modification landscape in human disease. RNA 23, 1754–1769. https://doi.org/10.1261/rna.063503.117

Juhling, F., Morl, M., Hartmann, R.K., Sprinzl, M., Stadler, P.F., Putz, J., 2009. tRNAdb 2009: compilation of tRNA sequences and tRNA genes. Nucleic Acids Research 37, D159–D162. https://doi.org/10.1093/nar/gkn772

Jurkowski, T.P., Jeltsch, A., 2011. On the Evolutionary Origin of Eukaryotic DNA Methyltransferases and Dnmt2. PLoS ONE 6, e28104. https://doi.org/10.1371/journal.pone.0028104

Jurkowski, T.P., Shanmugam, R., Helm, M., Jeltsch, A., 2012. Mapping the tRNA Binding Site on the Surface of Human DNMT2 Methyltransferase. Biochemistry 51, 4438–4444. https://doi.org/10.1021/bi3002659

Kaiser, S., 2017. The RNA methyltransferase Dnmt2 methylates DNA in the structural context of a tRNA. RNA BIOLOGY 14, 11. https://doi.org/10.1080/15476286.2016.1236170

Kasai, H., Ohashi, Z., Harada, F., Nishimura, S., Oppenheimer, N.J., Crain, P.F., Liehr, J.G., Von Minden, D.L., McCloskey, J.A., 1975. Structure of the modified nucleoside Q isolated from Escherichia coli transfer ribonucleic acid. 7-(4,5-cis-Dihydroxy-1-cyclopenten-3-ylaminomethyl)-7-deazaguanosine. Biochemistry 14, 4198–4208. https://doi.org/10.1021/bi00690a008

Katze, J.R., Gunduz, U., Smith, D.L., Cheng, C.S., McCloskey, J.A., 1984. Evidence that the nucleic acid base queuine is incorporated intact into tRNA by animal cells. Biochemistry 23, 1171–1176. https://doi.org/10.1021/bi00301a022

Klimasauskas, S., Kumar, S., Roberts, R.J., Cheng, X., 1994. Hhal methyltransferase flips its target base out of the DNA helix. Cell 76, 357–369. https://doi.org/10.1016/0092-8674(94)90342-5

Konevega, A.L., 2004. Purine bases at position 37 of tRNA stabilize codon-anticodon interaction in the ribosomal A site by stacking and Mg2+-dependent interactions. RNA 10, 90–101. https://doi.org/10.1261/rna.5142404

Kuge, H., 1998. Cap ribose methylation of c-mos mRNA stimulates translation and oocyte maturation in Xenopus laevis. Nucleic Acids Research 26, 3208–3214. https://doi.org/10.1093/nar/26.13.3208

Leach, A.R., Hann, M.M., Burrows, J.N., Griffen, E.J., 2006. Fragment screening: an introduction. Mol. BioSyst. 2, 429. https://doi.org/10.1039/b610069b

Lee, B.W.K., Van Lanen, S.G., Iwata-Reuyl, D., 2007. Mechanistic Studies of Bacillus subtilis QueF, the Nitrile Oxidoreductase Involved in Queuosine Biosynthesis. Biochemistry 46, 12844–12854. https://doi.org/10.1021/bi701265r

Leulliot, N., Chaillet, M., Durand, D., Ulryck, N., Blondeau, K., van Tilbeurgh, H., 2008. Structure of the Yeast tRNA m7G Methylation Complex. Structure 16, 52–61. https://doi.org/10.1016/j.str.2007.10.025

Li, J., Fu, A., Zhang, L., 2019. An Overview of Scoring Functions Used for Protein–Ligand Interactions in Molecular Docking. Interdiscip Sci Comput Life Sci 11, 320–328. https://doi.org/10.1007/s12539-019-00327-w

Li, S., Du, J., Yang, H., Yin, J., Ding, J., Zhong, J., 2013. Functional and structural characterization of DNMT2 from Spodoptera frugiperda. Journal of Molecular Cell Biology 5, 64–66. https://doi.org/10.1093/jmcb/mjs057

Liu, Q., Gao, Yang, Yang, W., Zhou, H., Gao, Yongxiang, Zhang, X., Teng, M., Niu, L., 2008. Crystallization and preliminary crystallographic analysis of tRNA m7G46 methyltransferase from Escherichia coli. Acta Crystallogr F Struct Biol Cryst Commun 64, 743–745. https://doi.org/10.1107/S1744309108020241

Liu, Y., Dong, Y., Chen, Y.-Y.M., Burne, R.A., 2008. Environmental and Growth Phase Regulation of the Streptococcus gordonii Arginine Deiminase Genes. AEM 74, 5023–5030. https://doi.org/10.1128/AEM.00556-08

Liu, Y., Santi, D.V., 2000. m5C RNA and m5C DNA methyl transferases use different cysteine residues as catalysts. PNAS 97, 8263–8265. https://doi.org/10.1073/pnas.97.15.8263

Lodish, H. (Ed.), 2002. Molecular cell biology, 4. ed., [Nachdr.]. ed, Media connected. Freeman, New York, NY.

Louise K. Francois Watkins, Grace D. Appiah, 2019. Chapter 4 Travel-Related Infectious Diseases-Shigellosis. URL https://www.cdc.gov/travel/yellowbook/2020/travel-related-infectious-diseases/shigellosis

Machnicka, M.A., Olchowik, A., Grosjean, H., Bujnicki, J.M., 2014. Distribution and frequencies of post-transcriptional modifications in tRNAs. RNA Biology 11, 1619–1629. https://doi.org/10.4161/15476286.2014.992273

Magee, R., Rigoutsos, I., 2020. On the expanding roles of tRNA fragments in modulating cell behavior. Nucleic Acids Research 48, 9433–9448. https://doi.org/10.1093/nar/gkaa657

Martin, J.L., McMillan, F.M., 2002. SAM (dependent) I AM: the S-adenosylmethionine-dependent methyltransferase fold. Current Opinion in Structural Biology 12, 11. https://doi.org/10.1016/S0959-440X(02)00391-3

Mathews, I., Schwarzenbacher, R., McMullan, D., Abdubek, P., Ambing, E., Axelrod, H., Biorac, T., Canaves, J.M., Chiu, H.-J., Deacon, A.M., DiDonato, M., Elsliger, M.-A., Godzik, A., Grittini, C., Grzechnik, S.K., Hale, J., Hampton, E., Han, G.W., Haugen, J., Hornsby, M., Jaroszewski, L., Klock, H.E., Koesema, E., Kreusch, A., Kuhn, P., Lesley, S.A., Levin, I., Miller, M.D., Moy, K., Nigoghossian, E., Ouyang, J., Paulsen, J., Quijano, K., Reyes, R., Spraggon, G., Stevens, R.C., van den Bedem, H., Velasquez, J., Vincent, J., White, A., Wolf, G., Xu, Q., Hodgson, K.O., Wooley, J., Wilson, I.A., 2005. Crystal structure of S-adenosylmethionine:tRNA ribosyltransferase-isomerase (QueA) from Thermotoga maritima at 2.0 Å resolution reveals a new fold. Proteins 59, 869–874. https://doi.org/10.1002/prot.20419

Matsumoto, K., Toyooka, T., Tomikawa, C., Ochi, A., Takano, Y., Takayanagi, N., Endo, Y., Hori, H., 2007a. RNA recognition mechanism of eukaryote tRNA m7G46) methyltransferase (Trm8-Trm82 complex). FEBS Letters 581, 1599–1604. https://doi.org/10.1016/j.febslet.2007.03.023

Matsumoto, K., Toyooka, T., Tomikawa, C., Ochi, A., Takano, Y., Takayanagi, N., Endo, Y., Hori, H., 2007b. RNA recognition mechanism of eukaryote tRNA (m7G46) methyltransferase (Trm8-Trm82 complex). FEBS Letters 581, 1599–1604. https://doi.org/10.1016/j.febslet.2007.03.023

Matsuyama, S., Ueda, T., Crain, P.F., McCloskey, J.A., Watanabe, K., 1998. A Novel Wobble Rule Found in Starfish Mitochondria. Journal of Biological Chemistry 273, 3363–3368. https://doi.org/10.1074/jbc.273.6.3363

McCarty, R.M., Somogyi, Á., Bandarian, V., 2009a. Escherichia coli QueD Is a 6-Carboxy-5,6,7,8-tetrahydropterin Synthase. Biochemistry 48, 2301–2303. https://doi.org/10.1021/bi9001437

McCarty, R.M., Somogyi, Á., Lin, G., Jacobsen, N.E., Bandarian, V., 2009b. The Deazapurine Biosynthetic Pathway Revealed: In Vitro Enzymatic Synthesis of PreQ0 from Guanosine 5′-Triphosphate in Four Steps. Biochemistry 48, 3847–3852. https://doi.org/10.1021/bi900400e

McClain, W.H., 1993. Rules that govern tRNA identity in protein synthesis. J Mol Biol 234, 257–280. https://doi.org/10.1006/jmbi.1993.1582

Meitert, T., Pencu, E., Ciudin, L., Tonciu, M., 1984. Vaccine strain Sh. flexneri T32-Istrati. Studies in animals and in volunteers. Antidysentery immunoprophylaxis and immunotherapy by live vaccine Vadizen (Sh. flexneri T32-Istrati). Arch Roum Pathol Exp Microbiol 43, 251–278.

Miles, Z.D., McCarty, R.M., Molnar, G., Bandarian, V., 2011. Discovery of epoxyqueuosine (oQ) reductase reveals parallels between halorespiration and tRNA modification. Proceedings of the National Academy of Sciences 108, 7368–7372. https://doi.org/10.1073/pnas.1018636108

Miles, Z.D., Myers, W.K., Kincannon, W.M., Britt, R.D., Bandarian, V., 2015. Biochemical and Spectroscopic Studies of Epoxyqueuosine Reductase: A Novel Iron–Sulfur Cluster- and Cobalamin-Containing Protein Involved in the Biosynthesis of Queuosine. Biochemistry 54, 4927–4935. https://doi.org/10.1021/acs.biochem.5b00335

Motorin, Y., Lyko, F., Helm, M., 2009. 5-methylcytosine in RNA: detection, enzymatic formation and biological functions. Nucleic Acids Research 38, 1415–1430. https://doi.org/10.1093/nar/gkp1117

Mueller, S.O., Slany, R.K., 1995. Structural analysis of the interaction of the tRNA modifying enzymes Tgt and QueA with a substrate tRNA. FEBS Letters 361, 259–264. https://doi.org/10.1016/0014-5793(95)00169-A

Müller, M., Hartmann, M., Schuster, I., Bender, S., Thüring, K.L., Helm, M., Katze, J.R., Nellen, W., Lyko, F., Ehrenhofer-Murray, A.E., 2015. Dynamic modulation of Dnmt2-dependent tRNA methylation by the micronutrient queuine. Nucleic Acids Res 43, 10952–10962. https://doi.org/10.1093/nar/gkv980

Murín, R., Abdalla, M., Murínová, N., Hatok, J., Dobrota, D., 2018. The Metabolism of 5-methylcytosine Residues in DNA. Physiol Res 383–389. https://doi.org/10.33549/physiolres.933550

Nar, H., Huber, R., Auerbach, G., Fischer, M., Hosl, C., Ritz, H., Bracher, A., Meining, W., Eberhardt, S., Bacher, A., 1995. Active site topology and reaction mechanism of GTP cyclohydrolase I. Proceedings of the National Academy of Sciences 92, 12120–12125. https://doi.org/10.1073/pnas.92.26.12120

Nelp, M.T., Bandarian, V., 2015. A Single Enzyme Transforms a Carboxylic Acid into a Nitrile through an Amide Intermediate. Angew. Chem. Int. Ed. 54, 10627–10629. https://doi.org/10.1002/anie.201504505

Nicola, G., Abagyan, R., 2009. Structure-Based Approaches to Antibiotic Drug Discovery. Current Protocols in Microbiology 12, 1–10. https://doi.org/10.1002/9780471729259.mc1702s12

Ohgi, T., Kondo, T., Goto, T., 1979. Total synthesis of optically pure nucleoside Q. Determination of absolute configuration of natural nucleoside Q. J. Am. Chem. Soc. 101, 3629–3633. https://doi.org/10.1021/ja00507a032

Okamoto, H., Watanabe, K., Ikeuchi, Y., Suzuki, T., Endo, Y., Hori, H., 2004. Substrate tRNA Recognition Mechanism of tRNA (m7G46) Methyltransferase from Aquifex aeolicus. J. Biol. Chem. 279, 49151–49159. https://doi.org/10.1074/jbc.M408209200

Patel, D., Bauman, J.D., Arnold, E., 2014. Advantages of crystallographic fragment screening: Functional and mechanistic insights from a powerful platform for efficient drug discovery. Progress in Biophysics and Molecular Biology 116, 92–100. https://doi.org/10.1016/j.pbiomolbio.2014.08.004

Pereira, M., Francisco, S., Varanda, A., Santos, Mafalda, Santos, Manuel, Soares, A., 2018. Impact of tRNA Modifications and tRNA-Modifying Enzymes on Proteostasis and Human Disease. IJMS 19, 3738. https://doi.org/10.3390/ijms19123738

Phalke, S., Nickel, O., Walluscheck, D., Hortig, F., Onorati, M.C., Reuter, G., 2009. Retrotransposon silencing and telomere integrity in somatic cells of Drosophila depends on the cytosine-5 methyltransferase DNMT2. Nat Genet 41, 696–702. https://doi.org/10.1038/ng.360

Phillips, G., El Yacoubi, B., Lyons, B., Alvarez, S., Iwata-Reuyl, D., de Crécy-Lagard, V., 2008. Biosynthesis of 7-Deazaguanosine-Modified tRNA Nucleosides: a New Role for GTP Cyclohydrolase I. JB 190, 7876–7884. https://doi.org/10.1128/JB.00874-08

Philpott, D.J., Edgeworth, J.D., Sansonetti, P.J., 2000. The pathogenesis of Shigella exneri infection: lessons from in vitro and in vivo studies. Philosophical Transactions Of The Royal Society B 575–586. https://doi.org/10.1098/rstb.2000.0599

Purta, E., van Vliet, F., Tricot, C., De Bie, L.G., Feder, M., Skowronek, K., Droogmans, L., Bujnicki, J.M., 2005. Sequence-structure-function relationships of a tRNA (m7G46) methyltransferase studied by homology modeling and site-directed mutagenesis. Proteins 59, 482–488. https://doi.org/10.1002/prot.20454

Ranjbar, R., Farahani, A., 2019. Shigella: Antibiotic-Resistance Mechanisms And New Horizons For Treatment. IDR Volume 12, 3137–3167. https://doi.org/10.2147/IDR.S219755

Razin, A., Cedar, H., 1991. DNA Methylation and Gene Expression. MICROBIOL. REV. 55, 8. https://doi.org/10.1128/MR.55.3.451-458.1991

Santi, D.V., Norment, A., Garrett, C.E., 1984. Covalent bond formation, between a DNA-cytosine methyltransferase and DNA containing 5-azacytosine. Biochemistry 6993–6997. https://doi.org/10.1073/pnas.81.22.6993

Sargentini, N.J., Gularte, N.P., Hudman, D.A., 2016. Screen for genes involved in radiation survival of Escherichia coli and construction of a reference database. Mutation Research/Fundamental and Molecular Mechanisms of Mutagenesis 793–794, 1–14. https://doi.org/10.1016/j.mrfmmm.2016.10.001

Schaefer, M., Lyko, F., 2010. Solving the Dnmt2 enigma. Chromosoma 119, 35–40. https://doi.org/10.1007/s00412-009-0240-6

Schaefer, M., Pollex, T., Hanna, K., Tuorto, F., Meusburger, M., Helm, M., Lyko, F., 2010. RNA methylation by Dnmt2 protects transfer RNAs against stress-induced cleavage. Genes & Development 24, 1590–1595. https://doi.org/10.1101/gad.586710

Schimmel, P., 2017. The emerging complexity of the tRNA world: mammalian tRNAs beyond protein synthesis. RNA Processing and Modifications 14. https://doi.org/10.1038/nmr.2017.77

Schubert, H.L., Blumenthal, R.M., Cheng, X., 2003. Many paths to methyltransfer: a chronicle of convergence. Trends in Biochemical Sciences 28, 329–335. https://doi.org/10.1016/S0968-0004(03)00090-2

Schuberth-Wagner, C., Ludwig, J., Bruder, A.K., Herzner, A.-M., Zillinger, T., Goldeck, M., Schmidt, T., Schmid-Burgk, J.L., Kerber, R., Wolter, S., Stümpel, J.-P., Roth, A., Bartok, E., Drosten, C., Coch, C., Hornung, V., Barchet, W., Kümmerer, B.M., Hartmann, G., Schlee, M., 2015. A Conserved Histidine in the RNA Sensor RIG-I Controls Immune Tolerance to N1-2′O-Methylated Self RNA. Immunity 43, 41–51. https://doi.org/10.1016/j.immuni.2015.06.015

Schulz, E.C., Roth, H.M., Ankri, S., Ficner, R., 2012. Structure Analysis of Entamoeba histolytica DNMT2 (EhMeth). PLoS ONE 7, e38728. https://doi.org/10.1371/journal.pone.0038728

Shaheen, R., Abdel-Salam, G.M.H., Guy, M.P., Alomar, R., Abdel-Hamid, M.S., Afifi, H.H., Ismail, S.I., Emam, B.A., Phizicky, E.M., Alkuraya, F.S., 2015. Mutation in WDR4 impairs tRNA m7G46 methylation and causes a distinct form of microcephalic primordial dwarfism. Genome Biol 16, 210. https://doi.org/10.1186/s13059-015-0779-x

Shanmugam, R., Aklujkar, M., Schäfer, M., Reinhardt, R., Nickel, O., Reuter, G., Lovley, D.R., Ehrenhofer-Murray, A., Nellen, W., Ankri, S., Helm, M., Jurkowski, T.P., Jeltsch, A., 2014. The Dnmt2 RNA methyltransferase homolog of Geobacter sulfurreducens specifically methylates tRNA-Glu. Nucleic Acids Research 42, 6487–6496. https://doi.org/10.1093/nar/gku256

Shanmugam, R., Fierer, J., Kaiser, S., Helm, M., Jurkowski, T.P., Jeltsch, A., 2015. Cytosine methylation of tRNA-Asp by DNMT2 has a role in translation of proteins containing poly-Asp sequences. Cell Discov 1, 15010. https://doi.org/10.1038/celldisc.2015.10

Shatkin, A., 1976. Capping of eucaryotic mRNAs. Cell 9, 645–653. https://doi.org/10.1016/0092-8674(76)90128-8

Shepherd, J., Ibba, M., 2015. Bacterial transfer RNAs. FEMS Microbiology Reviews 39, 280–300. https://doi.org/10.1093/femsre/fuv004

Shindo-Okada, N., Terada, M., Nishimura, S., 1981. Changes in Amount of Hypo-Modified tRNA Having Guanine in Place of Queuine during Erythroid Differentiation of Murine Erythroleukemia Cells. Eur J Biochem 115, 423–428. https://doi.org/10.1111/j.1432-1033.1981.tb05254.x

Singhal, R.P., 1981. MODIFICATION OF GUANINE TO QUHUINE IN TRANSFER RNAs DURING DEVELOPMFXV AND AGING. BIOCHEMICAL AND BIOPHYSICAL RESEARCH COMMUNICATIONS 99, 120–126. https://doi.org/10.1016/0006-291x(81)91721-6

Slany, R., Brsl, M., Kersten, H., 1994. Transfer and isomerization of the ribose moiety of AdoMet during the biosynthesis of queuosine tRNAs, a new unique reaction catalyzed by the QueA protein from Escherichia coil. Biochimie 389–393. https://doi.org/10.1016/0300-9084(94)90113-9

Theillet, F.-X., Binolfi, A., Frembgen-Kesner, T., Hingorani, K., Sarkar, M., Kyne, C., Li, C., Crowley, P.B., Gierasch, L., Pielak, G.J., Elcock, A.H., Gershenson, A., Selenko, P., 2014. Physicochemical Properties of Cells and Their Effects on Intrinsically Disordered Proteins (IDPs). Chem. Rev. 114, 6661–6714. https://doi.org/10.1021/cr400695p

Thiagarajan, D., Dev, R.R., Khosla, S., 2011. The DNA methyltranferase Dnmt2 participates in RNA processing during cellular stress. Epigenetics 6, 103–113. https://doi.org/10.4161/epi.6.1.13418

Thongdee, N., Jaroensuk, J., Atichartpongkul, S., Chittrakanwong, J., Chooyoung, K., Srimahaeak, T., Chaiyen, P., Vattanaviboon, P., Mongkolsuk, S., Fuangthong, M., 2019. TrmB, a tRNA m7G46 methyltransferase, plays a role in hydrogen peroxide resistance and positively modulates the translation of katA and katB mRNAs in Pseudomonas aeruginosa. Nucleic Acids Research 47, 9271–9281. https://doi.org/10.1093/nar/gkz702

Tomikawa, C., Ochi, A., Hori, H., 2007. The C-terminal region of thermophilic tRNA (m7G46) methyltransferase (TrmB) stabilizes the dimer structure and enhances fidelity of methylation. Proteins 71, 1400–1408. https://doi.org/10.1002/prot.21827

Tomikawa, C., Ohira, T., Inoue, Y., Kawamura, T., Yamagishi, A., Suzuki, T., Hori, H., 2013. Distinct tRNA modifications in the thermo-acidophilic archaeon, *Thermoplasma acidophilum*. FEBS Letters 587, 3575–3580. https://doi.org/10.1016/j.febslet.2013.09.021

Tomikawa, C., Takai, K., Hori, H., 2018. Kinetic characterization of substrate-binding sites of thermostable tRNA methyltransferase (TrmB). J. Biochem 163, 10. https://doi.org/10.1093/jb/mvx068

Tomikawa, C., Yokogawa, T., Kanai, T., Hori, H., 2010. N 7-Methylguanine at position 46 (m7G46) in tRNA from Thermus thermophilus is required for cell viability at high temperatures through a tRNA modification network. Nucleic Acids Research 38, 942–957. https://doi.org/10.1093/nar/gkp1059

Tomita, K., Ueda, T., Watanabe, K., 1998. 7-Methylguanosine at the anticodon wobble position of squid mitochondrial tRNASerGCU: molecular basis for assignment of AGA/AGG codons as serine in invertebrate mitochondria. Biochimica et Biophysica Acta (BBA) - Gene Structure and Expression 1399, 78–82. https://doi.org/10.1016/S0167-4781(98)00099-2

Trotman, J.B., Schoenberg, D.R., 2019. A recap of RNA recapping. WIREs RNA 10, e1504. https://doi.org/10.1002/wrna.1504

Tuorto, F., Herbst, F., Alerasool, N., Bender, S., Popp, O., Federico, G., Reitter, S., Liebers, R., Stoecklin, G., Gröne, H., Dittmar, G., Glimm, H., Lyko, F., 2015. The tRNA methyltransferase Dnmt2 is required for accurate polypeptide synthesis during haematopoiesis. EMBO J 34, 2350–2362. https://doi.org/10.15252/embj.201591382

Tuorto, F., Legrand, C., Cirzi, C., Federico, G., Liebers, R., Müller, M., Ehrenhofer-Murray, A.E., Dittmar, G., Gröne, H., Lyko, F., 2018. Queuosine-modified tRNAs confer nutritional control of protein translation. EMBO J 37. https://doi.org/10.15252/embj.201899777

Urbonavicius, J., Qian, Q., Durand, J.M., Hagervall, T.G., Björk, G.R., 2001. Improvement of reading frame maintenance is a common function for several tRNA modifications. EMBO J 20, 4863–4873. https://doi.org/10.1093/emboj/20.17.4863

Van Lanen, S.G., Iwata-Reuyl, D., 2003. Kinetic Mechanism of the tRNA-Modifying Enzyme S-Adenosylmethionine:tRNA Ribosyltransferase-Isomerase (QueA). Biochemistry 42, 5312–5320. https://doi.org/10.1021/bi034197u

Väre, V., Eruysal, E., Narendran, A., Sarachan, K., Agris, P., 2017. Chemical and Conformational Diversity of Modified Nucleosides Affects tRNA Structure and Function. Biomolecules 7, 29. https://doi.org/10.3390/biom7010029

Wang, C., Zou, P., Yang, C., Liu, L., Cheng, L., He, X., Zhang, L., Zhang, Y., Jiang, H., Chen, P.R., 2019. Dynamic modifications of biomacromolecules: mechanism and chemical interventions. Sci. China Life Sci. 62, 1459–1471. https://doi.org/10.1007/s11427-019-9823-1

Watson, J.D., Crick, F.H., 1953a. Genetical implications of the structure of deoxyribonucleic acid. Nature 171, 964–967. https://doi.org/10.1038/171964b0

Watson, J.D., Crick, F.H., 1953b. Molecular structure of nucleic acids; a structure for deoxyribose nucleic acid. Nature 171, 737–738. https://doi.org/10.1038/171737a0

WHO. Antimicrobial resistance (WHO Fact sheet)., 2018. . Geneva: World Health Organization.

Winiewska-Szajewska, M., Płonka, D., Zhukov, I., Poznański, J., 2019. Rational drug-design approach supported with thermodynamic studies — a peptide leader for the efficient bi-substrate inhibitor of protein kinase CK2. Sci Rep 9, 11018. https://doi.org/10.1038/s41598-019-47404-0

Yang, Y., Hsu, P.J., Chen, Y.-S., Yang, Y.-G., 2018. Dynamic transcriptomic m6A decoration: writers, erasers, readers and functions in RNA metabolism. Cell Res 28, 616–624. https://doi.org/10.1038/s41422-018-0040-8

Zegers, I., 2006. Crystal structure of Bacillus subtilis TrmB, the tRNA (m7G46) methyltransferase. Nucleic Acids Research 34, 1925–1934. https://doi.org/10.1093/nar/gkl116

Zegers, I., Gigot, D., Bujnicki, J.M., Kosinski, J., Droogmans, L., 2005. Crystal structure of Bacillus subtilis TrmB, the tRNA (m7G46) methyltransferase. NAR 34, 10. https://doi.org/10.1093/nar/gkl116

Zhou, H., Liu, Q., Yang, W., Gao, Y., Teng, M., Niu, L., 2009. Monomeric tRNA (m7G46) methyltransferase from Escherichia coli presents a novel structure at the function-essential insertion. Proteins 76, 512–515. https://doi.org/10.1002/prot.22413

Chapter 7 Abbreviations

5-mC	5-methyl-deoxycytidine
6xHis tag	hexa-histidine tag
A	adenosine
ADS	arginine deiminase system
BESSY	Die Berliner Elektronenspeicherring-Gesellschaft für Synchrotronstrahlung
C	cytidine
CDG	7-carboxy-7-deazaguanine
CPH_4	6-carboxy-5,6,7,8-tetrahydropterin
dA	deoxyadenosine
DNA	deoxyribonucleic acid
D-arm	dihydrouidine-arm
dC	deoxycytidine
DESY	Deutsches Elektronen Synchrotron
DFG	Deutsche Forschungsgemeinschaft
dG	deoxyguanosine
Dnmt	DNA methyltranferase
dT	deoxythimidine
EMBL	European Molecular Biology Laboratory
G	guanosine
G^+	archaeosine
GlmN6P	glucosamine-6-phosphate
GST	glutathione S-transferase
GTP	guanosine-5´-triphosphate
HEPES	4-(2-Hydroxyethyl)piperazine-1-ethanesulfonic acid
H_2NTP	7,8-dihydroneopterin triphosphate
I_sc	interface score
IPTG	Isopropy β-$_D$-1-thiogalactopyranoside
lncRNA	long non-coding RNA
m^1A	N1-methyladenosine
m^1G	N1-methylguanine
m^5C	C5-methylcytidine

m^6A	N6-methyladenosine
m^7G	N7-methylguanosine
manQ	mannosyl-queuosine
MES	2-(N-morpholino)ethanesulfonic acid
miRNA	micro RNA
mRNA	messenger RNA
MS	mass spectrometry
MTase	Methyltransferase
OD_{600}	optical density at 600 nm
oQ-tRNA	epoxy-queuosine-tRNA
PDB	Protein Data Bank
PEG	polythylene glycol
PP_i	Pyrophosphate
$preQ_1$	7-ammoniomethyl-7-deazaguanine
q	queuine
Q	queuosine
RMSD	root mean square deviation
RNA	ribonucleic acid
RT	room thermperature
SAH	S-adenosyl-L-homocystein
SAM	S-Adenosyl-L-methionine
SAXS	small-angle x-ray scattering
SD	standard deviation
SDS-PAGE	sodium dodecyl sulfate polyacrylamide gel electrophoresis
snoRNA	small nucelolar RNA
snRNA	small nuclear RNA
T-Arm	T-pseudouridine-C -Arm
TFA	Trifluoroacetic acid
TGT	tRNA-guanine transglycosylase
tRFs	tRNA fragments
Tris	tris(hydroxymethyl)aminomethane
tRNA	transfer RNA
U	uracil
UDP	uridine diphosphate
UV	ultraviolet fraction of electromagnetic radiation
v/v	volume / volume

yW	wybutosine
ψ	pseudouridine

Chapter 8 Acknowledgements

This thesis could not have been accomplished without a tremendous amount of help and support for which I would like to express my sincere appreciation.

The work underlying this thesis was carried out in the Department for Molecular Structural Biology at the Göttingen Centre for Molecular Biosciences (GZMB). I am deeply grateful for the opportunity to work on this project and want to thank the most important person during my studies, my supervisor Prof. Dr. Ralf Ficner. Thank you for providing a great research environment and letting me develop my own research ideas with guidance and criticism at the right places.

Further, I am grateful for the support and help of the members of my thesis committee, Prof. Dr. Jörg Stülke and Prof. Dr. Markus Bohnsack, who showed great interest in my work and always provided helpful input during our meetings. Furthermore, I want to thank Prof. Dr. Kai Tittmann, Dr. Sarah Adio, and Prof. Dr. Henning Urlaub for being part of my extended examination board.

I am deeply thankful for the constant support of Dr. Piotr Neumann. Thank you for always having time when I approached you. Your advice and ideas had a great impact on the work presented here in this thesis. Our countless scientific discussions have been inspiring, encouraging, and motivated me to become the best scientist I could be. Your sense of humour and ability to tell stories made working days truly joyful, especially during sleepless synchrotron trips (at least for us).

Furthermore, I want to thank Dr. Achim Dickmanns who always answered my questions and shared the excitement for diving into new scientific methods. His scientific expertise on lab work was always helpful.

Of course, I am in huge debt to all members of the MSB department for their friendship, asked and answered questions, and happy environment. Thanks to Marieke, Tim, Katharina, Patrick, and Flo for the joyful lunch breaks, coffee brakes, hallway talks, and welcoming environment. Especially I want to thank Jana and Alaa for being the best synchrotron squad of all times. I hold these times dearly to my heart. I also like to thank my students, Simon Bolz, Lukas Singhoff, and Fabienne Hahn for the opportunity of working together and participate in their scientific education.

Further, I am grateful to Marita Kalck and Daniel Weinrich for their bureaucratic and technical help and support. I want to thank Susanne van Beckum for all her warm words during more challenging times. Furthermore, I want to thank Annette Berndt and Beate Heinze. Vielen Dank für die unzähligen Momente in denen wir vor Lachen kaum noch Luft bekommen haben. Ihr habt mir in so manchen Situationen die Augen geöffnet und wart eine unglaubliche Hilfe, vielen Dank.

I express my sincere thanks to the members of the group of Prof. Dr. Kai Tittmann who made the socially distanced lunch breaks truly enjoyable. Especially I thank Fabian who never stopped asking to join in sportive activities and who shared my passion for flea markets.

Last but not least, I want to thank all my friends in Göttingen and elsewhere. Thank you for all the adventures we shared and for being there for me. Especially, I want to mention Anna, Jörn, and Felix, you are my favourite people to be locked into a room with. Dayana and Swantje, thank you for always catching me and for your wonderful friendship. And lastly, I am deeply thankful to Maximilian Hesselbarth. You have not only been my partner in crime, spent countless hours in noisy gyms, but also supported me in everything I did.

This thesis could have not been possible without the continuous support and love of my parents, Silvia Blersch and Erhard Blersch, as well as my sister Josephine and my brother Tobias. I am deeply grateful for every moment we have together.

I dedicate this thesis to them.